

Live Cell Studies of DNA Single Strand Break Repair Pathway:

The Road Map

By

Ismail Abdou

A thesis submitted in partial fulfillment of the requirements for the degree of

Doctor of Philosophy

In

Cancer Sciences

Department of Oncology

University of Alberta

© Ismail Abdou, 2015

ABSTRACT

The repair of damaged DNA is critically important for maintaining a stable cellular environment to ensure proper and high fidelity segregation and transmission of genetic information from one generation to the next. DNA can be subjected to many forms of DNA damage that are handled by dedicated signaling pathways and repair complexes. The most common DNA lesions are DNA single strand breaks (SSBs). Most of our current understanding of DNA SSB repair (SSBR) has been derived from biochemical studies. In our work, we employed live cell imaging techniques in addition to biochemical approaches to better define the steps in this repair pathway, thus providing clearer insight for how SSBR is orchestrated in live cells.

Our focus was mainly on (i) how rapidly different SSBR proteins accumulate at sites of DNA damage, (ii) how DNA SSBs are detected, (iii) providing mechanistic explanations for the association of different polymorphisms of the SSBR scaffold protein X-ray cross-complementing protein 1 (XRCC1) with cancer, and (iv) how the DNA SSBR end-processing enzyme, polynucleotide kinase/phosphatase (PNKP) is regulated in response to DNA damage.

Importantly, we provide evidence, for the first time in live cells, that DNA ligase III (LIG3), in addition to its established downstream nick sealing activity in SSBR, functions as an alternative SSB sensor to poly-ADP-ribose polymerase 1 (PARP1). Furthermore, we observed that LIG3 and PARP1 detect different types of SSBs. Given the current success of PARP inhibitors targeting PARPs 1 and 2 in cancer therapy, our finding expands the number of potential targets for small molecule inhibitor development and drug intervention.

We also show that two of the cancer associated XRCC1 polymorphisms, R194W and R280H, give rise to XRCC1 variant proteins that impede the accumulation and catalytic activity of PNKP at sites of DNA damage. This might lead to increased background mutations in cells harboring these polymorphisms providing a further driving force towards tumorigenesis.

Finally, our published data in agreement with others, show that the phosphorylation of two serine residues within the linker region of PNKP tightly regulate the protein behavior at DNA damage sites. We extended this work by carrying out preliminary studies on the behavior of the FHA domain of PNKP in live cells in response to DNA damage.

PREFACE

Chapter 1 provides a brief introduction to help understand the current working models for the DNA Double and Single Strand Break Repair (DSBR and SSBR respectively) pathways.

Chapter 2 provides detailed procedures for experimental work presented in this thesis.

Chapter 3 encompasses original work by Ismail Abdou recently published in the journal of Nucleic Acids Research, “DNA ligase III acts as a DNA strand break sensor in the cellular orchestration of DNA strand break repair”. All the experiments and manuscript preparation were carefully designed and carried out by Ismail Abdou, under the supervision of Michael Weinfeld and Michael Hendzel.

Chapter 4 is collaborative work between the laboratories of Michael Weinfeld and Mark Glover, where Rajam S. Mani conducted the biochemical experiments for the binding assays and circular dichroism analyses. Protein expression and purification were carried out by Ismail Abdou. The enzymatic and functional assays were designed and performed through concerted efforts of Mesfin Fanta and Ismail Abdou. Live cell imaging experiments were designed and carried out by Ismail Abdou.

Finally, in chapter 5 we aim to build on the previous work published by others (Yosi Shiloh) and ourselves (collaboration between Susan P. Lees Miller and Michael Weinfeld). In the latter publication, Ismail Abdou contributed by designing and performing the live cell imaging to investigate the impact of PNKP phosphorylation on the recruitment of the protein to sites of DNA damage. The preliminary work in this chapter is original work carried out by Ismail Abdou. Additionally, we provided

perspectives and views emanating from our findings that might pave the way for the therapeutic exploitation of LIG3.

DEDICATION

All gratitude is due to God, he is the first without predecessor and he is the last without a successor and to him and his mercy all my gratitude and prayers shall belong and rest.

if anyone saves a life, it shall be as though he had saved the lives of all mankind”

{AlMa'ida, verse 32, Holy Quraan}

(وَمَنْ أَحْيَاهَا فَكَأَنَّمَا أَحْيَا النَّاسَ جَمِيعًا)

سورة المائدة آية 32

First and foremost I dedicate this work to my family. They all have been, and will always be, an inspiration and great support to me in times of hardship and ease. My parents, in spite of being thousands of miles away, were very close to me with their prayers, supplications and blessings. My wife took care of many responsibilities so that I could focus on my work. She provided me with exceptional emotional support. My son has been an inspiration to me, bearing my absences from several of his activities on weekends because I had to work, and he even had to come to the laboratory with me sometimes. Finally, my baby daughter, sorry I didn't have enough time to hang around watching you growing by the minute.

A very important and dear person to me is Mr. Mesfin Fanta, from the very first moments in Dr. Weinfeld's laboratory, it was you who made me feel at ease and forget about home sickness, at least during our working hours. Mesfin, with unquestionable practical expertise in laboratory bench work and work ethic was very generous with

passing these qualities to me and everyone in the lab. On the personal level, Mesfin is an exceptional work colleague and a big brother.

Also I would like to thank past and current members of Dr. Weinfeld's laboratory, Mrs. Jane Lee, Dr. Aghdass Rasouli-Nia, Dr. Todd Mereniuk, Dr. Feridoun Karimi-Busheri, and Mr. Sudip Subedi, for their continuous support and fruitful discussions.

Finally, I dedicate this work to the welfare of cancer patients wishing them all good health and prosperous times to come after all the hardships they and their family members have faced, and I wish that one day my work would be the missing piece in the puzzle of treating such a calamitous condition.

ACKNOWLEDGEMENTS

I would like to take the opportunity and give a special dedication to my mentors and supervisors, Dr. Michael Weinfeld and Dr. Michael Hendzel. They helped a lot in moulding me personally and technically to become the scientist I am today. They were of constant support and involvement in my work and provided me with a highly flexible environment to pursue my research goals.

Also, I would like to thank Dr. Mark Glover for his help and support for my work.

I would like to thank Dr. Zhao-Qi Wang of Jena University, Germany, for providing us with PARP1 wild-type and knock out mouse embryonic fibroblasts. Additionally, Dr. Heinrich Leonhardt of Ludwig-Maximilians University, Germany, generously provided us with LIG3 constructs. I would like to thank Darin McDonald for technical assistance. I also thank the Cell Imaging Facility members (Dr. Sun and Geraldine Barron) at the Cross Cancer Institute (Edmonton) for providing space and support in cell imaging experiments.

Finally, I would like to thank our funding agencies for their financial support. Most of this research was supported by CIHR grants (MOP 15385 to Michael Weinfeld and Michael Hendzel). I held an Alberta Cancer Foundation Graduate Studentship (2011-2015).

LIST OF ABBREVIATIONS

Abbreviation	Full name
3'-OH	3'- hydroxyl
3'-P	3'-phosphate
3'-PUA	3'-polyunsaturated aldehyde
5'dRP	5'-deoxyribose phosphate
5'-OH	5'-hydroxyl
5'-P	5'-phosphate
53BP1	p53 binding protein 1
AOA1	Ataxia with Oculomotor Apraxia
APE1	Apurinic/aprimidinic endonuclease 1
AT	Ataxia Telangiectasia
ATM	Ataxia Telangiectasia Mutated
BER	Base excision repair
Bp	Base pairs
BRCA1	Breast Cancer 1, early onset
BRCA2	Breast Cancer 2, early onset
CtIP	C-terminal binding protein interacting protein
DBD	DNA binding domain
DDR	DNA Damage Response
DNA-PKcs	DNA-dependent protein kinase catalytic subunit
DSBR	Double strand break repair

DSBs	Double strand breaks
EGFP	Enhanced green fluorescent protein
EXO1	Exonuclease 1
FCS	Fetal calf serum
FEN1	Flap endonuclease 1
FHA	Fork Head Associated
FL	Full length
FRAP	Fluorescence recovery after photobleaching
GFP	Green fluorescent protein
HR	Homologous recombination
Ig	Immunoglobulin
IR	Ionizing radiation
IRI	Irinotecan
KO	Knockout
Laser μR	Laser micro-irradiation
LIG1	DNA Ligase 1
LIG3	DNA Ligase III
LIG4	DNA ligase IV
LP-BER	Long patch base excision repair
MCSZ	Microcephaly with Seizures
MDC1	Mediator of DNA damage checkpoint 1
MEFs	Mouse embryo fibroblasts
MMS	Methyl methanesulfonate

MRN	MRE11-RAD50-NBS1
NBS	Nijmegen Breakage Syndrome
NHEJ	Non-homologous end joining
OGG1	8-oxoguanine DNA glycosylase
PARP	Poly(ADP-ribose) polymerase
PARylation	Poly(ADP-ribosyl)ation
PCNA	Proliferating cell nuclear antigen
PNKP	Polynucleotide kinase/phosphatase
Polβ	DNA polymerase beta
RFP	Red fluorescent protein
ROS	Reactive oxygen species
RPA	Replication protein A
SCAN1	SpinoCerebellar Ataxia with Axonal Neuropathy
SDS	Sodium dodecyl sulphate
S.E.M.	Standard error of the mean
SNPs	Single Nucleotide Polymorphisms
SP-BER	Short patch base excision repair
SSBR	Single strand break repair
SSBs	Single strand breaks
ssDNA	Single stranded DNA
TDP1	Tyrosyl-DNA phosphodiesterase I
UV	Ultraviolet
WCE	Whole cell extracts

WT	Wild-type
XP	Xeroderma Pigmentosum
XRCC1	X-Ray Cross Complementing Protein 1
XRCC4	X-Ray Cross Complementing Protein 4
ZnF	Zinc finger

TABLE OF CONTENTS

List of Figures	xvi
Chapter 1: DNA damage and repair: Cellular regulation and importance for cellular homeostasis.....	1
Introduction	2
DNA damage and repair: Cellular regulation and importance for cellular homeostasis	2
DNA Single Strand Break Repair (SSBR)	5
DNA DSB: importance and pathways involved	15
The DNA DSB-SSBR alliance for repair: aNHEJ	26
Tools to study DNA repair, biochemical and cellular assays	28
Thesis Focus and working hypotheses	35
1) How are SSBs detected? Current perspective	35
PARP1, the sensor revisited	35
LIG3, a candidate sensor in SSBR	39
2) XRCC1 polymorphisms and links to cancer.....	41
3) PNKP structure and post-translational modifications.....	42
Chapter 2: Experimental procedures.....	46
Cell Culture.....	47
Lysate preparation.....	47
Mammalian and bacterial expression plasmids	48
List 1, expression plasmids.....	49
List 2, PCR primers.....	49
Western blotting.....	53
List 3, antibodies for western blotting	55
Protein expression and purification.....	55
In vitro phosphorylation of XRCC1 fragments and purification	57
Steady-state fluorescence spectroscopy	58
Circular dichroism spectroscopy	59
Measurement of single strand break repair (alkaline COMET assay).....	59

Immunofluorescence and microscopy	60
List 4, antibodies for immunofluorescence.....	61
Laser micro-irradiation (Two-photon laser micro-irradiation and 405 nm diode)	61
Fluorescence recovery after photobleaching (FRAP)	63
PNKP DNA Kinase Assays	64
Single time point kinase reaction.....	64
Turn over assay for PNKP kinase activity	65
Statistical analysis	65
Chapter 3: DNA ligase III acts as a DNA strand break sensor in the cellular orchestration of DNA strand break repair.....	66
ABSTRACT	67
INTRODUCTION	68
RESULTS	72
Establishment of a micro-irradiation system that specifically activates SSBR not BER	72
Rapid recruitment of SSBR machinery to DNA damage sites	79
PARP1 mediated poly(ADP-ribosyl)ation accelerates the initial recruitment of SSBR core proteins (XRCC1, LIG3, and PNKP) to sites of DNA damage but is not required for retention.....	83
The influence of LIG3 on the recruitment of SSBR core machinery	93
ZnF domain, a nick sensor in LIG3	102
ZnF domain is sufficient for the initial rapid recruitment of LIG3 to sites of DNA damage	105
Binding kinetics of SSBR proteins to damaged DNA is PARP1 independent	110
LIG3 and not PARP1 functions as a nick sensor in live cells	115
DISCUSSION.....	118
Indications of an alternative SSB sensor to PARP1	118
Chapter 4: Interaction between Polynucleotide Kinase/Phosphatase and the Scaffolding Protein XRCC1 is mediated through Linker-1 in the N-terminal domain of XRCC1.....	124
ABSTRACT	125

INTRODUCTION	127
RESULTS	131
Overview of the fluorescence-based analytical approach for studying PNKP interaction with XRCC1 fragments.....	131
Interaction between PNKP and the C-terminal domain of XRCC1.....	131
Interaction between PNKP and the extended BRCT1 domain of XRCC1	137
DNA binding to the extended BRCT1 domain of XRCC1.....	137
CD analysis of the extended BRCT1 domain of XRCC1 and interaction with DNA.....	141
Effect of XRCC1 and its fragments on the DNA kinase activity of PNKP	144
Influence of XRCC1 fragments on the turnover of PNKP.....	144
Cellular interaction of wild-type and mutant XRCC1 with PNKP.....	150
Discussion.....	154
Interactions of XRCC1 fragments with PNKP.....	154
Interactions of XRCC1 fragments with DNA.....	156
Effect of XRCC1 fragments on the kinase activity of PNKP.....	157
Chapter 5: Discussion and perspectives	159
LIG3, a damage sensor in SSBR: Implications for cancer therapy.....	160
LIG3 and DDR.....	160
LIG3 and links to cancer initiation and progression.....	160
Mechanistic Insights on the Assembly of PNKP at sites of DNA damage	168
<i>PNKP function and regulation</i>	<i>168</i>
Preliminary results and future experiments	179
Significance.....	183
References.....	184

LIST OF FIGURES

FIGURE 1: OUTLINE OF DIFFERENT FORMS OF DNA DAMAGE AND DELEGATED REPAIR PATHWAYS	3
FIGURE 2: OUTLINE OF BER-SSBR PATHWAY.....	7
FIGURE 3: ILLUSTRATION OF DIFFERENT MODES OF DAMAGED BASE ELIMINATION BY MONO- AND BI-FUNCTIONAL DNA GLYCOSYLASES.....	10
FIGURE 4: DIFFERENT TYPES OF DAMAGED 3' AND 5' ENDS AND SPECIFIC END PROCESSOR ENZYME	11
FIGURE 5: ILLUSTRATION OF REPAIR OF DSBS BY NHEJ (LEFT) AND HR (RIGHT).....	16
FIGURE 6: OUTLINE OF BASIC STEPS FOR DSBR VIA HOMOLOGOUS RECOMBINATION	20
FIGURE 7: OUTLINE OF DSBR VIA NHEJ	24
FIGURE 8: PROPOSED MODEL FOR A-NHEJ	27
FIGURE 9: OUTLINE OF PNKP KINASE ASSAY	30
FIGURE 10: SCHEMATIC REPRESENTATION OF LASER μ IR TO STUDY DDR IN REAL TIME.....	32
FIGURE 11: SCHEMATIC REPRESENTATION OF FRAP TECHNIQUE.....	34
FIGURE 12: PROPOSED MECHANISM OF PNKP KINASE ACTIVITY	43
FIGURE 13: OUTLINE OF PNKP PHOSPHATASE ACTIVITY.....	44
FIGURE 14: SCHEMATIC OUTLINE FOR GENERATED EXPRESSION PLASMIDS	52
FIGURE 15: COMPARATIVE INDUCTION OF BASE DAMAGE AND STRAND BREAKS BY DIFFERENT LASER MICRO-IR CONDITIONS	73
FIGURE 16: RECRUITMENT OF OGG1 AND XRCC1 UNDER DIFFERENT LASER CONDITIONS.....	75
FIGURE 17: RECRUITMENT AND RETENTION OF SSBR PROTEINS FOLLOWING MULTI-PHOTON 750 NM LASER MICRO-IRRADIATION	80
FIGURE 18: RECRUITMENT OF XRCC1 AND PNKP IN PARP1 WT AND KO CELLS.....	85
FIGURE 19: PARP1 INHIBITION AND THE RECRUITMENT OF SSBR PROTEINS TO SITES OF DNA DAMAGE	87
FIGURE 20: LIG3 KNOCKDOWN AND THE RECRUITMENT OF XRCC1 AND PNKP TO SITES OF DNA DAMAGE.....	95
FIGURE 21: LIG3 AND PARP1 ARE NON-REDUNDANT DAMAGE SENSORS.....	99
FIGURE 22: COMPARISON BETWEEN THE RECRUITMENT OF FULL LENGTH LIG3 AND LIG3 LACKING THE ZINC FINGER TO SITES OF DNA DAMAGE	103
FIGURE 23: THE ZNF DOMAIN IS REQUIRED AND SUFFICIENT FOR THE DAMAGE SENSING FUNCTION OF LIG3.....	107
FIGURE 24: PARP1 INHIBITION AND THE RETENTION OF SSBR PROTEINS AT SITES OF DNA DAMAGE	111
FIGURE 25: LIG3 IS AN <i>IN VIVO</i> NICK SENSOR FOR IRINOTECAN INDUCED DNA DAMAGE	116
FIGURE 26: TWO PATHWAYS EXIST FOR THE SHORT PATCH REPAIR OF SSBS.....	122
FIGURE 27: SCHEMATIC OF HUMAN XRCC1. THE DIAGRAM SHOWS THE MAJOR IDENTIFIED DOMAINS WITHIN XRCC1 AND THE PROTEIN FRAGMENTS USED FOR THIS STUDY.....	129
FIGURE 28: FLUORESCENCE TITRATION OF PNKP ^{WFX402-AC} VERSUS PEB2.....	133
FIGURE 29: FLUORESCENCE TITRATION OF PNKP ^{FHA-AC} VERSUS PEB2 AND PBLB	136
FIGURE 30: FLUORESCENCE TITRATION OF EB1 VERSUS DUPLEX DNA WITH A SINGLE NUCLEOTIDE GAP	139
FIGURE 31: CD ANALYSIS FOR WT AND MUTANT EB1	142
FIGURE 32: ACTIVATION OF PNKP BY FULL LENGTH XRCC1 AND XRCC1 FRAGMENTS.....	146

FIGURE 33: THE EFFECT OF XRCC1 VARIANTS ON THE RECRUITMENT OF PNKP TO SITES OF DNA DAMAGE	151
FIGURE 34: HALLMARKS OF CANCER.....	162
FIGURE 35: ENABLING CHARACTERISTICS THAT PROMOTE CARCINOGENESIS	163
FIGURE 36: PLAUSIBLE ROLES OF LIG3 AT DIFFERENT STAGES OF TUMOR EVOLUTION.....	165
FIGURE 37: FORMATION OF TOPOISOMERASE 1 CLEAVAGE COMPLEXES AND REPAIR VIA TDP1/PNKP COOPERATION	170
FIGURE 38: ROLE OF ATM/DNA-PKS IN THE RECRUITMENT OF PNKP TO LASER INDUCED DAMAGE TRACKS	174
FIGURE 39: PROPOSED MODEL FOR THE ACCUMULATION OF PNKP AT SITES OF DNA DAMAGE	177
FIGURE 40: RECRUITMENT OF FHA-LINKER TO SITES OF DNA DAMAGE.....	180

Chapter 1: DNA damage and repair: Cellular regulation and importance for cellular homeostasis

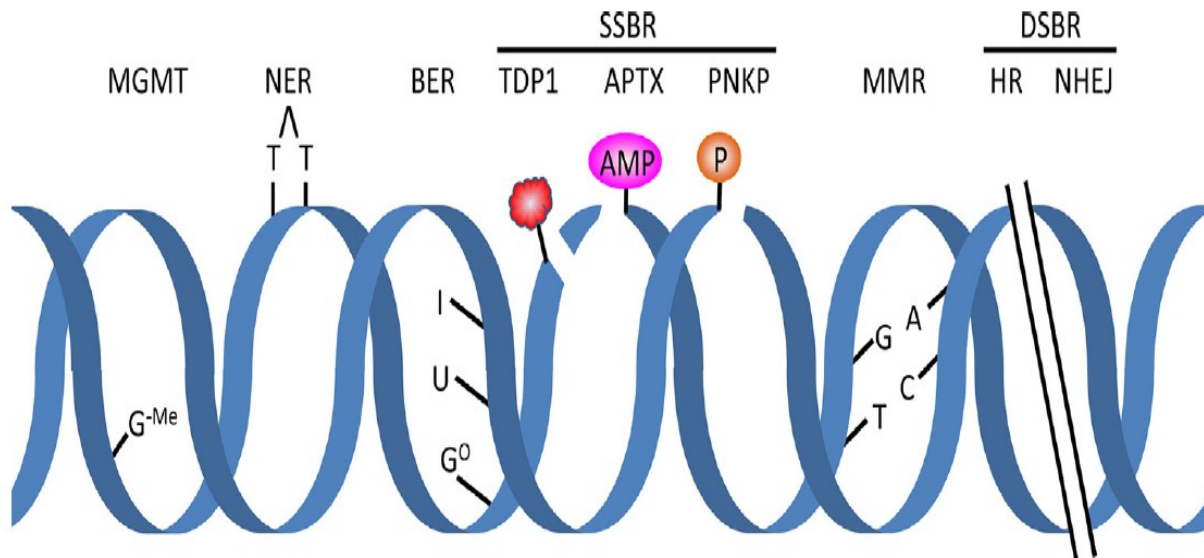
Introduction

DNA damage and repair: Cellular regulation and importance for cellular homeostasis

DNA is the carrier of genetic material in cells, and therefore, protecting cellular DNA is critical for maintaining homeostasis. The integrity of cellular DNA is continually challenged by exposure to intracellular e.g. reactive oxygen species (ROS) and extracellular agents e.g. ultraviolet (UV) light, ionizing radiation (IR) and genotoxic chemicals. Accordingly, living cells possess a large repertoire of DNA repair proteins involved in multiple damage specific pathways (outlined in **Figure 1**)^{1,2}. These proteins are clustered in different repair pathways, collectively known as the DNA Damage Response (DDR), that function as classical signalling cascades. The DNA lesion serves as the signal, which is detected by specific damage sensors that in turn relay to downstream scaffolding and effector proteins, resulting ultimately in the repair of DNA lesion.

Defective repair of different DNA lesions, due to mutations resulting in either the absence or loss of function of certain DDR proteins, has been linked to several diseases. Neurological disorders, e.g. Nijmegen Breakage Syndrome (NBS), Ataxia telangiectasia (AT)³, SpinoCerebellar Ataxia with Axonal Neuropathy 1 (SCAN1)⁴, Ataxia Oculomotor Apraxia (AOA)⁵, Microcephaly and Seizures (MCSZ)⁶ and Xeroderma Pigmentosum (XP)⁷, and increased predisposition to cancer are the most prevalent associations. Therefore, understanding the regulation of different DDR pathways is imperative and has been the subject of considerable study.

Figure 1: Outline of different forms of DNA damage and delegated repair pathways



DNA damage and repair responses. DNA repair pathways (top) and examples of corresponding DNA damage (bottom) are shown. The detailed molecular mechanisms for the repair responses are provided in the text. APTX, aprataxin; BER, base excision repair; DSBR, DNA double strand break repair; HR, homologous recombination; MGMT, O6-methylguanine-DNA methyltransferase; MMR, mismatch repair; NER, nucleotide excision repair; NHEJ, non-homologous end joining; P, 3' phosphate; PNKP, polynucleotide kinase/phosphatase; SSBR, DNA single strand break repair; SSBs, DNA single strand breaks; TC-NER, transcription-coupled NER; TDP1, tyrosyl-DNA phosphodiesterase 1; G-Me, O6-Methylguanine; T[^]T, thymine dimer; U, uracil; G[°], 8-oxoguanine. **DNA Repair 12 (2013) 620– 636**

Reproduced with permission from Elsevier. Copyright © 2013

Work in our laboratory mainly focuses on the DDR protein polynucleotide kinase/phosphatase (PNKP)⁸. PNKP participates in different DDR pathways, including double strand break repair (DSBR) and single strand break repair (SSBR). A final step that the majority of DDR pathways converge on is resealing of DNA ends. Often, DDR is associated with DNA ends that are incompatible with ligation (i.e. not the conventional 3'-OH and 5'-P) either as a direct consequence of the damage or as a repair intermediate⁹. At damaged DNA ends, PNKP possesses dual enzymatic activities, 5' kinase and 3' phosphatase, which help restore '*ligatable*' DNA termini. Genetic defects in PNKP are associated with the neurological disorder MCSZ⁶. Additionally, recent evidence has linked the neurodegenerative disorder, Spinocerebellar ataxia type 3 (SCA3), with abnormal functioning of PNKP^{10,11}.

The work presented herein aimed to provide deeper insights into the interplay between PNKP and associated proteins, primarily in SSBR and to a lesser extent in DSBR, taking place in the living cellular environment. In the following section a brief description of the current understanding of DNA DSBR and SSBR will be provided.

DNA Single Strand Break Repair (SSBR)

DNA single strand breaks (SSBs) are lesions that interrupt and compromise the integrity of single strands of DNA. Importantly, cellular DNA is subject to SSBs on a scale of thousands per cell per day ¹². If left unrepaired, SSBs can lead to blocking either transcription or replication, with apoptosis or formation of the more lethal and/or mutagenic DSBs respectively being the ultimate outcome ¹³. Consistently, defects in SSBR due to mutations in core proteins, TDP1, PNKP and APTX have been linked with several neurological disorders, including SCAN1, MCSZ and AOA1 respectively ¹⁴. Additionally, mutations in other SSBR core machinery proteins, XRCC1 and DNA Pol β , have been associated with cancer ^{15,16}. Accordingly, repair of such lesions in a rapid (usually on the scale of min ¹⁷) and robust manner is crucial for optimal cellular functioning.

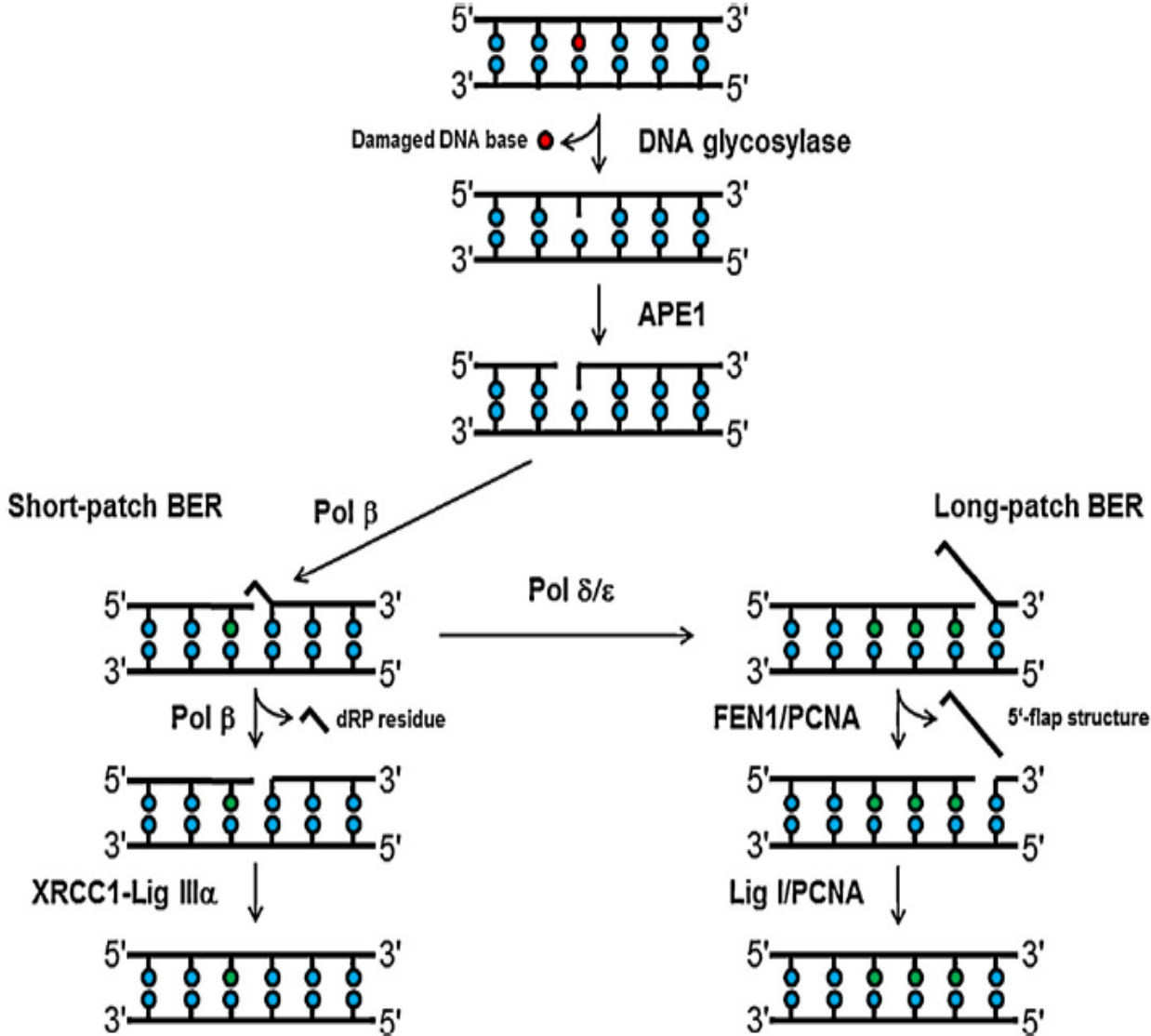
DNA SSBs arise from DNA insults either within the intracellular environment (e.g. ROS) or from extracellular agents. Collectively, this variety of damaging agents gives rise to direct SSBs or indirect SSBs. In the latter scenario SSBs are intermediates produced during the repair of damaged bases, which are first dealt with by the base excision repair (BER) or nucleotide excision repair (NER) pathway ¹⁸⁻²⁰. In the case of direct SSBs, the insult to DNA causes direct loss of nucleotides (gaps) and / or damage to the sugar phosphate backbone of the DNA without base loss (nicks). In either scenario (direct and indirect SSBs), the repair is relayed through the SSBR core machinery. The following section will briefly describe the current understanding for the mechanisms regulating BER/SSBR.

The current model for DNA BER/SSBR

Damage to DNA bases is one of the most frequently encountered classes of DNA lesions. Different insults to DNA can result in alkylation, deamination and oxidative reactions that directly damage DNA bases (purines and pyrimidines) ^{20,21}. If not recognized and removed by damaged base specific enzymes, known as DNA glycosylases ²², the damaged bases could result in transition ²³ and transversion ²⁴ mutations.

Biochemically, canonical BER (outlined in **Figure 2**) is orchestrated via four distinct steps and a “passing the baton” model has been proposed to be the operational mechanism for the process. First, the damaged base is recognized by a DNA glycosylase producing an abasic site (AP site). Then, depending on the type of the DNA glycosylase involved, the damaged DNA strand, containing the AP site, is incised by apurinic/apyrimidinic endonuclease 1 (APE1). Subsequently, gap filling and nick sealing are carried out by a DNA polymerase and ligase, respectively ²⁵.

Figure 2: Outline of BER-SSBR pathway

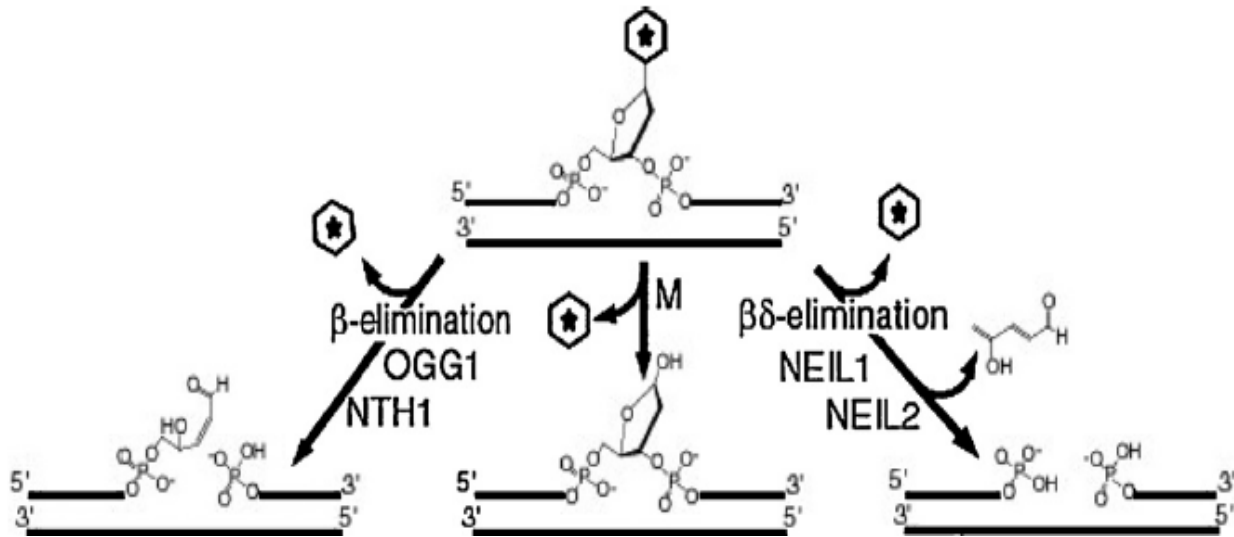


The BER pathway. BER is initiated by a damage-specific DNA glycosylase that excises the damaged base to create an abasic site. This is incised by APE1 to create a DNA SSB harbouring a 5'-deoxyribose phosphate (5'-dRP) residue. Pol β removes the 5'-dRP moiety and also adds a single nucleotide into the one-nucleotide gap. Finally, XRCC1–Lig III complex seals the remaining DNA ends to complete the short-patch BER pathway (left branch). However, if the 5'-dRP is resistant to cleavage by Pol β , then Pol δ/ϵ adds 2–8 more nucleotides into the repair gap, generating a 5'-flap structure that is removed by FEN-1 in a PCNA-dependent manner. Lig I then seals the remaining DNA ends to complete the long-patch BER pathway (right branch). **DNA Repair (Amst). 2013 May 1;12(5):326-33.**

Reproduced with permission from Elsevier. Copyright © 2013

DNA glycosylases scan the DNA for damaged bases. When detected, the repair glycosylase flips the damaged base into the active site pocket and then catalyzes its removal²². This mechanism is carried out by both mono- and bifunctional glycosylases. The latter cleave the DNA backbone via an additional 3' AP lyase activity, which catalyzes either β - or $\beta\delta$ -elimination reactions yielding replication and ligation blocking lesions, 3' α,β unsaturated aldehyde (3'-PUA), or 3'-P respectively (illustrated in **Figure 3**). Due to differences in substrate affinities among end processors, the type of damaged 3' end dictates which end processor is to be involved (see **Figure 4** for illustration of different damaged ends and dedicated end processors). Usually, APE1 catalyzes the removal of 3'-PUA whereas 3'-P ends are removed by PNKP⁹. The strand incision activity of APE1 results in the formation of 5' deoxyribose phosphate (5'dRP) termini, which are removed via the 5'dRPase action of DNA Pol β ²⁶ restoring the 5'P.

Figure 3: Illustration of different modes of damaged base elimination by mono- and bi-functional DNA glycosylases

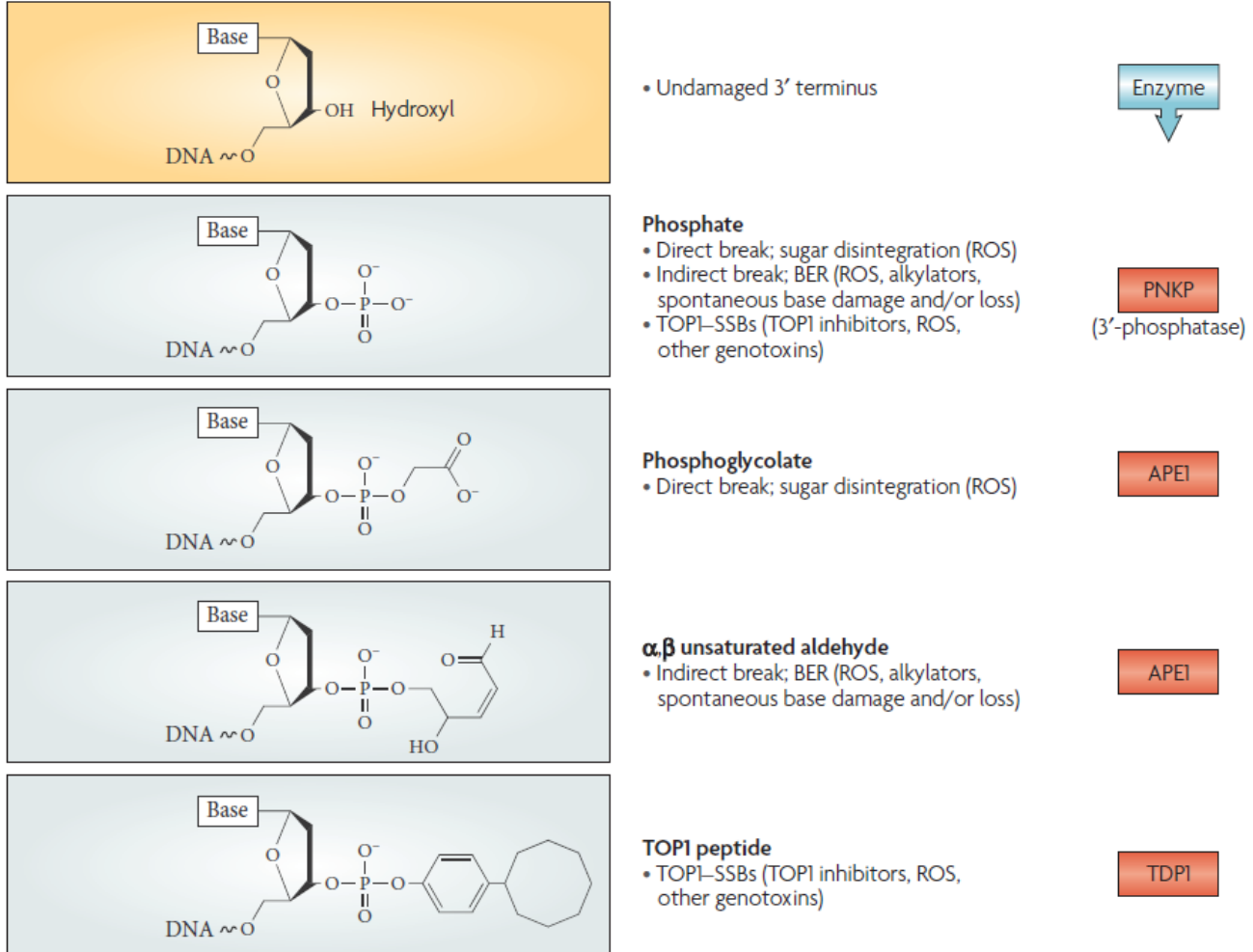


Mono- and bi-functional glycosylases and elimination reactions. In the case of mono-functional glycosylases (middle) e.g. Uracil-DNA Glycosylase (UDG), the glycosylase removes the base without incising the DNA backbone (i.e. no additional AP lyase activity); hence the AP site is cleaved by APE1 (text for details). On the other hand, bi-functional glycosylases possess an additional AP lyase activity e.g., OGG1 and NEIL1, cleaving the DNA backbone after removal of damaged base. The elimination reaction can proceed either via β -elimination e.g. OGG1 leaving a 3'-PUA which is a substrate for APE1 or via $\beta\delta$ -elimination e.g. NEIL1 resulting in a 3'-P end that is processed by PNKP. **DNA Repair 6 (2007) 470–480**

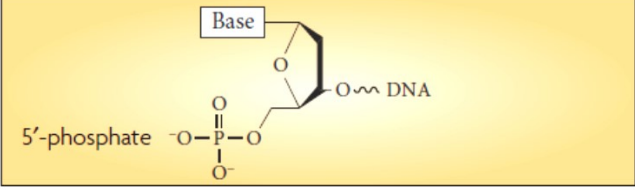
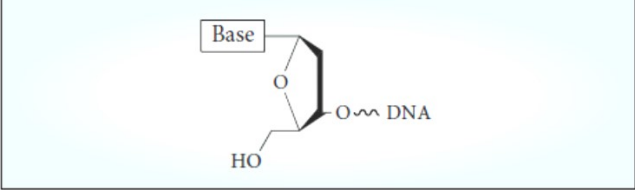
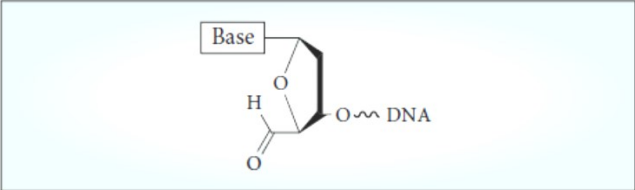
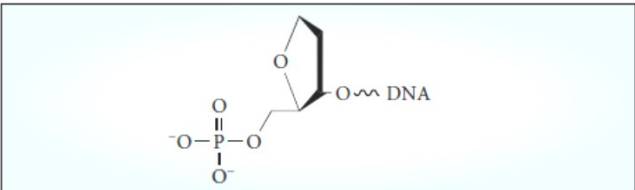
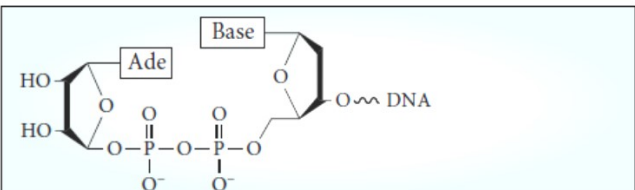
Reproduced with permission from Elsevier. Copyright © 2007

Figure 4: Different types of damaged 3' and 5' ends and specific end processor enzyme

a Types of damaged 3' termini



b Types of damaged 5' termini

	<ul style="list-style-type: none"> • Undamaged 5' terminus 	<div style="border: 1px solid black; background-color: #ADD8E6; padding: 2px; text-align: center;">Enzyme</div> <div style="text-align: center;">↓</div>
	<p>5'-hydroxyl</p> <ul style="list-style-type: none"> • TOP1-SSBs (TOP1 inhibitors, ROS, other genotoxins) 	<div style="border: 1px solid black; background-color: #FF8C00; padding: 2px; text-align: center;">PNKP (5'-kinase)</div>
	<p>5'-aldehyde</p> <ul style="list-style-type: none"> • Direct break; sugar disintegration (ROS) 	<div style="border: 1px solid black; background-color: #FF8C00; padding: 2px; text-align: center;">?</div>
	<p>5'-dRP (AP site)</p> <ul style="list-style-type: none"> • Indirect break; BER (ROS, alkylators, spontaneous base damage and/or loss) • Following ROS, this damage can be an oxidized dRP that might require LPR for removal 	<div style="border: 1px solid black; background-color: #FF8C00; padding: 2px; text-align: center;">Pol β</div>
	<p>5'-AMP</p> <ul style="list-style-type: none"> • Abortive ligase activity (can form at breaks with 5'-P) 	<div style="border: 1px solid black; background-color: #FF8C00; padding: 2px; text-align: center;">APTX</div>

Common types of damaged SSB termini and the enzymes that process them. For each type of SSB the mechanism of damage is summarized, with the causative agent(s) in parentheses. Ade, aldehyde: AP, apurinic/aprimidinic; APE1, AP endonuclease I; APTX, aprataxin; BER, base-excision repair; dRP, 5'-deoxyribose phosphate; FEN1, flap endonuclease 1; LPR, long-patch repair; P, phosphate; PNKP, polynucleotide kinase 3'-phosphatase; Pol β, DNA polymerase β; ROS, reactive oxygen species; TDP1, tyrosyl-DNA phosphodiesterase 1; TOP1, topoisomerase 1. **Nature Reviews Genetics, (2008), Vol 9, (619-631)**

Reproduced with permission from NPG. Copyright © 2008

After removal of the damaged bases, indirect SSBs are handed over to the operational machinery of SSBR and thereby dealt with in the same manner as direct SSB. Two sub pathways have been identified for SSBR/BER, namely, short patch (0-2 nt) BER (SP-BER) and long patch (2-14 nt) BER (LP-BER) (**Figure 2**)^{13,19,27}.

For SP-BER, end processing following damage allows for subsequent gap filling and ligation by DNA pol β and LIG3 respectively. XRCC1 is an integral scaffold protein that is required for optimal function and accumulation of other SP-BER proteins²⁶.

On the other hand LP-BER can be initiated by strand displacement activity of DNA Pol β , which results in having a flap of DNA. Alternatively, the pathway can utilize replication machinery proteins to accomplish repair. In this case, the loading platform, PCNA, is recruited. Then replicative DNA polymerases δ/ϵ catalyze gap filling, which results in the formation of a 5' flap structure. Flap endonuclease 1 (FEN1) is recruited and stimulated by PCNA and then cleaves the displaced patch. Finally DNA ligase 1 (LIG1) carries out nick sealing¹⁹.

SP-BER and LP-BER are not necessarily mutually exclusive processes. We and others²⁸⁻³⁰ observed that SP-BER repair proteins, XRCC1, LIG3 and Pol β accumulate at DNA damage sites more rapidly than the LP-BER scaffold PCNA, suggesting either SP-BER proteins are involved in the regulation of LP-BER, or LP-BER is activated downstream of SP-BER in response to certain types of damage. Both scenarios are likely to be true. Indeed PCNA recruitment to sites of DNA damage was shown to require XRCC1²⁸. Additionally, a role for XRCC1-LIG3 complex in regulating pathway choice between SP- and LP-BER has been postulated depending on the local ATP concentration at repair

sites ³¹. More importantly, the type of damage dictates the repair pathway. In many cases, after the accumulation of SP-BER at damage sites, 5' ends that are resistant to DNA pol β 5'dRPase activity, such as oxidised 5'dRP, results in strand displacement by DNA pol β and subsequently repair progresses via LP-BER. Notably, several lines of evidence support the hypothesis that the cell cycle phase is a determinant for repair progression via SP- or LP-BER ²⁷, with SP-BER being active throughout the cell cycle, while LP-BER is primarily active during S-phase owing to the proximity of the replication machinery.

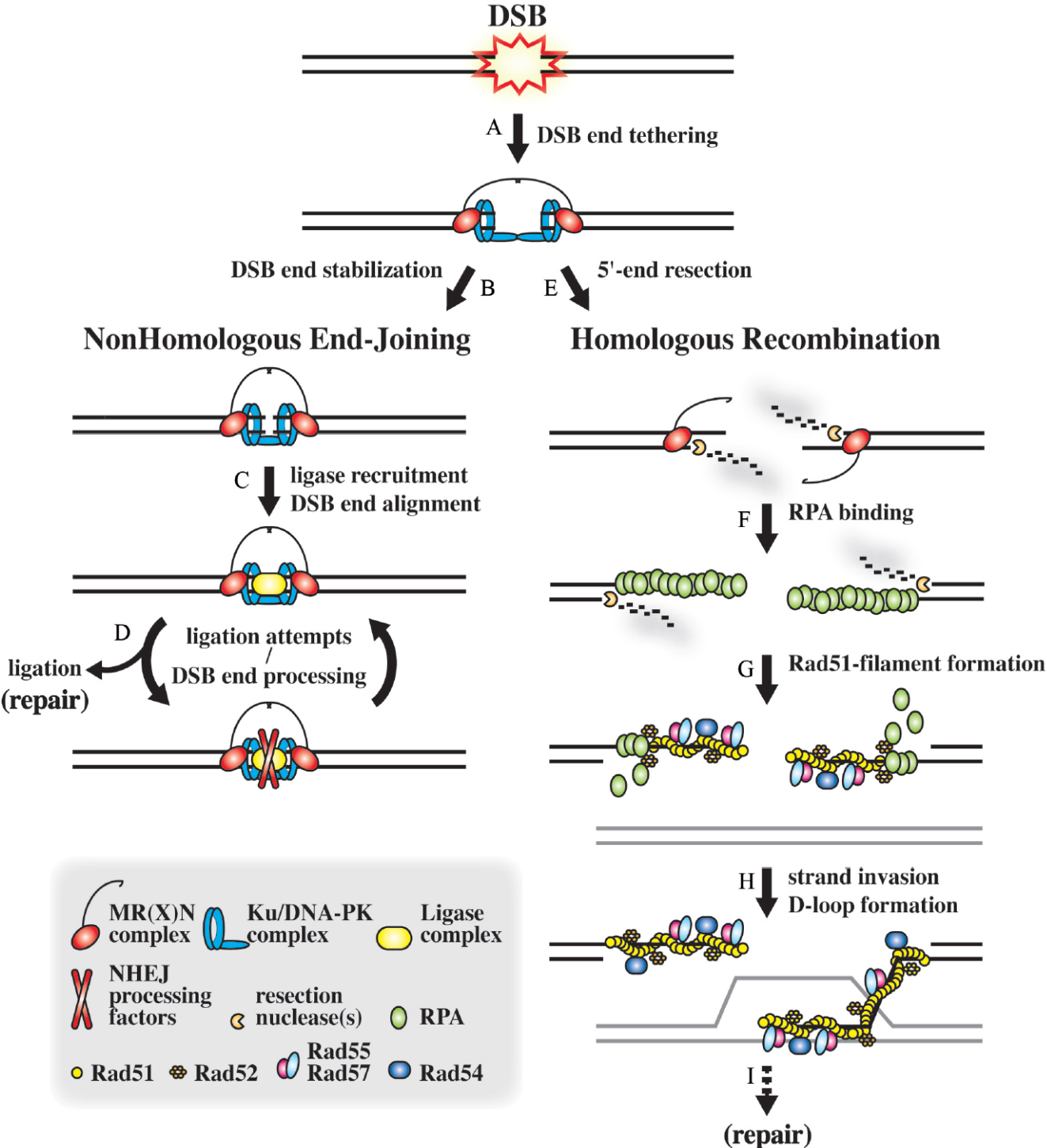
On the other hand several roles for the important DNA strand break sensor, PARP1 ³², in BER/SSBR have been proposed and will be discussed later on.

DNA DSB: importance and pathways involved

DSBs arise when two breaks in the double strand of DNA occur simultaneously within 10-20 bp. DSBs are the most deleterious type of DNA damage. If left unrepaired, DSBs result in either cell death, even from a single DSB³³, or mutagenicity via chromosomal rearrangements and translocations³⁴, and therefore, unrepaired DSBs have been implicated in driving carcinogenesis³⁵. As with other forms of DNA damage, DSBs arise in cells from intracellular and extracellular agents. Importantly, DSBs occur naturally in cells via programmed events associated with meiosis³⁶ and Immunoglobulin antigen receptor diversity generation via “V(D)J” recombination^{37 38}.

Two major pathways, with different founding operational principles, repair DNA DSBs, namely, homologous recombination (HR) and non-homologous end joining (NHEJ) (outlined in **Figure 5**). In HR, a template from a homologous strand of DNA, usually from a sister chromatid, is used in the repair of damaged DNA, thereby ensuring high fidelity and accuracy of repair. Accordingly, HR has been widely accepted to be an “*error free*” process. On the other hand, NHEJ involves re-ligation of the ends of broken DNA, which, depending on the nature of the DSB, might require extensive processing to render them ligatable. Therefore, NHEJ bears the possibility of being “*error prone*”. The two pathways are not mutually exclusive, while NHEJ is active throughout all phases of cell cycle, HR is mainly active during late S/G2 phases due to the requirement of a proximal intact sister chromatid to complete the repair.

Figure 5: Illustration of repair of DSBs by NHEJ (left) and HR (right)



Model of DSB repair by NHEJ and HR pathways. DNA undergoing a DSB and the homologous template used for repair are respectively represented by a close pair of black and grey lines. (A) DSB ends are tethered by MR(X)N and Ku/DNA-PK complexes. (B) In NHEJ, DSB ends are further stabilized by MR(X)N and Ku/DNA-PK. (C) MR(X)N and Ku/DNA-PK recruit the ligase complex and DSB ends are aligned. (D) DSB ends are ligated or are processed prior to ligation (repair). (E) In HR, 5' DSB ends are resected by MR(X)N and other nucleases. (F) RPA binds to single-stranded overhangs generated by resection. (G) RPA-coated single-stranded DNA is a substrate for Rad51-filament formation, involving Rad52, Rad55-Rad57 and Rad54. (H) Rad51-filament homology search and strand invasion lead to the formation of a D-loop. (I) From the D-loop, different HR pathways can result in DSB repair. MRX is the yeast orthologue of human MRN complex, where X denotes XRS2 protein, the yeast functional homologue for human NBS1. **Cell. Mol. Life Sci. 66 (2009) 1039 – 1056**

Reproduced with permission from SpringerLink. Copyright © 2009

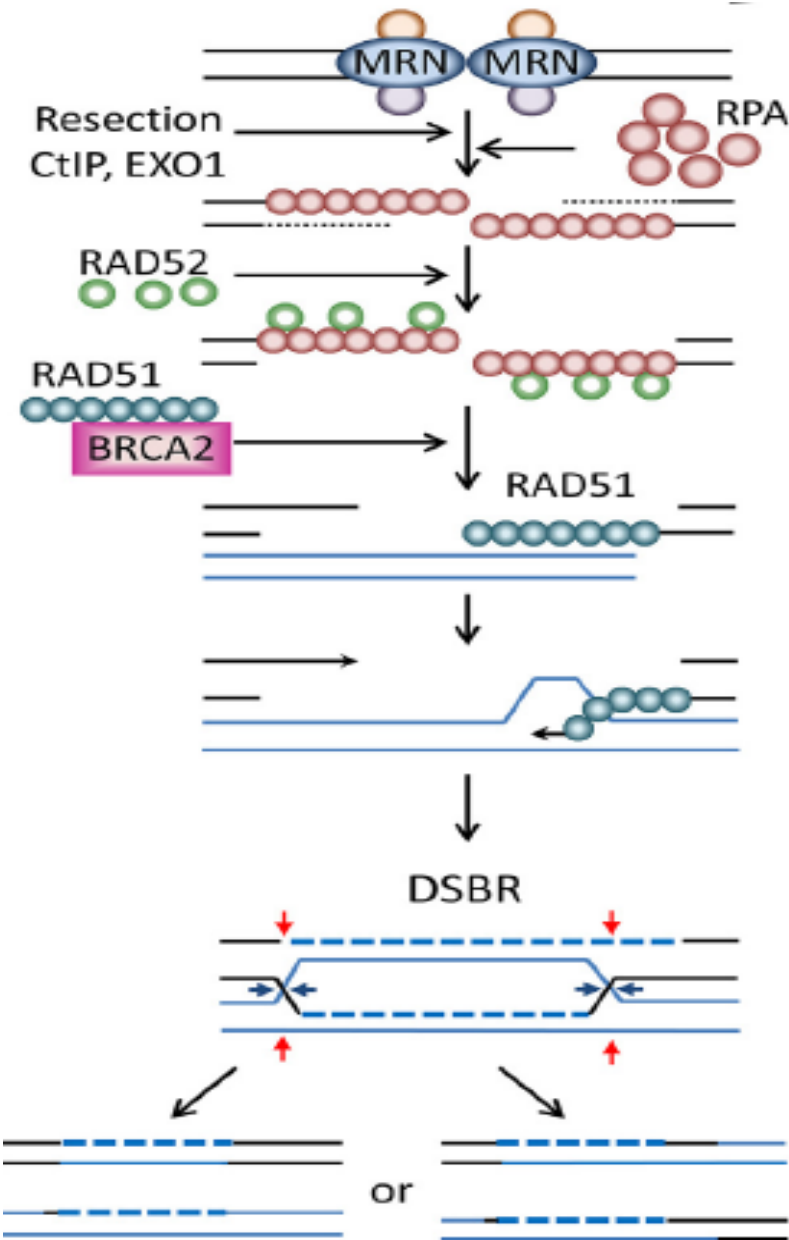
Homologous Recombination (HR)

In order to resynthesize damaged DNA with a DSB lesion using a sister chromatid template, the generation of ssDNA with 3' overhangs is required to facilitate the search for homologous sequences. Accordingly, end resection activities are pivotal to the process. Several steps coordinate DSBR by HR (outlined in **Figure 6**)³⁹⁻⁴¹. Usually, DSBs are detected and bound by the MRE11-RAD50-NBS1 (MRN) complex that recruits the protein kinase, ataxia telangiectasia mutated (ATM), which, upon binding to the MRN complex, becomes activated via auto-phosphorylation and further phosphorylates downstream proteins to facilitate amplifying the cascade. One of the key proteins phosphorylated by ATM is the histone protein H2AX, which is phosphorylated at serine 139. . Phosphorylated H2AX (γ H2AX) is recognized by mediator of DNA damage checkpoint 1 (MDC1) protein, which in turn recruits further MRN complexes, resulting in subsequent iterations of ATM recruitment and activation with H2AX phosphorylation, loading further MDC1, hence a feedback loop is generated. This ultimately leads to γ H2AX spanning up to 1Mbp surrounding the damage site, thereby amplifying the damage response^{42,43}. γ H2AX serves as a signal to help recruit and assemble DSBR proteins into subnuclear repair bodies, commonly detected microscopically as ionizing radiation induced foci (IRIF)⁴⁴. In HR, the step that follows DSB sensing is DNA end resection in which MRE11 (3'-5' exonuclease), and the yeast Sae1 (5'-3' exonuclease) orthologue, C-terminal binding protein interacting protein (CtIP), are initially activated followed by further end resection activity of enzymes like exonuclease 1 (EXO1) (5'-3' exonuclease) to generate ssDNA with 3' overhangs. Subsequently, the resected product, ssDNA of 3' overhangs, is stabilized and protected

against further damage by replication protein A (RPA). To initiate the search for homologous DNA sequences, the recombinase RAD51 coats the ssDNA by displacing RPA, a process that is facilitated by RAD52⁴⁵, breast cancer associated gene 2 (BRCA2)⁴⁶ and breast cancer associated gene 1 (BRCA1)⁴⁴ to help form the characteristic RAD51 nucleoprotein filament⁴⁷. The RAD51 nucleoprotein filament catalyzes the homology search, strand invasion, and exchange. Subsequently, the DNA repair synthesis is carried out by DNA polymerases, usually pol η ⁴⁸. A resultant repair intermediate in HR following strand invasion, exchange and resynthesis is a heteroduplex loop (D-loop) which is resolved by different mechanisms³⁹.

BRCA1 is an important scaffold protein that binds and interacts with several proteins involved in different steps of HR regulation⁴⁴. Since NHEJ is active throughout the cell cycle, in late S/G2 phases the commitment of cellular machinery to HR is important to ensure accurate repair. Therefore the repair pathway choice in DSB repair is thought to be a function of cell cycle phase as well as interplay between different proteins at the damage site such as BRCA1 and p53 binding protein 1 (53BP1)^{40,49}.

Figure 6: Outline of basic steps for DSBR via Homologous Recombination



The key steps in the repair of a DSB by homologous recombination. HR has been proposed to be initiated by recognition of the DSB by the MRN complex (MRE11-

RAD50-NBS1). The MRN complex associates with CtIP, which initiates 5'-3' end resection to create the 3' ssDNA overhang. Further resection is carried out by exonucleases (possibly EXO1), and the resulting ssDNA is stabilized by binding of RPA. RAD52 is recruited to RPA. The RAD51-BRCA2 complex then replaces the RAD52-RPA complex to form RAD51 nucleoprotein filaments, whereas, in SSA, RPA and RAD52 carry out the recombination process in a RAD51-independent manner. RAD51-coated ssDNA enables strand invasion of the intact homologous DNA region. In classic DSBR, the second DSB end can be captured by the D-loop to form an intermediate with double Holliday junctions, which can result in a non-crossover (cleavage at blue arrows) or a crossover (cleavage at blue arrows on one side and red arrows on other side) products. **DNA Repair 12 (2013) 620– 636**

Reproduced with permission from Elsevier. Copyright © 2013

Non-Homologous End Joining (NHEJ)

Being active throughout the cell cycle, NHEJ is considered to be the major DSB repair pathway in mammalian cells ³⁴. Two main NHEJ sub-pathways have been identified, classical NHEJ (cNHEJ) and alternative NHEJ (aNHEJ) ⁵⁰. In this section we will discuss the regulation of cNHEJ and will shed light on the aNHEJ later on.

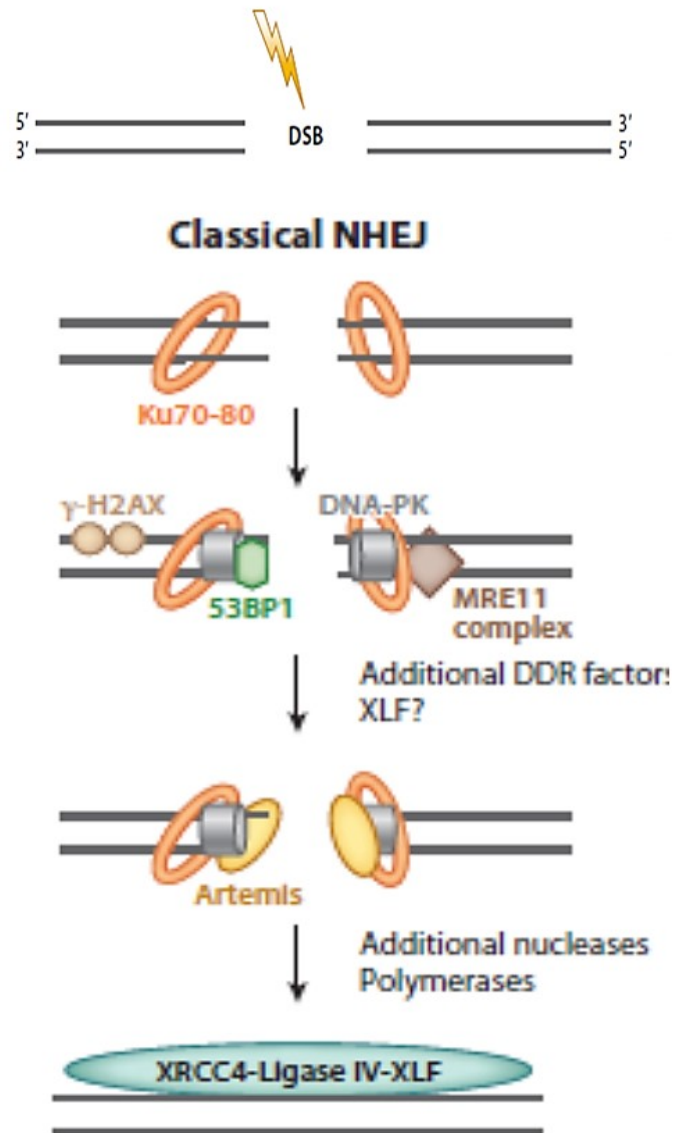
In contrast to HR, NHEJ does not require a homologous template for repair; rather, NHEJ involves direct religation of broken ends. cNHEJ (illustrated in **Figure 7**) can be biochemically reconstituted by phylogenetically conserved (yeast to mammalian cells) core machinery proteins involving, Ku70/80 heterodimer, DNA protein kinase catalytic subunit (DNA-PKcs), and the DNA ligase complex comprised of X-ray cross complementing protein 4 - DNA ligase 4 (XRCC4-LIG4) and XRCC4 like factor (XLF) ⁵¹. One of the earliest proteins in cNHEJ that binds and senses the DSB is the Ku 70/80 heterodimer. Ku binds to different dsDNA substrates with very high affinity, and in a fashion that mimics proliferating cell nuclear antigen (PCNA), it fully encircles the DNA and slides inwards across the DNA for about 1 helical turn after loading DNA-PKcs. The tethering and sliding actions of Ku are important to help avoid straying of DNA ends surrounding the break and subsequently load downstream repair proteins ⁵².

Biochemically, the order of recruitment of downstream repair factors is highly variable since Ku bound to DNA can bind different downstream cNHEJ proteins in a nonspecific order ⁵³. Based on studies showing that DNA-PKcs is required for the efficient accumulation and activation of other cNHEJ proteins at sites of damage ⁵⁴⁻⁵⁶, a current consensus is that Ku recruits and loads DNA-PKcs and the interaction of the latter with

Ku:DNA complex results in activation of its protein kinase activity leading to autophosphorylation and phosphorylation of other NHEJ proteins, including Artemis, XRCC4, LIG4 and XLF⁵⁷. These phosphorylation events are functionally significant for the progression of cNHEJ^{57,58}. Following the formation of the DNA-PK holoenzyme (Ku heterodimer and DNA-PKcs), end processing and gap filling ensue to accomplish repair⁵². The end processing is important to render damaged DNA ends ligatable. The first enzyme involved in the process is Artemis⁵⁹, then other end processors, e.g. PNKP, follow⁶⁰. Finally, gap filling and ligation occur via the stepwise actions of DNA polymerases μ and λ ⁵² and the resultant nicks are sealed by DNA ligase complex.

One of the key cNHEJ mediators is 53BP1. It is recruited to DSBs via the interactions of its domains (BRCT domains, Tudor domain and Ubiquitylation dependent recruitment (UDR) domain) with phosphorylated MDC1 and combination of histone codes, mainly methylation and ubiquitylation⁶¹. Similar to a role of BRCA1 in promoting HR, 53BP1 plays a pivotal role in cellular commitment to cNHEJ. First, it stabilizes DNA ends across DSBs to avoid their straying and allow subsequent ligation⁴⁰. Second, it inhibits DNA resection activities of the nucleases that are required for HR and aNHEJ, therefore it stabilizes the binding of Ku to DSB ends thus promoting cNHEJ⁴⁰.

Figure 7: Outline of DSBR via NHEJ



Outline of DSBR by NHEJ DNA DSB is detected by the Ku heterodimer which subsequently binds the ends of the lesion, tethering them together. The exact mechanism by which Ku heterodimer is recruited to DSB is unknown, suggesting that the heterodimer is recruited independent of other known DSB factors. Following, Ku moves inwards, allowing recruitment and loading of DNA-PKcs at the DSB site.

Altogether the Ku heterodimer and DNA-PKcs form the DNA-PK holoenzyme complex which triggers autophosphorylation of DNA-PKcs in addition to phosphorylation of other downstream NHEJ proteins that are substrates to DNA-PKcs. Finally, DSB end processing, gap filling and ligation occur as described in text. **Annu. Rev. Genet. 2013. 47:433–55**

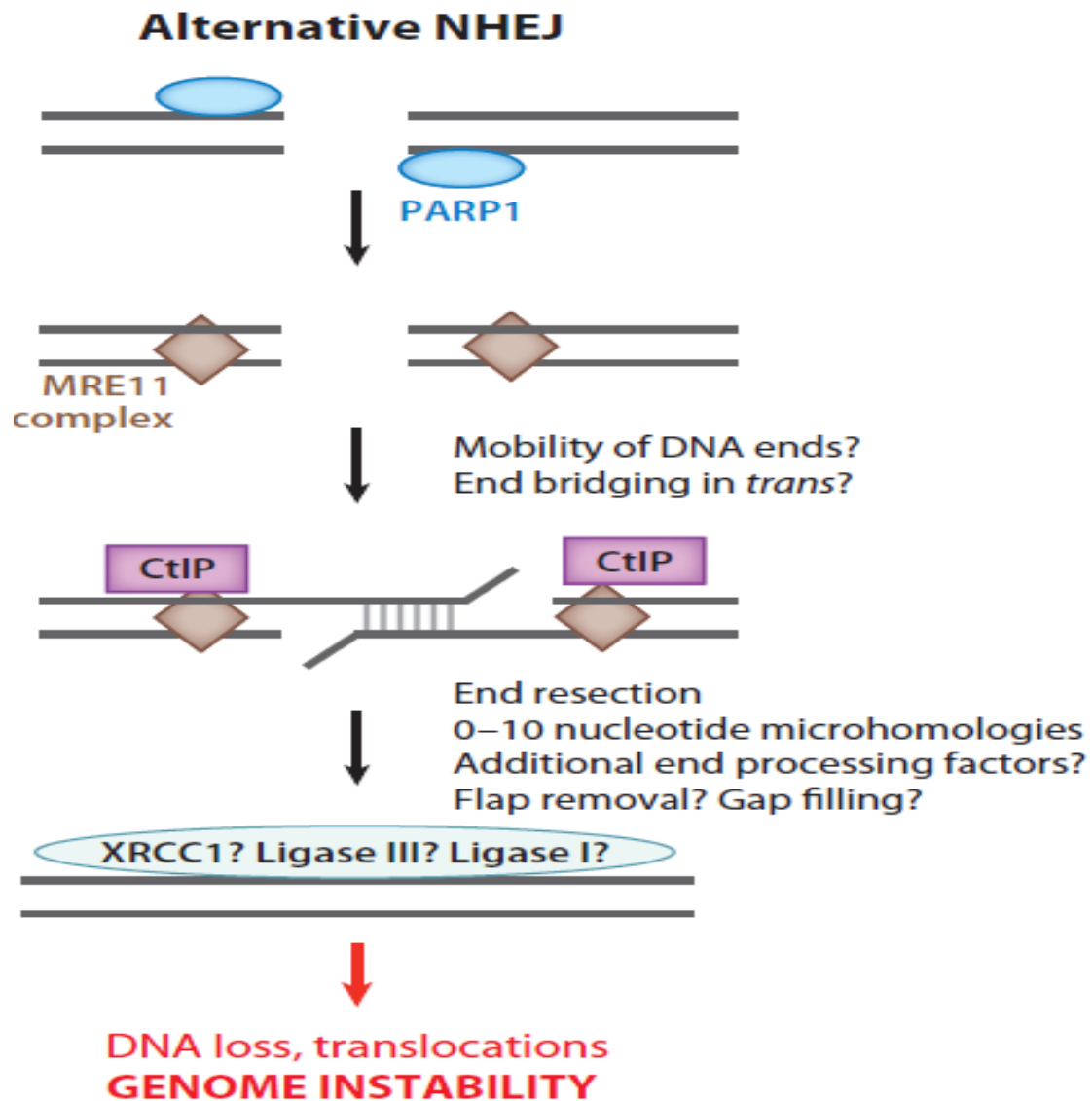
Reproduced with permission from Annual Reviews. Copyright © 2013

The DNA DSB-SSBR alliance for repair: aNHEJ

Cross talk between different DDR pathways exists in order to provide fail safe mechanisms for the repair of different lesions, especially those arising from extracellular insults to DNA^{62,63}. A recently discovered backup mechanism for DSB in cells lacking cNHEJ components is aNHEJ (outlined in **Figure 8**)^{64,65}. Several studies have identified key proteins required for repair via this pathway^{52,66,67}. Mainly HR and SSBR proteins, PARP1, MRE11, CtIP, LIG3 and LIG1^{40,52,67} are the candidate components in aNHEJ. Although LIG3 and XRCC1 form a biochemically stable complex⁶⁸, a controversial role for XRCC1 in aNHEJ has been proposed^{69,70}. Due to the characteristic features of repair junctions of aNHEJ (large deletions, insertions and microhomologies), a working model has been proposed. First, the DSB is recognized by PARP1, and a competition between PARP1 and Ku^{71,72} for the DSB has been proposed to be the rate limiting step to repair via aNHEJ⁷³. PARP1 function is required for MRN complex recruitment to sites of DNA damage⁷⁴ and may facilitate loading the complex along with CtIP to mediate end resection activities⁵² required for microhomology searching to further stabilize repair intermediates. Finally, the break is sealed by either LIG3 or LIG1⁶⁷. Paradoxically repair of DSBs via aNHEJ does not necessarily result in a favourable cellular outcome. aNHEJ has been proposed to be an important driver for chromosomal translocations that underlie several types of cancer

⁷⁵.

Figure 8: proposed model for a-NHEJ



Proposed model for a-NHEJ. In a-NHEJ damage sensing is carried out by PARP1. Then DNA ends are tethered together by bridging action of MRN complex, following end resection ensues by CtIP to facilitate microhomology search. Finally, DNA ligases (LIG3/LIG1) carry out sealing the damage site. **Annu. Rev. Genet. 2013. 47:433–55**

Reproduced with permission from Annual Reviews. Copyright © 2013

Tools to study DNA repair, biochemical and cellular assays

Cellular survival assays after treatment with genotoxic agents are indicative of certain DNA repair defects depending on the nature of damage introduced by the agent. Examples of genotoxins that have been widely used include hydrogen peroxide, which introduces SSBs (gaps and nicks) and oxidative base damage via ROS generation ^{76,77}; IR, which also introduces SSBs as well as DSBs in a ratio of 1:25 (DSBs : SSBs) per gray ⁷⁸; alkylating agents e.g. methyl methanesulfonate (MMS) that introduce alkylation base damage ⁷⁹, UV and cisplatin that damage DNA via formation of bulky lesions such as photo-dimerization and intra-strand crosslinks respectively ²; and the chemotherapeutic topoisomerase 1 and 2 poisons ^{80,81} that result in the formation of SSBs and DSBs respectively.

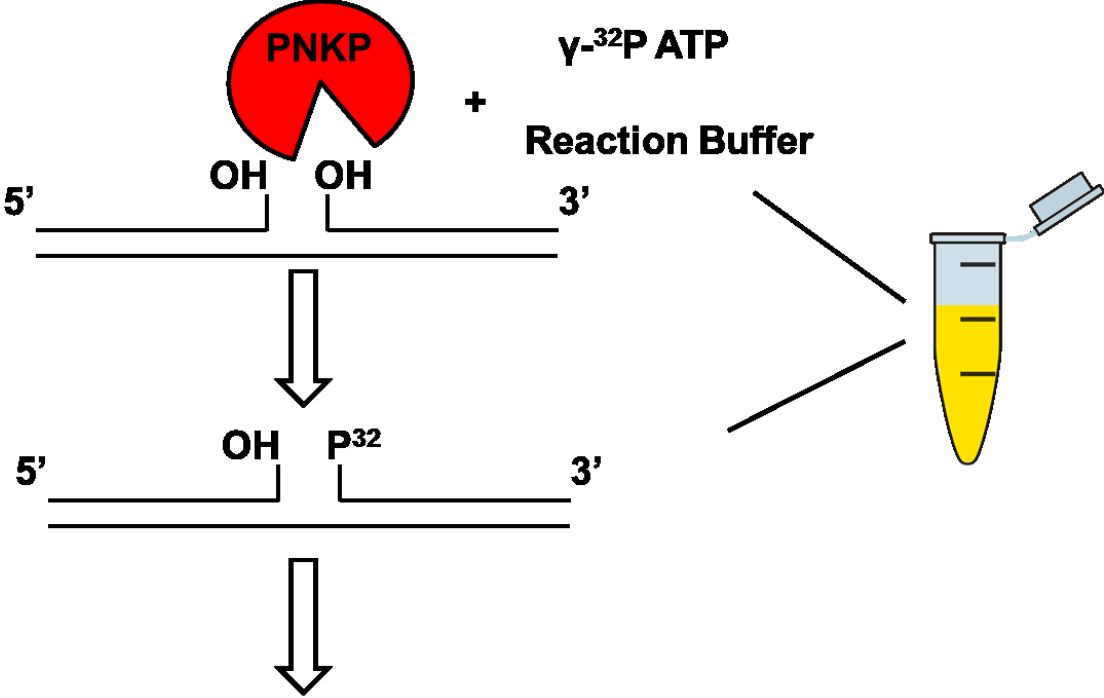
In spite of the pivotal role of cellular survival assays in unravelling DNA repair defects, an inherent drawback in the assays is the lack of mechanistic information about DNA repair mechanisms. This has been complemented by two fundamental approaches, namely biochemical *in vitro* reconstitution assays and live cell imaging techniques. Both have significantly contributed to our current understanding for the orchestration of DNA repair ⁸².

Biochemical assays involve reconstitution of repair reactions or complete pathways by incubation of damage containing DNA substrates with candidate repair protein(s) then analysing repair efficiency often using gel electrophoresis. Examples of DNA repair pathways that have been reconstituted *in vitro* include cNHEJ ⁸³ and BER-SSBR ^{84,85}.

In our laboratory, we routinely employ two functional assays (outlined in **Figure 9**, kinase assay) to monitor variations in the dual DNA 5' kinase and 3' phosphatase activities of PNKP (i.e., kinase and phosphatase assays)⁸.

Importantly, biochemical assays lack the exact replication of the cellular chromatin milieu and post-translational modifications to DNA repair proteins occurring in response to damage. Therefore, the use of live cell microscopy techniques has become an integral tool to elucidate DDR in real time within the cellular environment.

Figure 9: Outline of PNKP kinase assay



Run on gel and detected by autoradiography

Laser micro-irradiation (μ IR) and fluorescence recovery after photobleaching

(FRAP)

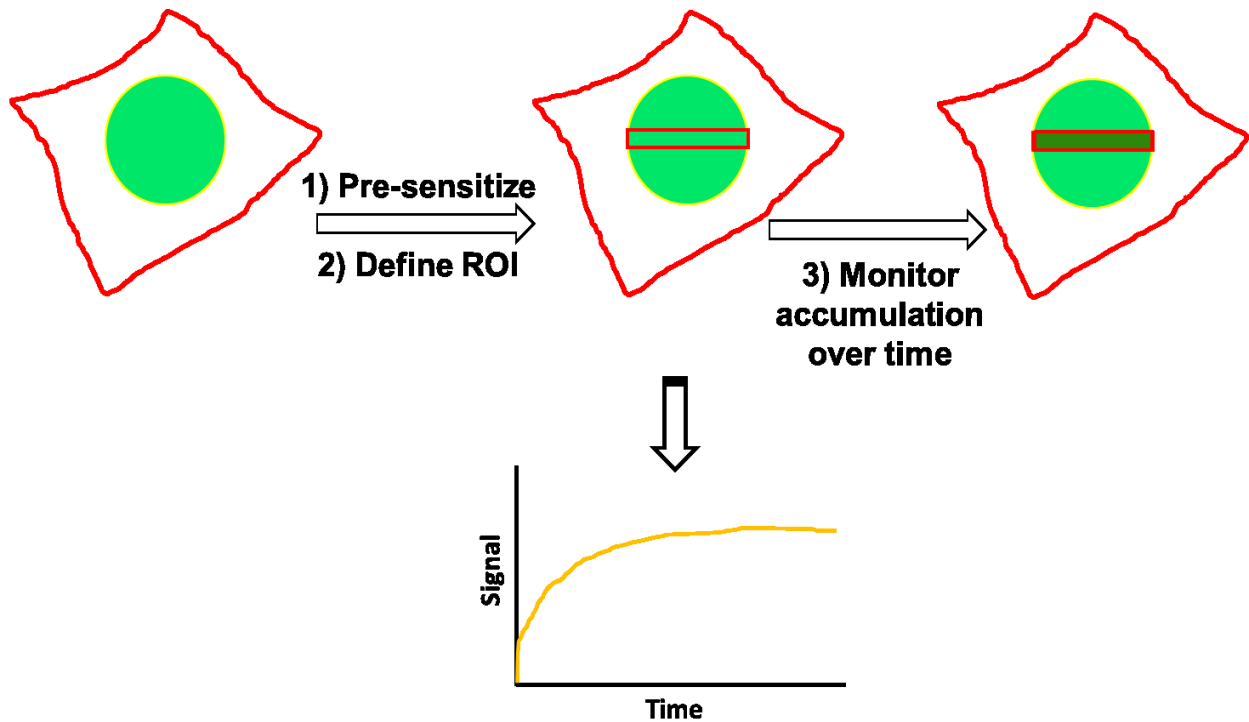
Early studies by Cremer et al. ^{86,87} provided the foundation for recent advances in microscopy to be integrated into the visualization of DNA lesions and monitoring kinetics and dynamics of repair proteins at damage sites ⁸⁸. The two live cell microscopy techniques that are commonly employed in DNA repair studies are laser μ IR and FRAP.

In laser μ IR (outlined in **Figure 10**) a pre-defined sub-micrometer region of the cell, usually within the nucleus, is irradiated with a laser beam to generate DNA damage at a defined site. The technique can be combined with either indirect immunofluorescence or time-lapse microscopy to monitor and quantify accumulation of an endogenous protein (indirect immunofluorescence) or a fluorescently tagged version (time-lapse microscopy) of the protein of interest. One advantage of time-lapse microscopy is the possibility of monitoring very early events (fraction of a second) in DDR, which due to practical considerations, cannot be followed by indirect immunofluorescence.

Laser μ IR has become the common standard for real time study of DDR. Importantly, different laser wavelengths and modes (single photon vs multi-photon) and the presence and type of photosensitizer used result in different forms of damage being generated in different proportions, hence protein responses vary from one laser μ IR setup to the other ^{89,90}. Therefore, careful consideration should be paid when interpreting results of such experiments and complementation with other biochemical and cellular assays is imperative.

Figure 10: Schematic representation of laser μ IR to study DDR in real time

Cell expressing fluorescent protein of interest



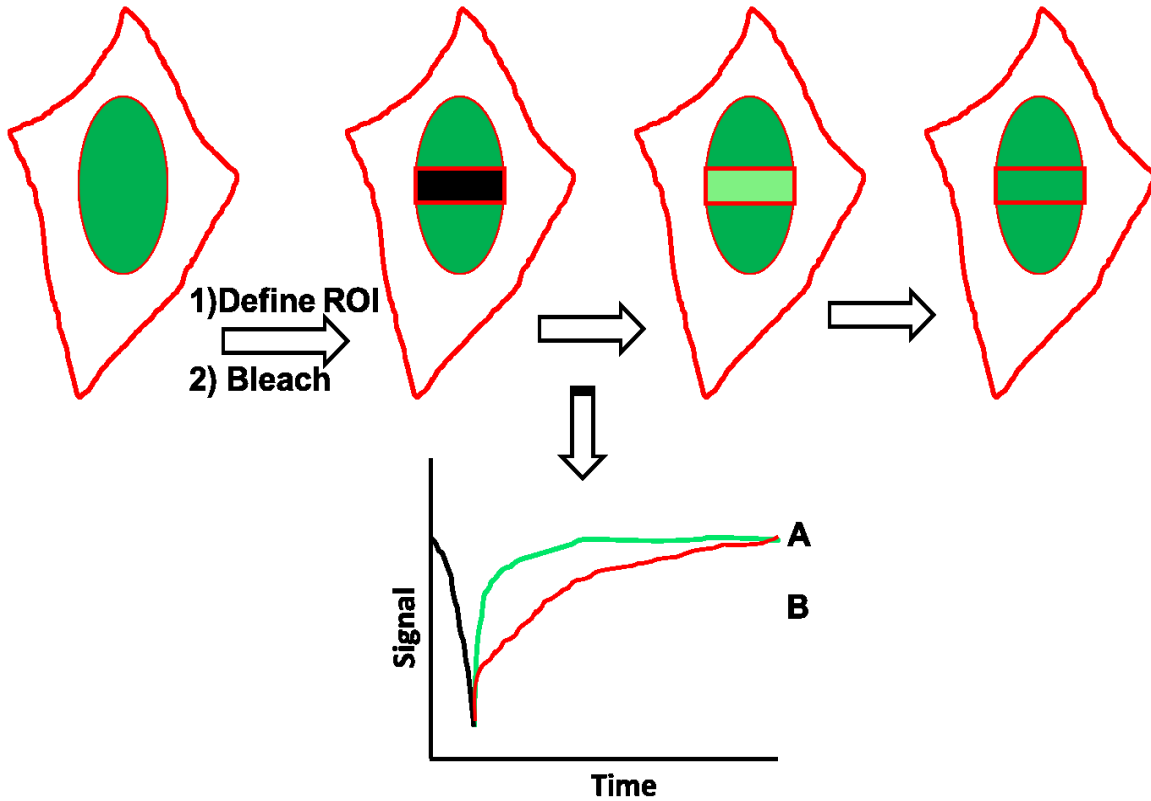
Outline of laser micro-irradiation. Cells expressing fluorescent tagged version of protein of interest are sensitized to laser induced damage using appropriate photosensitizer. A focused laser beam is introduced to region of interest (ROI). Accumulation of protein is monitored over time and signal quantification can be carried out. Alternatively, endogenous protein can be tested by indirect immunofluorescence.

The FRAP technique (outlined in **Figure 11**) was developed in the 1970's by Axelrod and co-workers⁹¹. Technically, FRAP experiments employ a similar setup to that of time-lapse microscopy with laser μ IR, where a pre-defined sub-micrometer region of a cell expressing a fluorescent tagged version of a protein of interest is irreversibly photobleached with the compatible laser line. Photobleaching involves the excitation of the fluorescent molecule to a triplet state where it loses its ability to cycle between excitation and emission phases⁹¹. Subsequently, the repopulation of the photobleached region by neighbouring fluorescent molecules termed '**recovery**' is monitored over time. Several factors contribute to the recovery of fluorescent proteins post photobleaching⁹¹⁻⁹³, including diffusion and binding of the fluorescent protein to other cellular macromolecules e.g. proteins and DNA. Therefore it is expected that if a protein binds to damaged DNA, its movement through the nucleus will slow, resulting in a slower recovery relative to the movement of the protein without damage.

Laser μ IR and FRAP can be combined in a single application in order to provide insights into the changes in recovery of proteins of interest in response to damaged and undamaged DNA within the same cell^{29,94}. Thus specific involvement for these proteins in DDR can be studied in real time using a fluorescence microscope.

Figure 11: Schematic representation of FRAP technique

Cell expressing fluorescent protein of interest



Outline of FRAP experiment. Two scenarios for recovery are shown. (A), green curve describes the kinetics of fast recovering protein which is indicative mainly of low binding events. (B), red curve describes the kinetics of slow recovering protein that mainly reflects tight binding events

Thesis Focus and working hypotheses

In the following chapters (3, 4 and 5), different aspects of the DDR that we addressed experimentally will be discussed. We focused on (i) sensing SSBs in live cells, (ii) impact of XRCC1 polymorphisms on its interaction with PNKP, and (iii) the possible interplay between different PNKP domains and PTMs and their potential effect on the behaviour of PNKP at sites of DNA damage, particularly DSBs.

1) How are SSBs detected? Current perspective

DNA damage sensing is essential to generate a signal for downstream proteins. In the case of indirect SSBs arising from damaged bases, the specific glycosylase fulfils the sensor role by scanning the DNA backbone. Upon detection of perturbed base pairing, the glycosylase cleaves the N-glycosidic bond leaving an abasic site. Repair ensues in 'passing the baton' fashion, where the lesion site is handed over from one repair protein to the other as previously described ⁹⁵⁻⁹⁷.

PARP1, the sensor revisited

In contrast to SSBs created during BER, evidence from biochemical and live cell imaging experiments has strongly suggested that PARP1 is the sole damage sensor for direct SSBs. PARP1 binds damaged DNA through its ZnF domains with very high affinity ⁹⁸. Upon binding damaged DNA substrates, PARP1 undergoes a conformational change and becomes activated to catalyze poly(ADP-ribose)ation, "PARylation", of several acceptor proteins including PARP1 itself, "auto-PARylation" ³². Based on the nature of the break, two models have been postulated for the fashion by which PARP1

binds the damage site and subsequent auto-PARylation occurs ⁹⁹. In the first model, PARP1 binds the damage site as a monomer where auto-PARylation occurs in cis ¹⁰⁰. Alternatively, PARP1 forms dimers at the DNA break where auto-PARylation occurs in trans ¹⁰¹. These models have been proposed based on the binding of the PARP1 DNA binding domain (DBD), which is composed of two ZnF domains (ZnF1 and ZnF2) and a nuclear localization signal, to a DNA substrate containing an SSB. Due to charge repulsion forces, the auto-PARylated PARP1 possesses a very low affinity to DNA, hence allowing for the disengagement of PARP1 from the damage site and facilitating loading of other repair proteins ¹⁰²⁻¹⁰⁴.

Early evidence that implicated PARP1 in the DDR was the finding that mice lacking PARP1 demonstrate extreme sensitivity to different DNA damaging agents including ionizing radiation and the DNA alkylating agent methylnitrosourea (MNU) ^{105,106}. Further studies supported PARP1 as a sensor for SSBs. We and others have shown in live cells that PARP1 accumulates very rapidly at sites of DNA damage ^{103,104,107}. Importantly, PARP1-mediated PARylation has been postulated to serve several roles in SSBR. In cells treated with hydrogen peroxide or subjected to laser μ IR, the accumulation of XRCC1 at sites of DNA damage was shown to be PARP1 dependent ^{103,104,108,109}. Consistently, cells treated with PARP inhibitor show reduced SSBR rates in response to treatment with ionizing radiation ¹⁰³. The XRCC1 recruitment to DNA damage sites is PARP1-dependent but this might be explained by the observation that DNA damage associated PARP1 PARylation allows for chromatin expansion and decondensation ^{110,111}, thus permitting the access of the SSBR scaffold protein XRCC1 to damage sites. Importantly, XRCC1 has been shown to accumulate with the same efficiency at sites of

DNA damage within the less compact chromatin compartment, euchromatin, and the more compact chromatin compartment, heterochromatin¹¹². Alternatively, PAR residues might serve as a scaffold to which SSB proteins bind and recognize the damage site. This is supported by the finding that both XRCC1 and LIG3 bind PAR *in vitro*^{113–115}. Additionally, PARP1 might be implicated in the repair of indirect SSBs, since PARP1 was found to interact with 8-oxoguanine DNA glycosylase (OGG1), and the auto-PAR-ylated PARP1 inhibits OGG1 activity¹¹⁶. This, in turn, might facilitate the handover of damaged DNA from OGG1 to downstream proteins thereby accelerating repair. Clinically, the sensor role of PARP1 in SSB has provided an explanation for why HR defective breast cancer cells are hypersensitive to PARP inhibitors alone^{117,118}. This observation serves as a paradigm for therapeutic use of synthetic lethality in which cells that are defective in a specific DNA repair pathway can be selectively killed by inhibiting another repair pathway without exposing cells to exogenous DNA damaging treatments. In this case, BRCA1/BRCA2 defective cancer cells, which have non-functioning HR, survive normally since SSB is still functioning. However, interfering with SSB sensing by treatment with PARP inhibitors leads to their conversion to DSBs, which, in a HR defective background are mainly funnelled through the error prone NHEJ¹¹⁹ resulting in lethal chromosomal rearrangements and cell death.

In contrast to the observations supporting the role of PARP1 as a SSB sensor, other experimental evidence exists to question this role. First, it was shown that PARP1 null mice repair UV and alkylating damage efficiently in a manner similar to wild-type counterparts¹²⁰. It is worth mentioning that in this study, PARP1 null mice displayed early delay in thymocyte recovery following ionizing radiation treatment, however the

recovery reached normal levels at later time points following irradiation ¹²⁰. Furthermore SSBs generated by treating plasmid DNA substrates with X-rays were repaired with the same efficiency by extracts derived from PARP1 null and wild-type cells ¹²¹. Similar results were observed in DNA substrates containing alkylation damage ¹²¹, lending further support that PARP1 is dispensable for BER/SSBR. Notably, in these studies, the absence of NAD in reactions using wild-type PARP1 extracts slowed the rate of repair in both scenarios (SSBs and alkylation damage) while not having an impact in experiments using PARP1 null extracts. This might provide an explanation for why SSBR is defective only with chemical inhibition of PARP1 and not with the absence of PARP1. Since PARP inhibitors work by competitive inhibition with the NAD substrate, in the presence of inhibitors, PARP1 cannot be auto-PAR-ylated and hence will remain bound to damaged DNA due its high affinity. This might impede access of core SSBR repair proteins (XRCC1-LIG3 complex, PNKP, pol β) and slow down repair. Strikingly, it was shown that PARP1 and XRCC1 are synthetically lethal as the chemical inhibition of PARP in cells devoid of XRCC1 (EM9 cells) led to cellular death in the absence of DNA damage ¹²². This finding shows that PARP1 and XRCC1 do not necessarily have epistatic roles in SSBR. Consistently, PARP inhibition and lack of XRCC1 had an additive effect on the retardation of SSBR ¹²² further disconnecting PARP1 from a required role in the core SSBR machinery. In live cells, treatment with PARP inhibitors did not affect the accumulation of core SSBR proteins XRCC1, pol β and PNKP, at sites of DNA damage ³⁰.

Collectively these observations add to our current understanding of SSBR in several ways. First, these observations highlight the possibility that despite the fact that PARP1

binds SSBs with high affinity, this binding might reflect a protective rather than a sensor role of PARP1 where PARP1 protects the damaged DNA from nucleases or their conversion to DSBs ¹²³. Hence PARP1 binding to SSBs might be a failsafe mechanism if the number of SSBs exceeds the saturation capacity of core SSBR proteins ¹⁸.

Second, care should be taken when interpreting the synthetic lethality between PARP1 and HR defective tumors. It should be noted that chemical inhibition of PARP1 locks the protein on SSBs rather than interfering with PARP1 as a sensor for SSBs, since different results were obtained by PARP1 depletion in HR defective backgrounds ¹¹⁷.

Third, these controversial observations regarding the role of PARP1 in SSBR suggest the existence of an alternative SSBR sensor in live cells.

LIG3, a candidate sensor in SSBR

PARP1 binds damaged DNA through its ZnF domain, which shows a substrate preference for gaps over nicks ^{98,124}. On the basis of *in vitro* experiments, Mackey et al. postulated that among the other SSBR proteins, LIG3 uniquely has a bona fide damage sensing module ascribed to its ZnF domain at the N-terminus that is homologous to that of PARP1 ¹²⁵. Additionally, the LIG3 ZnF, in contrast to that of PARP1, shows a substrate preference for nicks over gaps ¹²⁶. The latter study demonstrated that the ZnF domain of LIG3 cooperates with a downstream DNA binding domain (DBD) within LIG3 to comprise a nick sensing module. This module, together with another nick sensing module involving the catalytic core, orchestrates a dynamic switch between the initial nick sensing and the subsequent sealing events in a 'jack knife' fashion. However, these two studies were performed using the LIG3 β isoform and not the ubiquitously

expressed LIG3 α ^{126,127}. A notable difference between the two LIG3 isoforms, apart from the differences in expression patterns, is the interaction with XRCC1. It was shown that LIG3 α and not LIG3 β exists in a complex with XRCC1 and this interaction is required for LIG3 stability and optimal catalytic activity ^{68,127}.

Previous work alluded to the possibility of LIG3 being involved in early damage sensing steps of SSBR. Importantly, biochemical studies indicated that LIG3 inhibits PARP1 catalytic activity upon encountering DNase I treated DNA ¹²⁸, implying that the two proteins bind competitively at strand breaks. Consistent with the possibility of LIG3 being a damage sensor, it was shown that among the three different DNA ligases implicated in DNA damage responses, LIG3 shows a very rapid recruitment to sites of DNA damage introduced by laser micro-irradiation ¹²⁹. However an involvement of the LIG3 ZnF in damage sensing was not demonstrated in this study ¹²⁹. Based on these observations, we hypothesized a role for LIG3 in sensing SSBs.

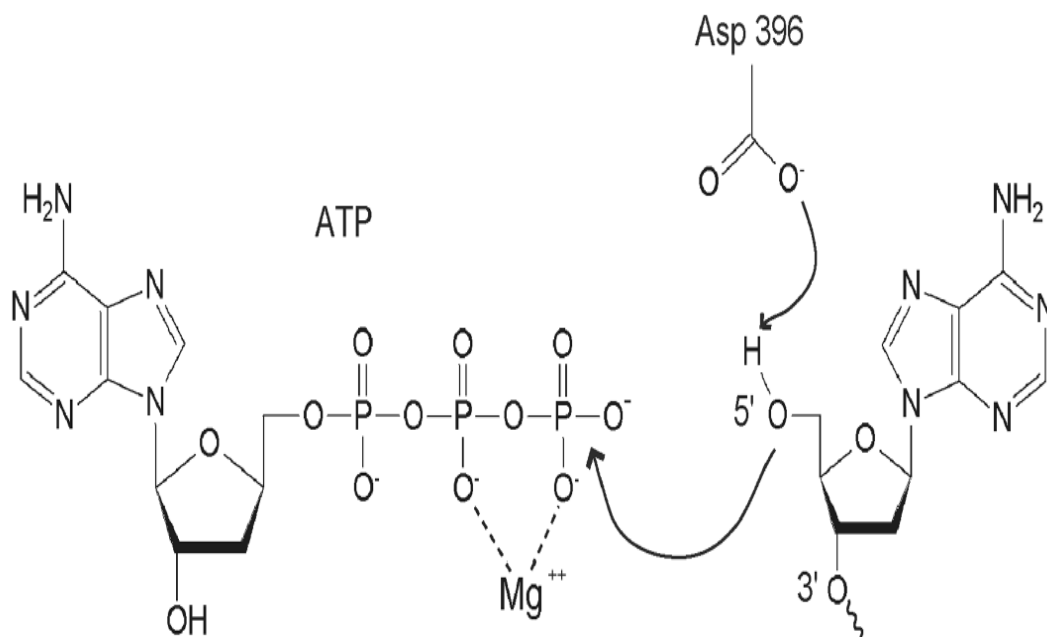
2) XRCC1 polymorphisms and links to cancer

Three XRCC1 SNPs have been positively associated with cancer risk for particular types of cancer in certain populations. These three sequence variants are located within the coding region of XRCC1, namely, R194W (rs1799782), R280H (rs25489) and R399Q (rs25487) ¹⁵. Evidence, albeit contradictory, from meta-analyses highlighted the association of these missense SNPs with tumorigenic potential ^{130–136} in breast, lung, and thyroid cancers. It appears that the links between such polymorphisms and cancer may depend on other risk factors, including ethnicity and lifestyle. Subtle differences in BER-SSBR capacity between cell lines expressing these XRCC1 variants and wild-type XRCC1 have been reported ¹⁵. The latter work showed that these XRCC1 variants could still support the accumulation of PNKP at sites of DNA damage in a manner similar to wild-type protein. This might not be surprising since these mutations lie outside the cluster of CK2 phosphorylation sites (515-526 aa) on XRCC1 that support the phosphorylation dependent interaction with PNKP ¹³⁷. In further investigating the interaction of XRCC1 and PNKP, our aim was to assess the binding affinities of two of the XRCC1 variants (R194W and R280H) to substrate DNA. Additionally, we tested the effect of these mutations on the scaffolding function of XRCC1 by comparing the repair kinetics of PNKP when incubated with wild-type and variant forms of XRCC1.

3) PNKP structure and post-translational modifications

PNKP is comprised of two major conserved domains¹³⁸. At the N-terminus of the protein is the FHA domain that supports interaction with phosphorylated proteins, mainly XRCC1¹³⁹ and XRCC4⁶⁰. The catalytic domain possesses two modules, the phosphatase and the kinase domains that confer the 3' DNA phosphatase and 5' DNA kinase activities of PNKP, respectively⁹. The mechanism for the 5' DNA kinase activity (**Figure 12**) has been proposed to proceed via an aspartic acid residue (Asp396 in mouse PNKP) which facilitates the attack of 5'-OH group on the γ -phosphate of ATP via hydrogen bonding^{9,140,141}. The PNKP phosphatase domain belongs to the conserved haloacid dehalogenase family of phosphotransferases¹⁴⁰. The phosphatase activity (**Figure 13**) requires Mg^{2+} to stabilize the interaction between phosphate (substrate) and active site Lys and Thr (Lys259 and Thr216 in mouse PNKP) forming a phospho-aspartate intermediate. Ultimately, the intermediate is hydrolysed into free enzyme and inorganic phosphate is released¹⁴⁰. The FHA domain is linked to the catalytic core of PNKP via a highly flexible unstructured 30 amino acid linker¹³⁸. Interestingly, this linker region contains two serine residues (Ser114 and Ser126) that have been shown to be phosphorylated *in vivo* by ATM and ATM/DNA-PKcs respectively^{55,142,143}. The proposed roles for these modifications are: (1) regulating levels of PNKP by protection against ubiquitin mediated degradation¹⁴² and (2) maintaining the optimal levels and enzymatic function of PNKP at sites of DNA damage introduced by laser μ IR. Mutations in PNKP that disrupt these PTMs conferred radiosensitivity possibly due to impaired PNKP activity⁵⁵.

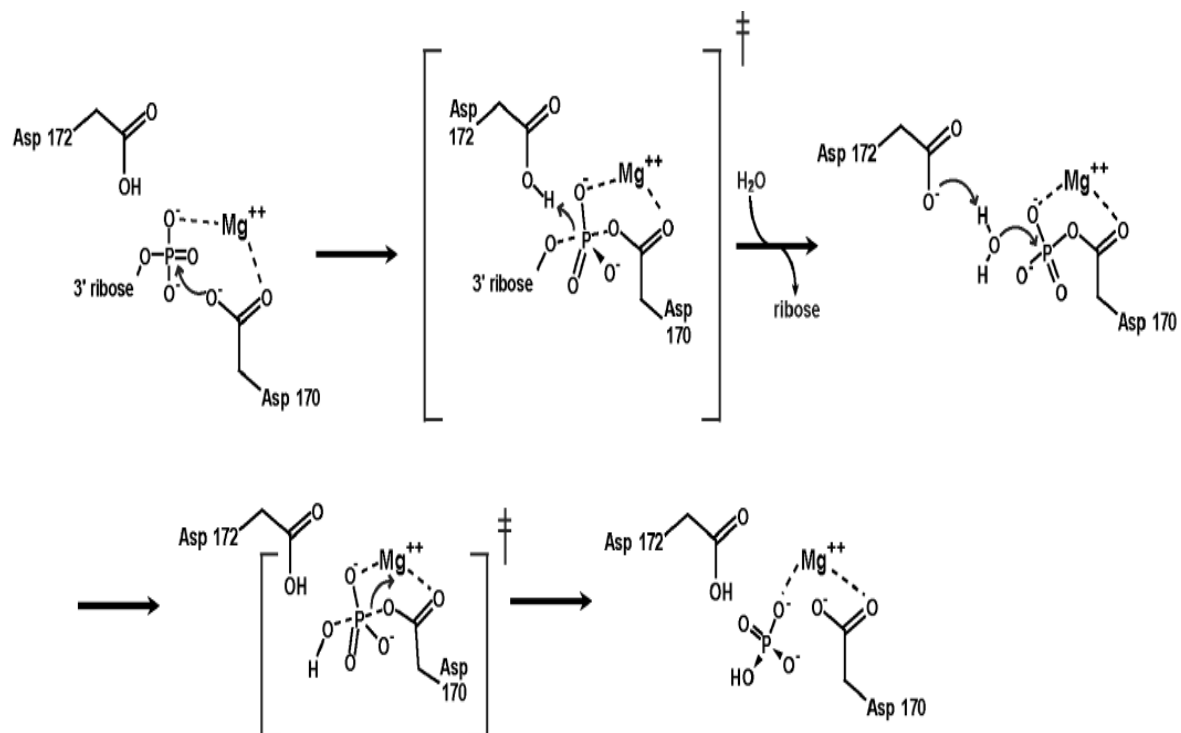
Figure 12: Proposed mechanism of PNKP kinase activity



Anticancer Agents Med Chem. 2008 May; 8(4): 358–367.

Reproduced with permission from Bentham Science publishers

Figure 13: Outline of PNKP phosphatase activity



Anticancer Agents Med Chem. 2008 May; 8(4): 358–367.

Reproduced with permission from Bentham Science publishers

The exact mechanism by which PNKP is recruited to sites of DNA damage in live cells has yet to be elucidated. It has been proposed that PNKP accumulates at damage sites via its FHA mediated interaction with the scaffold protein XRCC1^{144,145}. We (unpublished data) and others³⁰ have observed that PNKP accumulates in EM9 cells devoid of XRCC1, albeit with a lesser efficiency compared to XRCC1 wild-type counterparts. This by-and-large normal recruitment might be due to the binding of the FHA domain to PAR residues¹⁴⁶ or direct binding of PNKP to damaged DNA. We aimed to study the recruitment kinetics of different domains of PNKP (FHA and catalytic domain) and the linker region, in order to provide deeper insights into the interplay between these regions of PNKP and its impact on the behaviour of PNKP at sites of DNA damage.

Chapter 2: Experimental procedures

Cell Culture

Human HeLa cells were obtained from Dr. David Murray (University of Alberta) and cultured in DMEM-F12 media supplemented with 10% Fetal Calf Serum (FCS). Chinese Hamster Ovary cells (XRCC1 WT - AA8, and XRCC1 deficient - EM9) were kindly provided by Dr. Keith Caldecott (University of Sussex) and cultured in DMEM supplemented with 10% FCS. PARP1^{+/+} (F20) and PARP1^{-/-} (A1) mouse embryo fibroblasts (MEFs) were kindly provided by Dr. Zhao-Qi Wang (Jena University, Germany) and cultured in DMEM low glucose media supplemented with 10% FCS. For PARP-1^{-/-} MEFs, growth media contained neomycin at a final concentration of 600 µg/ml. Transfection of plasmid DNA, either mammalian expression plasmids or plasmids containing sequences coding for short hairpin RNA (shRNA), into cell lines was performed using Turbofectin 8.0 reagent (Cat. no. TF81001OriGene, Rockville, MD) according to the manufacturer's protocol. Briefly, cells were plated on either 6 well tissue culture plates (for subsequent lysate preparation) or 35-mm glass bottom dishes (for microscopy and live cell imaging) then allowed to adhere and grow. The next day (24 h after plating) cells were transfected with Turbofectin-DNA complexes containing 500 ng – 1 µg of plasmid DNA. 24-48 h later cells were analysed for downstream applications (i.e. microscopy and lysate preparation)

Lysate preparation

Whole cell extracts (WCE) for analysis of either protein expression or knock down were prepared using RIPA buffer (25 mM Tris-HCl pH 7.6, 150 mM NaCl, 1% NP-40, 1% sodium deoxycholate, 0.1% SDS) containing phenylmethanesulfonyl fluoride (PMSF)

and protease inhibitor cocktail (Thermo Scientific, Cat. no. 78430). 24-48 h following transfection of plasmid DNA, adherent cells were washed twice with 1X ice cold phosphate buffered saline (PBS), then cells were harvested by trypsin treatment. Trypsin was inactivated by the addition of complete growth medium containing FCS and then cells were centrifuged at 800 rpm/4 °C for 5 min. Cells were then washed twice in ice cold PBS and finally incubated on ice with RIPA buffer for 5 min. Finally, cells were centrifuged at 14000g/4 °C for 15 min to pellet cellular debris and supernatant was analyzed by Bradford assay for protein concentration. Aliquots of WCE were stored at -80 °C.

Mammalian and bacterial expression plasmids

Mammalian expression plasmids, pEGFPC1- Δ ZnF LIG3, pEGFPC1 LIG3 and pmRFPC1 LIG3 were kindly provided by Dr. Heinrich Leonhardt (Ludwig-Maximilians University, Germany), pEGFP-N3-hOGG1 plasmid was a kind gift from Dr. Akira Yasui (Institute of Development, Aging and Cancer, Tohoku University, Japan). pEGFPC1-hPARP1 has been previously described in ⁷⁴. Generated expression plasmids (outlined in **Figure 14** with representative PAGE analysis and western blotting for expressed proteins) included pCMV6-AC-mGFP/mRFP (PNKP/XRCC1/LIG3/ Δ ZnF-LIG3/pol β /PARP1), pCMV6-AN-mGFP (PNKP/XRCC1/LIG3/ Δ ZnF-LIG3/L360D XRCC1 (XR1)/R194W XR1/R280H XR1/166-436 XR1), pCMV6-AC-mKate (PNKP/LIG3/XRCC1/PARP1/pol β , pEGFP-C1ZnF-LIG3/ZnF-DBDLIG3/R31I-ZnF-LIG3) and pEX-N-His (PNKP/XRCC1/R194W XR1/R280H XR1/166-436 XR1/166-436 R194W XR1/ 166-436 R280H XR1).

All plasmids were generated by cloning the PCR (list 2, primers) product of the protein of interest into the destination vector via restriction digestion and ligation. Plasmids encoding mutant and/or truncated versions of proteins were generated by either overlap extension PCR or Quick change II site directed mutagenesis kit (Agilent, Cat. no. 200523). Plasmids were sequence validated and expression of protein of interest was verified by western blotting.

List 1, expression plasmids

Vector name	Supplier
pCMV6-AC-mGFP (mammalian)	OriGene, Cat. no. PS100040
pCMV6-AN-mGFP (mammalian)	OriGene, Cat. no. PS100048
pCMV6-AC-mRFP (mammalian)	OriGene, Cat. no. PS100041
pCMV6-AC-mKate (mammalian)	OriGene, Cat. no. PS100039
pEX-N-His (bacterial)	OriGene, Cat. no. PS100030

List 2, PCR primers

Primer name	Sequence
Fwd PNKP for AC vectors	5'GAG GCG ATC GC ATG GGC GAG GTG GAG GCC3'
Rev PNKP for AC vectors	5'GCG ACG CGTGCC CTC GGA GAA CTG GCA GTA3'
Fwd XRCC1 for AC vectors	5'GAG GCG ATC GCC ATG CCG GAG ATC CGC CTC3'
Rev XRCC1 for AC vectors	GCGACG CGT GGC TTG CGG CAC CAC CCC ATA3'
Fwd LIG3 for AC vectors	AGCAGCGCGGCGCGCCATGGCTGAGCAACGGTTCTGTGTG 3'
Rev LIG3 for AC vectors	AGCAGCGCCGGTCCGCTGCAGGGAGCTACCAGTCTCCGTTT
Fwd pol β for AC vectors	GGAGCAGCGGCGCGCCA ATGAGCAAACGGAAGGCG
Rev pol β for AC vectors	GGAGCAGCCGGTCCGC7TTTCGCTCCGGTCCTTGGGT

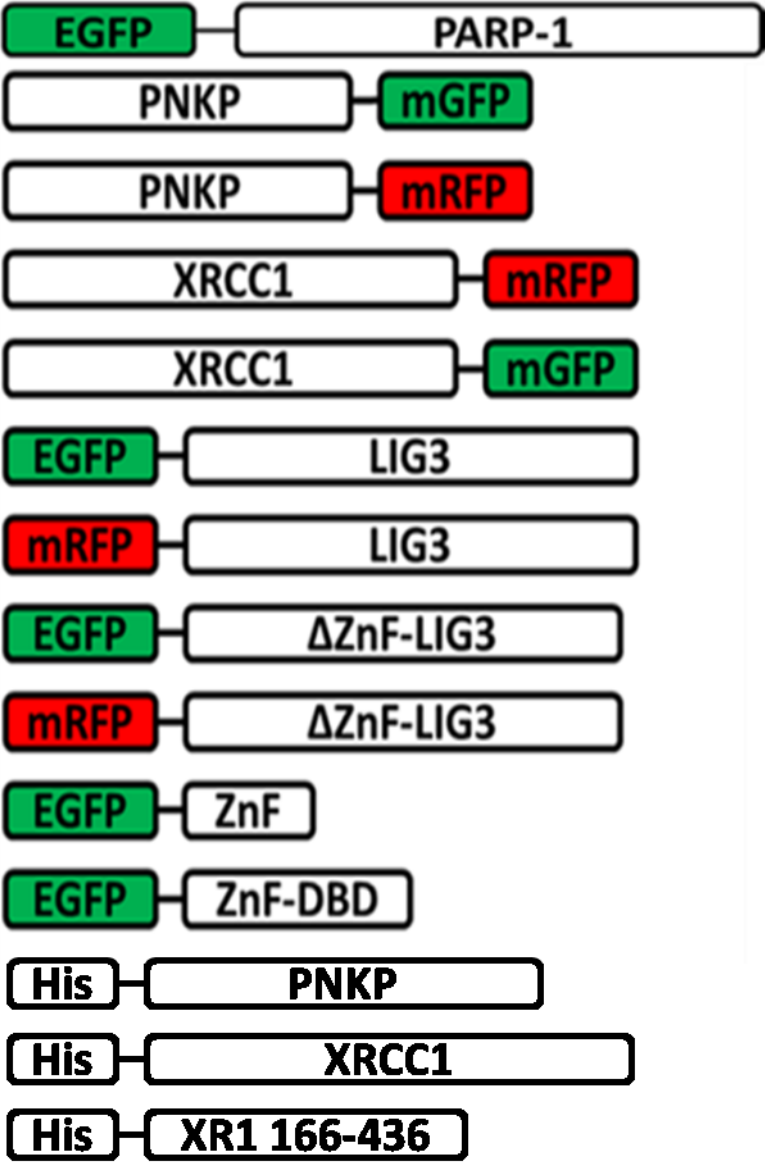
Fwd PARP1 for AC vectors	ACGGCGGCGATCGCCATGGCGGAGTCTTCGGATAA
Rev PARP1 for AC vectors	GACGCGACGCGTCCACAGGGAGGTCTTAAAATT
Fwd Δ ZnF LIG3 for AC vectors	AGCAGCGCGGCGCGCCATGTTTGAGAACTAGAGCGG
Rev Δ ZnF LIG3 for AC vectors	AGCAGCGCCGGTCCGCTGCAGGGAGCTACCAGTCTCCGTTT
Fwd PNKP for AN vectors	AGCAGCGCGGATCGCCATGGGCGAGGTGGAG
Rev PNKP for AN vectors	AGCAGCGCACGCGTTCAGCCCTCGGAGAA
Fwd XRCC1 for AN vectors	AGCAGCGCGGCGCGCCAATGCCGGAGATCCGCCT
Rev XRCC1 for AN vectors	AGCAGCGCCGGTCCGTCAGGCTTGCGCCACCA
Fwd LIG3 for AN vectors	AGCAGCGCGGCGCGCCAATGGCTGAGCAACGGTT
Rev LIG3 for AN vectors	AGCAGCGCCGGTCCGTCATCTCCTGCCTGCTG
Fwd Δ ZnF LIG3 for AN vectors	AGCAGCGCGGCGCGCCAATGTTTGAGAACTAGA
Rev Δ ZnF LIG3 for AN vectors	AGCAGCGCCGGTCCGTCATCTCCTGCCTGCTG
Fwd 166-436 XR1 for AN vectors	AGCAGCGCGGCGCGCCAATGGTGACCAAGCTTGCCAGTTC
Rev 166-436 XR1 for AN vectors	AGCAGCGCCGGTCCGTCATTTGGTCTGGGGTTGCTTCT
Fwd R194W XR1 for AN vectors	GGGCTCTTCTTCAGCTGGATCAACAAGACATCC
Rev R194W XR1 for AN vectors	GGATGTCTTGTTGATCCAGCTGAAGAAGAGAGCCC
Fwd R280H XR1 for AN vectors	GCCAGCTCCAACCTACATACCCAGCCACAG
Rev R280H XR1 for AN vectors	CTGTGGCTGGGGTATGAGTTGGAGCTGGC
Fwd L360D XR1 for AN vectors	CGGGACAGCACGCACGACATCTGTGCCTTTGC
Rev L360D XR1 for AN vectors	GCAAAGGCACAGATGTCGTGCGTGCTGTCCCG
Fwd FHA PNKP for AC vectors	AGCAGCGGGCGATCGCC ATGGGCGAGGTGGAGG
Rev FHA PNKP for AC vectors	AGCAGCGGACGCGTCCCAGCTGCGGTGAACA
Fwd ZnF LIG3	AGGGCGGTGACGCTGAGCAACGGTT
Rev ZnF LIG3	AGCCGCGGATCCTTATTTCCGGGGATTGGTACT
Fwd ZnF-DBD LIG3	AGGGCGGTGACGCTGAGCAACGGTT
Rev ZnF-DBD LIG3	AGCCGCGGATCCTTACAGCGAGGCCTGGACGCT
Fwd R311 ZnF LIG3	GGGCACCACTTTGCCAATTATGCATACGCCCTTACAATC

Rev R31I ZnF LIG3

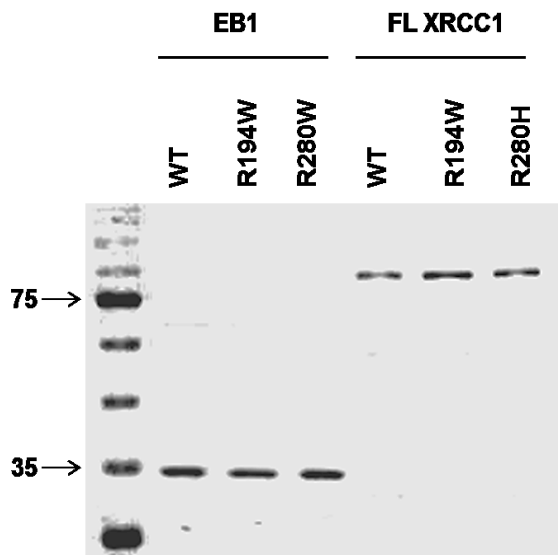
GATTGTGAAGGGCGTATGCATAATTGGCAAAGTGGTGCCC

Figure 14: Schematic outline for generated expression plasmids

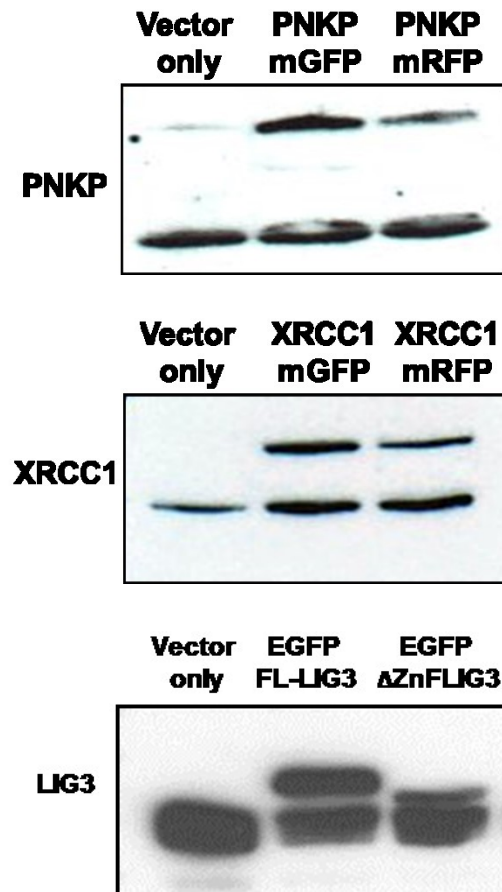
(A)



(B)



(C)



Validation of bacterial and mammalian expression plasmids. (A) Schematic representation for mammalian and bacterial expression plasmids generated. (B) SDS-PAGE analysis of purified proteins; EB1 represents XRCC1 fragment 166-436 aa. (C) Western blot analysis showing expression of fluorescently tagged versions of PNKP, XRCC1, LIG3 and Δ ZnF LIG3 (truncated LIG3 lacking N-terminal ZnF domain) following transient transfection in mammalian cells.

Western blotting

50 µg samples were mixed with 1X Tris-glycine sample buffer (63 mM Tris-HCl, 2.5% β-mercaptoethanol, 0.005% bromophenol blue, 4% sodium dodecyl sulphate (SDS) and 10% glycerol) then boiled for 5 min. Subsequently, denatured samples were loaded into wells of 10% denaturing (SDS)-polyacrylamide gels and run using Tris-glycine SDS running buffer (25 mM Tris, 192 mM glycine and 0.1% SDS) for 50 min at 180 V. Gels were transferred by tank blotting onto 0.45 µm pore size nitrocellulose membranes (BioRad, Cat. no. 162-0094). Transfer was performed in Towbin transfer buffer (25 mM Tris, 192 mM glycine, 0.1% SDS, 20% methanol) at 100 V for 70 min; alternatively transfer was carried out overnight at 30 V. Subsequently, membranes were blocked in 5% milk in PBS for 1 h, then washed in 0.1% Tween-PBS twice and incubated with primary antibody (list 3). After incubation with primary antibody (dilution and incubation were in accordance with manufacturer's recommendation), membranes were washed and incubated with horseradish peroxidase conjugated secondary antibodies (1:5000 dilution) for 45 min at room temperature and then washed. Chemiluminescent substrate was used for detection (Roche, Cat. no.12015200001).

List 3, antibodies for western blotting

Antibody	Supplier
Mouse monoclonal anti-DNA ligase 3	BD-transduction labs, Cat. no. 611876
Goat polyclonal anti-actin	Santa Cruz, Cat. no. sc-1616
Mouse monoclonal anti-XRCC1	Abcam, Cat. no. ab1838-250
Mouse monoclonal anti-PNKP	In house manufactured
Mouse monoclonal anti-EGFP	Clontech, Cat. no. 632375
Rabbit anti-goat HRP	Jackson immunoresearch, Cat. no. 305-035-003
Rabbit anti-mouse HRP	Jackson immunoresearch, Cat. no. 315-035-003
Mouse anti-rabbit	Jackson immunoresearch, Cat. no. 211-035-109

Protein expression and purification

Escherichia coli (*E. coli*) BL21-Gold DH5 α cells (Cat. no. 230130, Agilent) were transformed with bacterial expression plasmids encoding for hexa-histidine tagged versions of proteins of interest (wild-type and variants). 1 or 2 L bacterial cultures were grown in LB media containing appropriate selection antibiotic (100 μ g/mL ampicillin). At an OD₆₀₀ of 0.7-0.9, IPTG was added to a final concentration of 1 mM (for XRCC1 WT, variants and fragments) or 0.1 mM for PNKP. Induction was carried out at 37 °C for different versions of XRCC1 for 3 h and at 16 °C for PNKP for 18 h. Induction was confirmed by comparing samples of induced cultures to non-induced control on 10% SDS-PAGE gel and confirmation with Coomassie stain. Subsequently, bacterial pellets were obtained by spinning down cultures at 10,000 rpm for 15 min at 4 °C and pellets

were stored at -80 °C. His-tagged proteins were purified on Pro-Bond Nickel Chelating resin (Life Technologies, Cat. no. R801-01) following the manufacturer's protocol for lysis and purification.

Purified proteins were dialyzed and concentrated using Millipore concentrators and stored in storage buffer (50 mM Tris-HCl pH 7.5, 100 mM NaCl, 5 mM MgCl₂, and 1 mM DTT) at -80 °C for further downstream applications.

Human PNKPWFX402 and the FHA domain of PNKP were expressed in *E. coli* BL21(DE3)pLysS (Millipore, Etobicoke, ON), purified as previously described¹⁴⁷⁻¹⁴⁹, and kept in storage buffer (50 mM Tris-HCl, pH 7.4, 100 mM NaCl, 5 mM MgCl₂ and 1 mM dithiotreitol) at -80°C.

For XRCC1 fragments 511-633 and 295-633 the encoding cDNAs were cloned into the pET28a vector (Millipore) using a restriction-free cloning (RF-cloning) procedure¹⁵⁰. Briefly, in the first step a regular PCR amplification was performed employing a template vector of human XRCC1, which was kindly provided by Dr. Tom Ellenberger (Washington University, St Louis). In the second step further PCR amplification was carried out using primers designed to have 30 bp overlap with the sites of integration in the destination vector. The amplified products then served as mega-primers for insertion into the vector. The parental plasmid DNA was removed by DpnI treatment, and then DNA was directly transformed into competent *E. coli* DH5α cells. The selected colonies were checked by DNA sequence verification. The cDNA encoding full length XRCC1 and residues 166-436 was amplified by PCR and inserted into the bacterial expression plasmid pEX-N-His (OriGene, Rockville, MD) using AscI-RsrII restriction sites. Point mutations encoding R280H and R194W were introduced into wild-type XRCC1 using

overlap extension PCR technique with the following forward and reverse primers for R194W mutant: 5'-GGGCTCTCTTCTTCAGCTGGATCAACAAGACATCC-3' and 5'-GGATGTCTTGTTGATCCAGCTGAAGAAGAGAGCCC-3'; and for the R280H mutant: 5'-GCCAGCTCCAACTCATACCCCAGCCACAG-3' and 5'-CTGTGGCTGGGGTATGAGTTGGAGCTGGC-3'. All generated plasmids were sequence verified.

His-tagged proteins were expressed in *E. coli* BL21 gold transformed with bacterial expression plasmids after reaching OD600 0.6 followed by induction with 1 mM IPTG at 37°C for 3 h. Subsequently, proteins were purified using Pro-Bond Nickel Chelating resin (Life Technologies) following the manufacturer's protocol for lysis and purification. The purified proteins were dialyzed against 50 mM Tris, pH 7.4, 100 mM NaCl and 5 mM MgCl₂.

In vitro phosphorylation of XRCC1 fragments and purification

The XRCC1 cDNAs encoding residues 511–633 (EB2) and 295-633 (BLB) followed by a C-terminal hexahistidine were cloned into the pET28a vector (Millipore) using a restriction free cloning. The expression plasmids were transformed into BL21(DE3) *E. coli* cells and grown in LB-kanamycin media. Starting culture (2 ml) was transferred to 100 ml TYM media (2% bacto-tryptone, 0.2% yeast extract, 0.1 M NaCl and 0.01 M MgCl₂). After reaching OD600 of 0.4 the cells were harvested at 3000 rpm for 10 min and the cells pellets were resuspended in 20 ml TFB2 buffer (10 mM Na-MOPS, pH 7.0, 75 mM CaCl₂, 10 mM KCl, 15% glycerol). Following incubation for 2 h on ice, the cells were harvested at 3000 rpm for 10 min again and the cells pellets were resuspended in

4 ml TFB1 (10 mM Na-MOPS, pH 7.0, 75 mM CaCl₂, 10 mM KCl, 15% glycerol). The cells were divided into aliquots of 50 µl and stored at -80°C. The XRCC1-fragment competent *E. coli* cells were further transformed with CK2α vector (pGEX-3x cut by BamHI\BamHI, Ampicilin resistance).

After growth to OD₆₀₀ 0.4, the culture was cooled to 18°C and protein expression was induced with 1 mM IPTG for 18 h. The cells were harvested by centrifugation (6000g for 20 min), resuspended in lysis buffer (20 mM imidazole, 20 mM Tris pH 8.0, 300 mM NaCl, 1 mM EDTA and 5 mM β-mecraptoethanol) and protease inhibitor cocktail was added before lysis by sonication. A cleared lysate was prepared by centrifugation and proteins were purified by immobilized metal affinity chromatography followed by gel filtration. The soluble fraction was added to Ni-NTA-agarose resin (Amersham Pharmacia Biotech) and mixed gently by shaking at 4°C for 2 h. The protein solution-Ni-NTA-agarose mixture was loaded into a column and washed with 300 ml of lysis buffer and 100 ml lysis buffer containing 25 mM imidazole. Bound protein was eluted with 10 ml lysis buffer containing 300 mM imidazole. The buffer was then exchanged for gel filtration buffer (20 mM Tris-HCl, pH 8, 150 mM NaCl, 1 mM EDTA, 5 mM MgCl₂ and 5 mM β-mecraptoethanol), and the protein was further purified on a Superdex 75 26/60 (Amersham) gel filtration column.

Steady-state fluorescence spectroscopy

Labelling of PNKPWFX402 and the PNKP FHA domain with 6-acryloyl-2-diamino naphthalene (AC) was carried out as described in our earlier studies¹⁵¹. The interaction between phosphorylated and non-phosphorylated XRCC1 fragments and PNKP was

studied using acrylodan-labelled PNKPWFX402 and the FHA domain as described previously^{151,152}. AC-labelled proteins were excited at 380 nm, and the changes in AC fluorescence at the emission maximum (490 nm) were monitored. The interaction between XRCC1 fragments and DNA substrates was studied using the intrinsic fluorescence due to tryptophan residues as detailed in our earlier work¹⁵⁰. All fluorescence and CD measurements were carried out in 50 mM Tris-HCl, pH 7.5, 100 mM NaCl, 5 mM MgCl₂ and 1 mM DTT. GraphPad Prism software (GraphPad Software Inc., La Jolla, CA) was used for the analysis of binding data.

Circular dichroism (CD) spectroscopy

Far-UV CD measurements were performed with an Olis DSM 17 CD spectropolarimeter (Bogart, GA) as described previously¹⁵⁰. Protein concentrations used for each determination are presented in the corresponding figure legends. The CD spectra were analyzed according to the method of Provencher and Glöckner¹⁵³.

Measurement of SSB (alkaline COMET assay)

Cells were treated with 100 µM hydrogen peroxide in PBS for 40 min on ice. then washed twice with PBS, and then growth medium was added. Finally, cells were harvested after 15, 60, 120 and 240 min incubation at 37°C. For sample preparation for the single-cell gel electrophoresis (comet) assay, we followed the kit manufacturer's (Trevigen, Gaithersburg, MD) protocol. Briefly, cells were trypsinized and washed twice with PBS. Then the cell count was adjusted to 2 X 10⁵ cells/ml in ice cold PBS. 25 µl of cell suspension was mixed with 250 µl molten LMP (low melting point) agarose, and 75

μ l of mixture was spread on each comet slide. Slides were kept in the dark for 60 min (gelling time) and then immersed in ice cold alkaline lysis buffer. Samples were kept overnight in the dark at 4°C, and the next day immersed in freshly prepared cold electrophoresis buffer for 45 min in the dark, and then transferred to a horizontal electrophoresis chamber. Electrophoresis was carried out at 1 volt/cm and 300 mA for 30 min. Slides were then immersed in 70% ethanol for 5 min, air dried, and stained with SYBR Green (1:3000 dilution). For scoring, slides were visualized with epifluorescence using an FITC filter with 10X objective, and the analysis was carried out using AutoComet software (TriTek, Sumerduck, VA).

Immunofluorescence and microscopy

Cells were plated on 35-mm glass bottom dishes at approximately 70-80% confluency. For immunofluorescence cells were fixed and permeabilized using ice cold methanol: acetone (1:1) mixture for 20 min. Then cells were rehydrated with PBS at room temperature for 15 min. For 8-oxo-dG staining, cells were treated with 2N HCl for 10 min at 37°C, then washed with PBS (three 5 min washes) prior to incubation with primary antibody (list 4). Subsequently, cells were blocked with 5% BSA for 1 h and incubated with primary antibodies for 1 h at room temperature or overnight at 4°C. After incubation, cells were washed once with 0.1% Triton-X-100 in PBS, then twice in PBS. Finally, cells were incubated with appropriate secondary antibodies for 30-45 min at room temperature, and then washed as described above. In the final wash, 4',6-diamidino-2-phenylindole (DAPI) was added for nuclear DNA staining and left for 15 min then washed with PBS. For image acquisition, fixed and stained cells were placed on the stage of a Zeiss confocal LSM 710 microscope. Images were acquired using either

40X or 63X objectives as 12 bit grayscale images, and then exported as Tiff 16 bit grayscale images for processing using ImageJ software. For immunofluorescence experiments, three independent experiments were carried out. In each experiment 15-20 cell images were acquired and analyzed.

List 4, antibodies for immunofluorescence

Antibody name	Supplier
Mouse monoclonal anti-8-oxo-dG	Cat. no. 4354-MC-050, Trevigen
Mouse monoclonal anti- γ H2AX	(Cat. no. 05-636, Millipore
Mouse monoclonal anti-53BP1	Cat. no. , Millipore
Mouse monoclonal anti-XRCC1	Cat. no. ab1838-250, Abcam
Rabbit polyclonal anti-DNA Ligase 3	Cat. no. GTX103197, GeneTex
Mouse monoclonal anti-poly(ADP-ribose)	Cat. no. ab14459, Abcam
Alexa Fluor 555 goat anti-rabbit	Cat. no. A-21430, Invitrogen
Alexa Fluor 488 goat anti-mouse	Cat. no. A-11017, Invitrogen

Laser micro-irradiation (Two-photon laser micro-irradiation and 405 nm diode)

For two-photon laser micro-irradiation, cells were grown on 35-mm glass bottom dishes. Before laser micro-irradiation, cells were incubated with Hoechst 33258 (Sigma, Cat. no. 94403) to a final concentration of 1 μ g/ml for 20 min and then fed with fresh growth medium for 10 min. Where indicated, cells were incubated with either 1 or 2 μ M AG14361 (IC₅₀ = 29 nM, Selleckchem, Cat. no. S2178), or with 2.5 and 10 μ M PJ-34 (IC₅₀ = 20 nM, Enzo Life Sciences, Cat. no. ALX-270-289) for 1-2 h prior to micro-

irradiation. Subsequently, cells were placed on a 37°C heated stage of a Zeiss LSM510 NLO laser-scanning confocal microscope. Micro-irradiation was carried out using a near infrared titanium sapphire laser. To introduce damage within nuclei of individual cells, a 1.2 µm wide region was pre-defined and subsequently micro-irradiated with 10 iterations of a 750 nm laser line (50 mW) at 10% power using a Plan-Neofluar 40X/1.3 NA oil immersion objective. For immunofluorescence of endogenous proteins and protein modifications, cells were fixed right after laser micro-irradiation and counterstained with antibodies of interest. For time lapse experiments of mRFP-tagged proteins, the fluorescent signal was recorded using excitation with a 543 nm He–Ne laser and a 559–634 nm band-pass emission filter. Similarly, for mGFP and EGFP tagged proteins, the signal was recorded after excitation with a 488 nm argon laser and a 515–540 nm band-pass emission filter. Cells with low to medium expression levels of fluorescent proteins were selected and accumulation of fluorescently tagged protein in micro-irradiated areas was quantified and compared to that in unirradiated regions. After background subtraction as previously described ¹⁵⁴, the intensity was normalized so that the total cell intensity remained constant throughout the experiment. This process compensates for photobleaching during acquisition ¹⁵⁴. Images were then realigned using ImageJ software and fluorescence signals of the exported Tiff images were subsequently quantified using Metamorph software 6.0 (Molecular Devices). Plotted results of recruitment kinetics represent averages of three independent experiments. For each experiment 10 -12 cells were analyzed (total 30-36 cells).

For the 405 nm laser micro-irradiation, we applied the same settings as described by Dinant et al ⁸⁹ (60% laser power, 30 iterations, 0.5 µg/mL Hoechst). Briefly, cells transiently expressing a fluorescent protein-tagged protein of interest were pre-sensitized with Hoechst dye for 20 min, at a final concentration of 0.5 µg/ml, and then the media was replaced prior to micro-irradiation. Cells were placed on a 37°C heated stage of a Zeiss LSM710 NLO laser-scanning confocal microscope. To introduce damage within nuclei of individual cells, a 1.2 µm wide region was pre-defined and subsequently micro-irradiated with 30 iterations of a 405 nm (30 mW) laser line at 60% power using a Plan-Neofluar 63X/1.3 N.A. (numerical aperture) oil immersion objective. For time lapse experiments of EGFP/mGFP tagged proteins, the signal was recorded after excitation with a 488 nm argon laser and a 515–540 nm band-pass filter. Cells with low to medium expression levels of fluorescent proteins were selected and analyzed. For quantification, analyses were performed as previously described ¹⁵⁴.

Fluorescence recovery after photobleaching (FRAP)

Cells were placed on a 37°C heated stage of a Zeiss LSM 510 confocal microscope. FRAP was carried out on 1.5 µm strips across the width of the nuclei of cells under investigation using a 488 nm Argon laser line set at 100% intensity for 30 iterations using a 40X 1.3 N.A. objective. Laser power used for scanning during post-bleach time lapses was 3% to minimize photobleaching during the acquisition of the time lapse data. For data quantification, fluorescence intensities were measured in the bleached region, the entire nucleus, and extracellular background using LSM image browser software. Each image was normalized for total fluorescence intensity relative to the first image

collected after photobleaching to correct for any photobleaching that occurred during the collection of the post-bleach time series¹⁵⁴. Data on FRAP curves were plotted based on readings of 20-25 cells that were scanned over two independent experiments for each curve. For drug treatments, AG14361 was added at the indicated concentrations 90-120 min before FRAP experiments, and 10 mM H₂O₂ was added immediately prior to data acquisition. For irinotecan (IRI) treatment, cells were treated with IRI, diluted to a final concentration of 5 mM, for 30 min. Then FRAP analysis was performed as described above.

PNKP DNA Kinase Assays

Single time point kinase reaction

PNKP (500 ng, 9 pmol) was premixed with 60 pmol of either XRCC1 or XRCC1 wild-type or mutant fragment in 5 µl and incubated at 37°C for 5 min. The volume was increased to 20 µl with addition of kinase buffer (80 mM succinic acid, pH 5.5, 10 mM MgCl₂, and 1 mM DTT), 0.2 nmol of 24 mer DNA substrate (Integrated DNA Technologies, Coralville, IA), and 3.3 pmol of [γ-³²P]ATP (PerkinElmer Life Sciences, Waltham, MA) and incubated for 5 more min. 4 µl samples were mixed with 2 µl of 3X sequencing gel loading dye (Fisher Scientific, Ottawa, ON), boiled for 10 min and run on a 12% polyacrylamide/7M urea sequencing gel at 200 V. Gels were scanned with a Typhoon 9400 variable mode imager (GE Healthcare, Bucks, UK) and the resulting bands were quantified using Image Quant 5.2 (GE Healthcare) .

Turn over assay for PNKP kinase activity

Reaction mixtures (50 μ l) containing kinase buffer (80 mM succinic acid, pH 5.5, 10 mM MgCl₂, and 1 mM dithiothreitol), 0.2 nmol of 24 mer DNA substrate, 0.4 nmol of unlabeled ATP, 3.3 pmol of [γ -³²P]ATP, and 0.9 pmol of PNKP were incubated at 37°C. From one of the reaction mixtures, 4 μ l samples were taken at 0, 1, 2, 5, 10, 20 and 30 min. To the other reaction mixtures, 60 pmol of full length XRCC1 or XRCC1 fragment was added after 20 min initial incubation and 4 μ l samples were taken after 1, 2, 5, 10, 20 and 30 min further incubation. The samples were mixed with 2 μ l of 3X sequencing gel loading dye (Fisher), boiled for 10 min and run on a 12% polyacrylamide/7 M urea sequencing gel at 200 V. Gels were scanned on a Typhoon 9400 variable mode imager and the resulting bands were quantified using Image Quant 5.2.

Statistical analysis

A two-tailed Student's t test was used to calculate statistical significance. Calculations were performed using Microsoft Excel 2010.

Chapter 3: DNA ligase III acts as a DNA strand break sensor in the cellular orchestration of DNA strand break repair *

Ismail Abdou¹, Guy G. Poirier², Michael J. Hendzel¹ and Michael Weinfeld^{1*}

¹Department of Oncology, University of Alberta, and Cross Cancer Institute, Edmonton, Alberta, Canada

² Cancer Axis, CHUQ Research Center and Faculty of Medicine, Laval University, Quebec City, Quebec, Canada.

* *Corresponding author:* Michael Weinfeld (mweinfel@ualberta.ca) and Michael Hendzel (mhendzel@ualberta.ca)

* This chapter describes work published in the journal of Nucleic Acids Research (NAR)

ABSTRACT

In the current model of DNA SSB, PARP1 is regarded as the sensor of SSBs. However, biochemical studies have implicated LIG3 as another possible SSB sensor. Using a laser micro-irradiation protocol that specifically generates SSBs, we were able to demonstrate that PARP1 is dispensable for the accumulation of different SSB proteins at sites of DNA damage in live cells. Furthermore, we show in live cells for the first time that LIG3 plays a role in mediating the accumulation of the SSB proteins XRCC1 and PNKP at sites of DNA damage. Importantly, the accumulation of LIG3 at sites of DNA damage did not require the BRCT domain-mediated interaction with XRCC1. We were able to show that the N-terminal ZnF domain of LIG3 plays a key role in the enzyme's SSB sensing function. Finally, we provide cellular evidence that LIG3 and not PARP1, acts as the sensor for DNA damage caused by the topoisomerase I inhibitor, irinotecan. Our results support the existence of a second damage-sensing mechanism in SSB involving the detection of nicks in the genome by LIG3.

INTRODUCTION

Protecting the integrity of DNA is pivotal in maintaining cellular homeostasis. However, cellular DNA is continually damaged by intracellular and extracellular agents such as reactive oxygen species, ionizing radiation, and genotoxic chemicals. These agents cause various forms of DNA insults, and accordingly, living cells possess a large repertoire of proteins that function in the repair of DNA in damage-specific pathways¹. One of the most frequently encountered forms of DNA damage is DNA SSBs. SSBs can arise as a direct consequence of exposure to endogenous or exogenous DNA damaging agents and are also generated during the base excision repair (BER) pathway (indirect SSBs)¹³. SSBs are defined as either short gaps (breaks involving loss of nucleotides) or nicks (breaks in the sugar-phosphate backbone with no missing nucleotides) that compromise the integrity of the DNA backbone. In this work we aimed to provide cellular insights into SSBR with a major emphasis on the SSB sensing step.

Based on biochemical studies, the current model for SSBR incorporates four distinct steps. The first step is SSB sensing mediated by PARP1 through its zinc finger domains (F1- F2 domains)³². In response to SSB detection, PARP1 catalyzes poly(ADP-ribose)ation (PARylation) of itself as well as other acceptor proteins. PAR residues serve two main functions (a) chromatin relaxation, which permits access of SSBR proteins and (b) generating a PAR scaffold that can bind and retain proteins near the damage site. Usually, DNA damage is associated with ends that are incompatible with gap filling and ligation steps, and therefore the step that follows damage sensing is end processing, which is catalyzed by various enzymes, such as polynucleotide kinase/phosphatase (PNKP), that are specific to the type of damaged termini resulting

from DNA insult⁹. After restoration of correct DNA ends, gap filling proceeds, which is mediated by DNA polymerase β ¹⁵⁵. Finally, the resulting nick is sealed by DNA ligase III (LIG3)¹⁵⁶. An integral component in the SSBR cascade is the scaffold protein XRCC1 that orchestrates the steps from end processing to ligation¹⁵⁷.

Previous biochemical and live cell work indicated that PARP1 is the only cellular SSB sensor and that the recruitment of SSBR core proteins, particularly XRCC1, to sites of DNA damage is PARP1 dependent^{103,104,158,159}. Contradicting these observations, it was also shown that recruitment of SSBR core proteins, XRCC1, pol β and PNKP, to sites of DNA damage was PARP1 independent³⁰. Intriguingly, PARP1 knockout mouse embryonic fibroblasts (MEFs) repair SSBs and damaged bases efficiently in a manner similar to wild-type (WT) MEFs^{121,122}. Collectively, the controversial involvement of PARP1 as a sensor in SSBR/BER suggests the possible existence of an alternative sensor. PARP1 binds damaged DNA through its zinc finger (ZnF) domain, which shows a substrate preference for gaps over nicks^{98,124}. On the basis of *in vitro* experiments, Mackey et al. postulated that among the other SSBR proteins, LIG3 uniquely has a bona fide damage sensing module ascribed to its ZnF domain at the N-terminus that is homologous to that of PARP1¹²⁵. Additionally, the LIG3 ZnF, in contrast to that of PARP1, shows a substrate preference for nicks over gaps¹²⁶. The latter study demonstrated that the ZnF domain of LIG3 cooperates with a downstream DNA binding domain (DBD) within LIG3 to comprise a nick sensing module. This module, together with another nick sensing module involving the catalytic core, orchestrates a dynamic switch between the initial nick sensing and the subsequent sealing events in a 'jack knife' fashion. However, these two studies were performed using the LIG3 β isoform and

not the ubiquitously expressed LIG3 α ^{126,127}. A notable difference between the two LIG3 isoforms, apart from the differences in expression patterns, is the interaction with XRCC1. It was shown that LIG3 α , through a BRCT module in the C-terminus of the α isoform, and not LIG3 β exists in a complex with XRCC1 and this interaction is required for LIG3 stability and optimal catalytic activity^{68,127}. Previous work alluded to the possibility of LIG3 being involved in early damage sensing steps of SSBR. Importantly, biochemical studies indicated that LIG3 α inhibits PARP1 catalytic activity upon encountering DNase I treated DNA¹²⁸, implying that both proteins can bind independently at strand breaks. Consistent with the possibility of LIG3 being a damage sensor, it was shown that among the three different DNA ligases implicated in DNA damage response, LIG3 shows a very rapid recruitment to sites of DNA damage introduced by laser micro-irradiation¹²⁹. However an involvement of LIG3 ZnF in damage sensing was not demonstrated in this study¹²⁹.

Based on these observations, we hypothesised a role for LIG3 α in sensing SSBs. Accordingly, we studied the early steps of SSBR in live cells. Here we show that PARP1 is dispensable for the recruitment and binding of SSBR proteins to sites of DNA damage. Furthermore, we identified a novel role for LIG3 α as an independent sensor for DNA damage that helps in regulating the accumulation of SSBR core machinery to DNA repair sites. We also demonstrate that LIG3 α can accumulate at sites of nuclear DNA damage independent of its BRCT domain-mediated interaction with XRCC1. We elucidated the mechanism by which LIG3 α (hereon referred to as LIG3) is recruited to damage sites and that the ZnF domain is required for the very rapid recruitment of LIG3 to damaged DNA, and indeed functions as a damage sensor in SSBR in live cells.

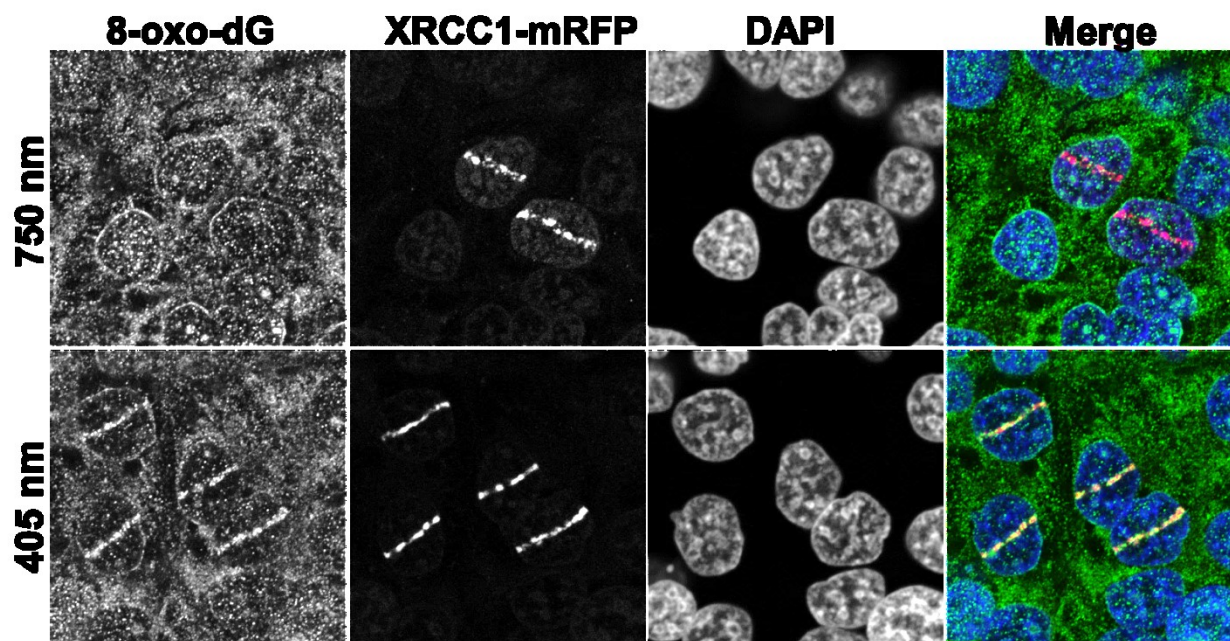
Importantly, we provide cellular evidence that LIG3 is the sensor of nicks introduced by treatment of cells with the chemotherapeutic agent irinotecan (IRI).

RESULTS

Establishment of a micro-irradiation system that specifically activates SSBR not BER

An inherent problem with studying SSBR proteins (PARP1, XRCC1, PNKP and LIG3) in real time is their participation in the BER pathway; therefore the establishment of a technique that clearly discriminates between both pathways would be pivotal to our work. It is known that different laser micro-irradiation systems enable the analysis of different DNA repair pathways in real time^{89,90}. However, a drawback can be the creation of multiple types of DNA damage, including SSBs and damaged bases. Accordingly, to study the behaviour of SSBR factors we established conditions that primarily activate the SSBR machinery rather than the BER machinery. We compared two different laser micro-irradiation systems, namely the 405 nm laser diode and the two-photon 750 nm Ti-Sapphire laser, and studied the nature of DNA damage introduced by both of them. Cells expressing XRCC1-mRFP were micro-irradiated by both systems, and 3-5 min after micro-irradiation cells were fixed and stained for 8-oxo-dG, which is one of the predominant base lesions that serve as substrates for the BER machinery. Whereas XRCC1 showed robust recruitment to sites of DNA damage following irradiation under both conditions, we found that 8-oxo-dG was produced by the 405 nm laser diode system but not the two-photon 750 nm laser (**Figure 15**).

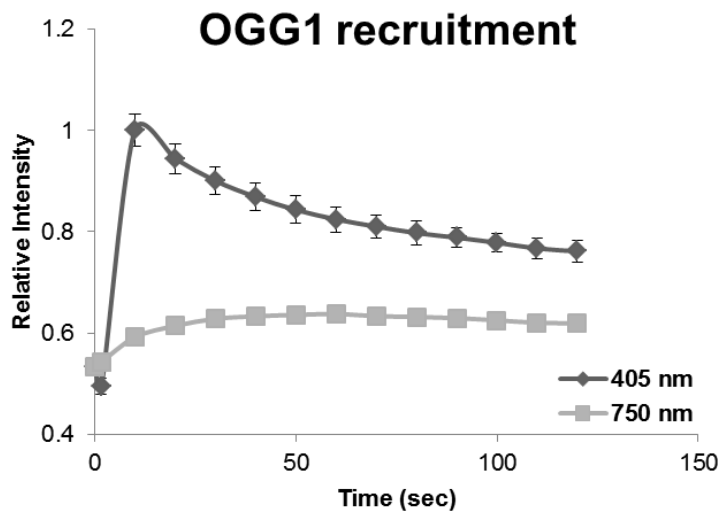
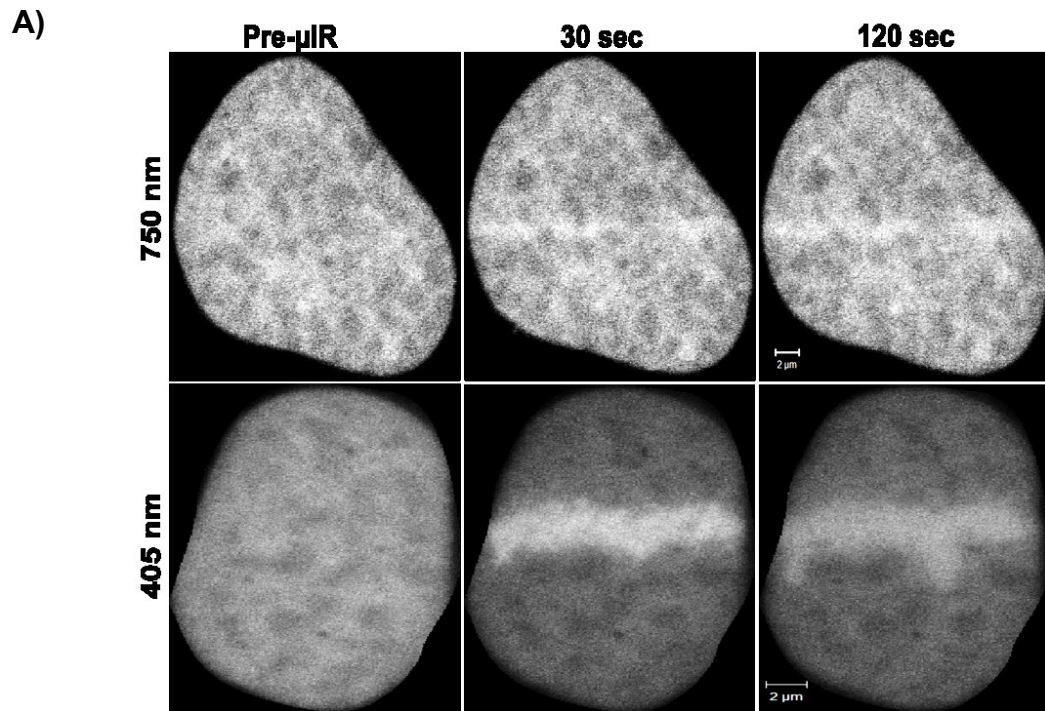
Figure 15: Comparative induction of base damage and strand breaks by different laser micro-IR conditions



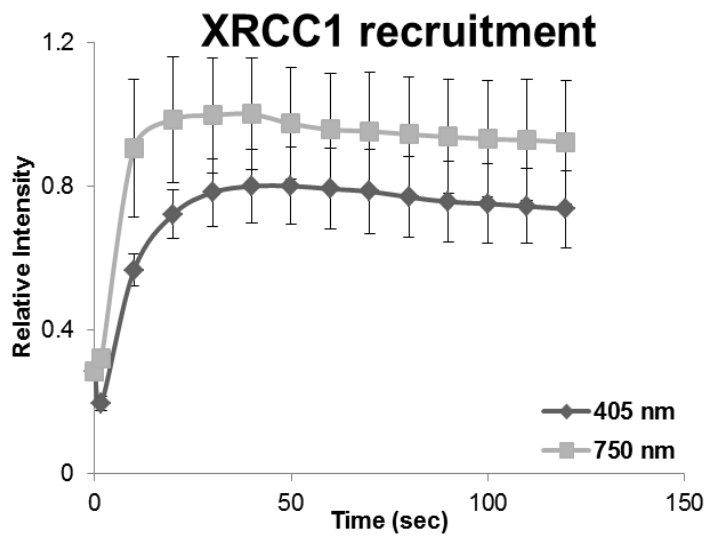
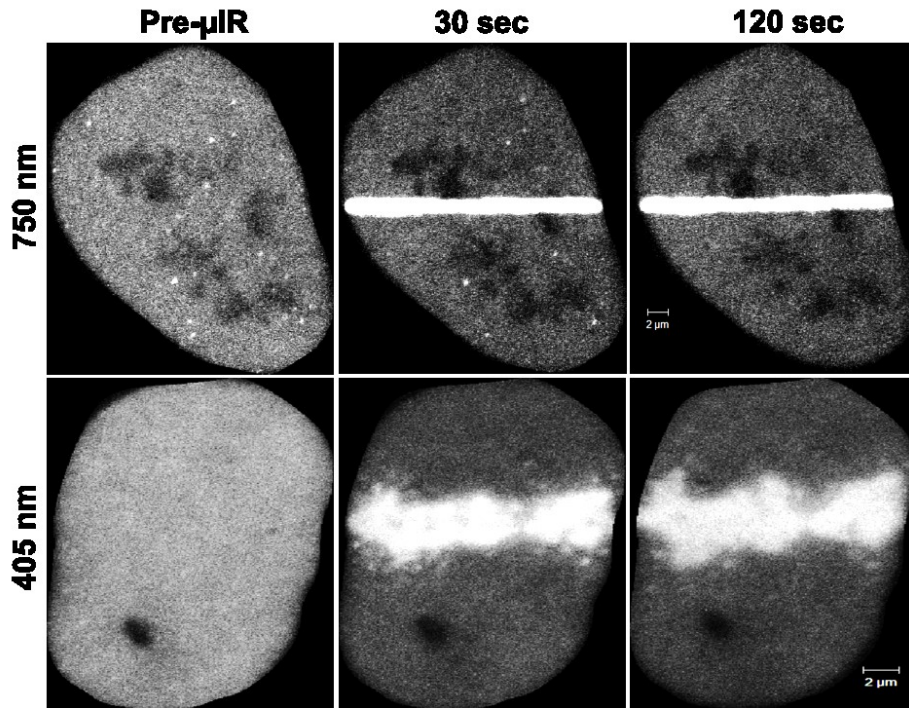
Comparative induction of base damage and strand breaks by different laser micro-IR conditions. Laser micro-irradiation was performed on HeLa cells using either 750 nm multi-photon excitation or a 405 nm laser diode. The production of base damage was gauged on the basis of production of 8-oxo-dG, while XRCC1 recruitment was used as a marker of strand break induction.

To further confirm our observation, we studied the impact of both micro-irradiation systems on the recruitment of the BER protein OGG1 and the SSBR/BER scaffold protein, XRCC1, in real time. Consistent with previous work, OGG1 showed robust recruitment to sites of DNA damage introduced by the 405 nm micro-irradiation, but only minimal accumulation at damage sites generated by the two photon micro-irradiation using 750 nm light (**Figure 16A**). Importantly, XRCC1 recruited to sites of DNA damage generated by both systems, consistent with its roles in both BER and SSBR (**Figure 16B**). Finally, it was previously shown that the L360D mutant of XRCC1 recruits specifically to sites of BER and not SSBs¹⁵⁹. Accordingly, we examined the recruitment of the mGFP-XRCC1 L360D mutant, in cells co-expressing WT XRCC1-mRFP, to sites of DNA damage introduced by both systems. Consistent with our observations, L360D mutant showed very limited accumulation at sites of DNA damage generated by the two-photon 750 nm laser, however it showed marked accumulation at sites generated by the 405 nm laser system (**Figure 16C**). Collectively, our observations indicate that the two-photon 750 nm laser system mostly generates direct SSBs with minimal activation of the BER machinery. Consequently, and distinct from other live cell studies of SSBR that were performed using the 405 nm laser micro-irradiation, we relied on the two-photon laser micro-irradiation system for studying SSBR in live cells.

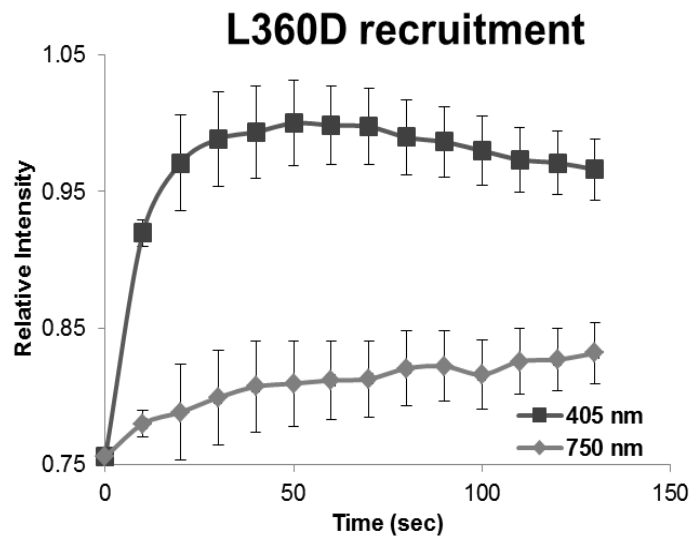
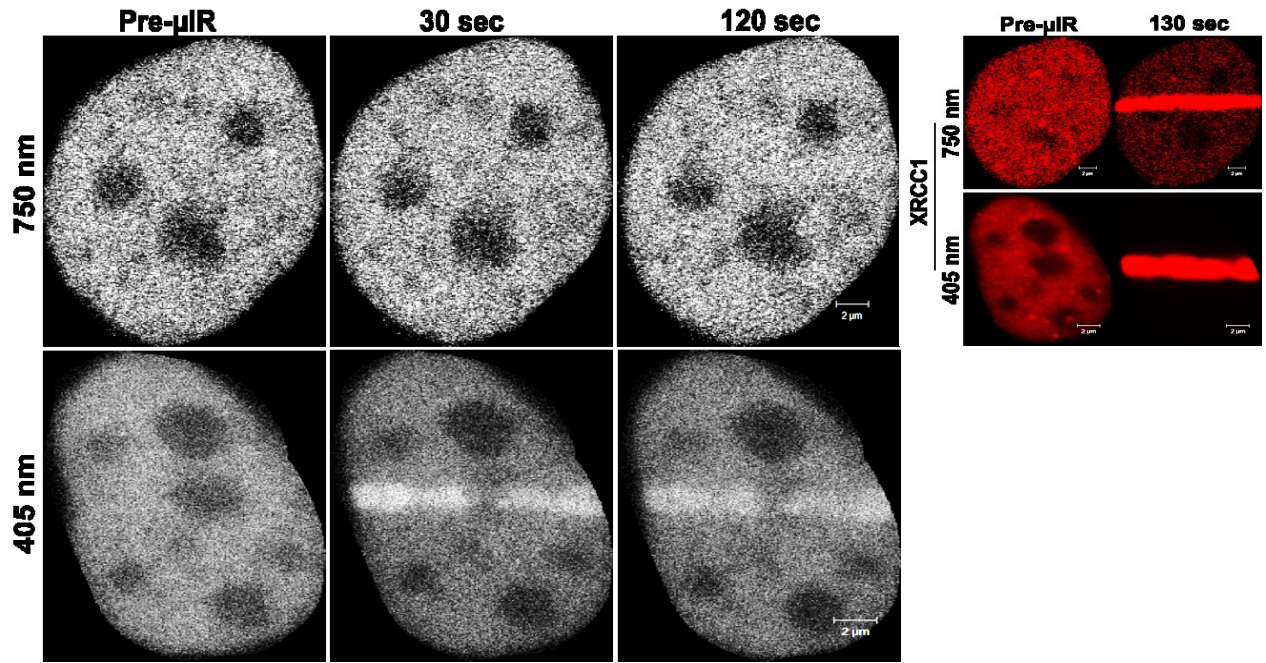
Figure 16: Recruitment of OGG1 and XRCC1 under different laser conditions



B)



C)



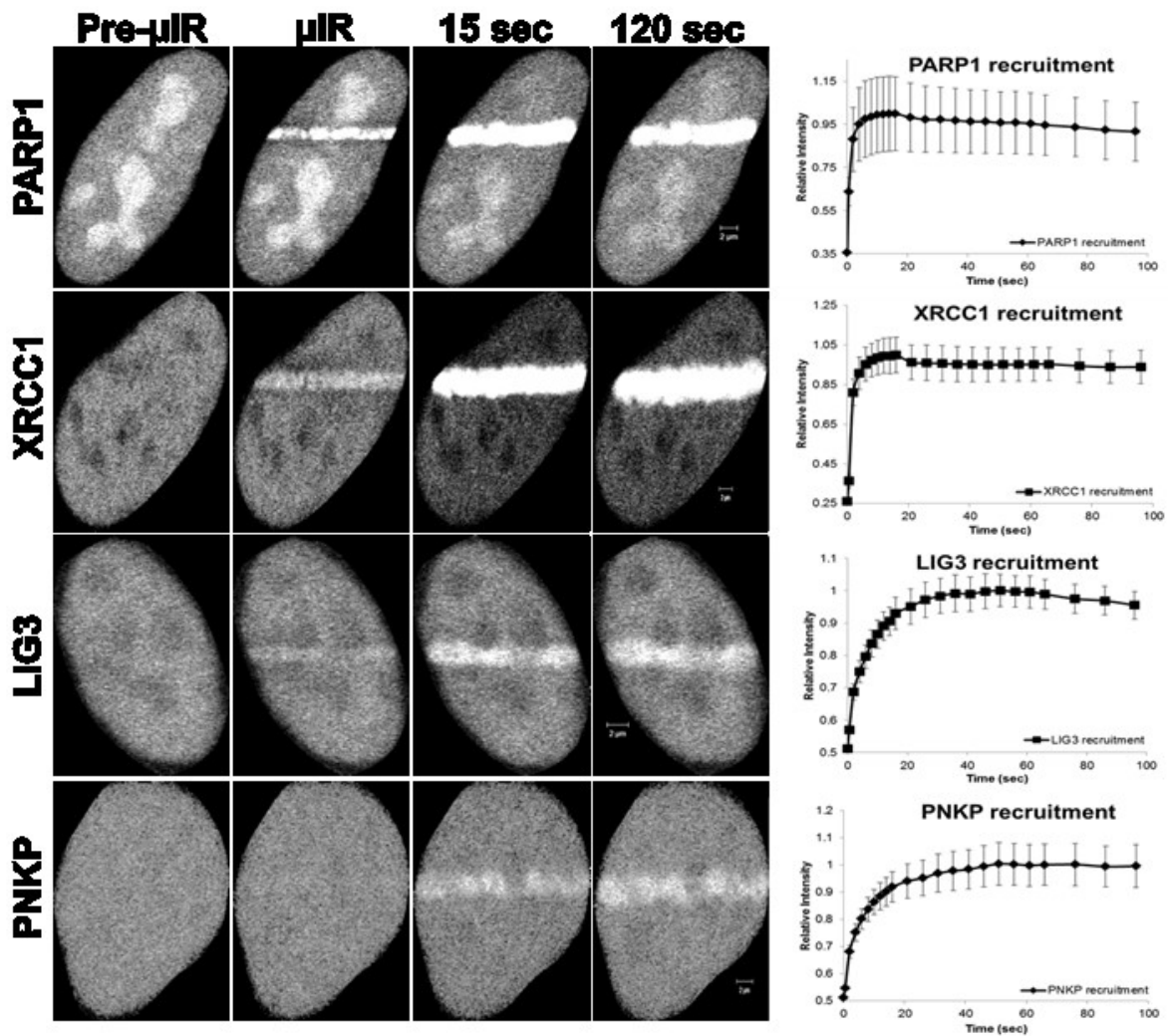
Recruitment of OGG1 and XRCC1 under different laser conditions. Recruitment kinetics of (A) the BER protein OGG1, (B) BER/SSBR scaffold protein XRCC1 and (C) XRCC1 mutant L360D were compared following irradiation of HeLa cells expressing pEGFP-OGG1 or wild-type or mutant XRCC1-mGFP with either 750 nm multi-photon excitation or 405 nm laser excitation. The recruitment of the XRCC1 mutant, L360D, was tested in cells co-expressing WT XRCC1-mRFP (shown in inset). Error bars represent S.E.M, from 3 independent experiments each analyzing 12 cells (i.e. n=36).

Rapid recruitment of SSBR machinery to DNA damage sites

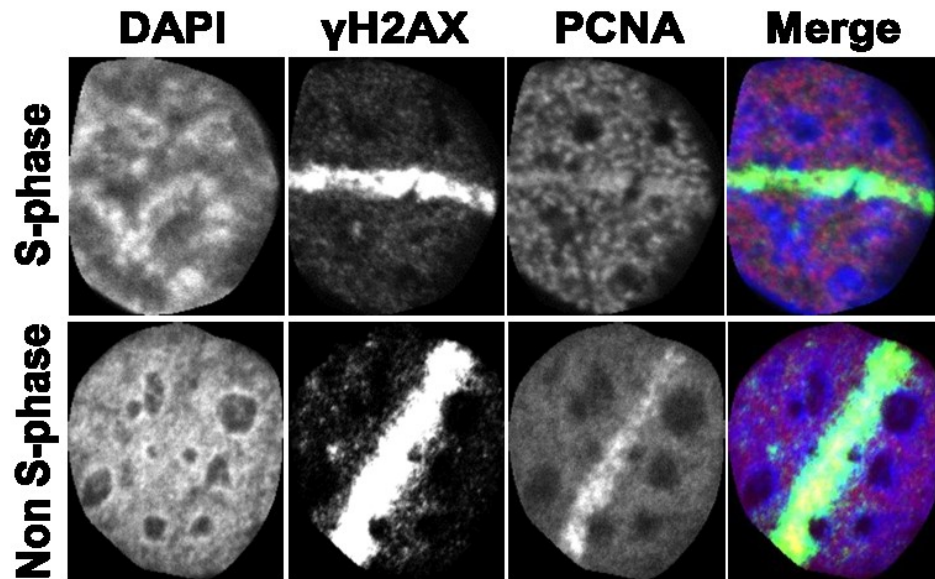
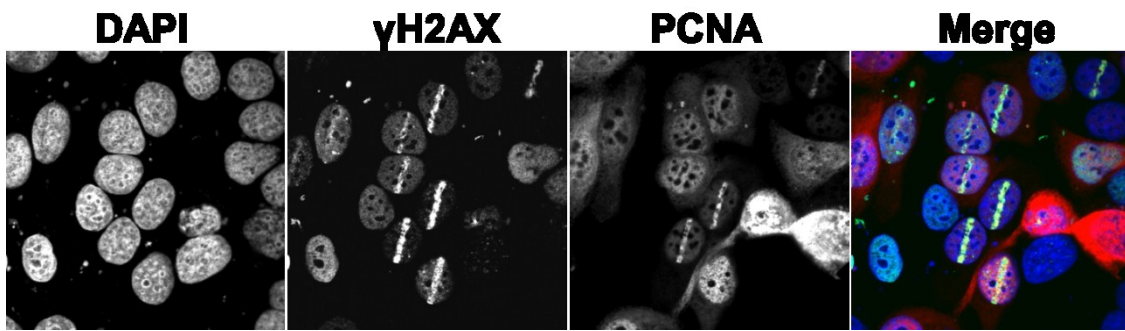
With the aim of studying early events of the SSBR cascade, we first examined the accumulation of SSBR core machinery proteins at sites of laser induced nuclear DNA damage. We employed laser micro-irradiation of HeLa cells that transiently expressed fluorescently tagged versions of PARP1, LIG3, XRCC1, and PNKP (a schematic representation of the fluorescent tagged proteins used in this work is shown in **Figure 14**). We observed rapid accumulation ($t_{1/2} \leq 5.3$ sec) of the proteins at 750 nm damage sites (**Figure 17A**). It is also clear that the retention of the proteins is longer than expected for conventional SSBR, which typically is regarded to have a $t_{1/2} \sim 2$ min¹⁶⁰. Others have similarly observed a long retention time of XRCC1 at laser micro-irradiation tracks¹⁶¹. This may be due to the generation of complex damage in the laser track, and indeed we observed the formation of DSB (using γ H2AX as a marker) under our irradiation conditions (**Figure 17B**), although others found that XRCC1 is rapidly released from DNA damage induced by high LET radiation¹⁶².

Figure 17: Recruitment and retention of SSBR proteins following multi-photon 750 nm laser micro-irradiation

A)



B)



Recruitment and retention of SSB proteins following multi-photon 750 nm laser micro-irradiation. (A) EGFP-PARP1, XRCC1-mGFP and EGFP-LIG3 show near instantaneous recruitment to sites of DNA damage, and PNKP-mGFP is also rapidly recruited. Laser micro-irradiation using multi-photon 750 nm was carried out as outlined in Materials and Methods using HeLa cells expressing fluorescently tagged versions of indicated proteins. Recruitment curves show quantification of signals over the observed time scale starting at the time when the damage is introduced by the laser ($t=0$). Error bars represent S.E.M from 3 independent experiments for a total of 36 individual cells. (B) To ensure that the γ H2AX seen in the laser micro-irradiated tracks did not arise from stalled replication (i.e. conversion of SSB into DSB), non-synchronized HeLa cells transiently expressing mRFP-PCNA (marker for S-phase) were subjected to multi-photon 750-nm laser micro-irradiation as described in experimental procedures (approximately 40 cells were analyzed). Subsequently (5-10 min post laser micro-irradiation) cells were fixed and stained for γ H2AX. A robust signal for γ H2AX was observed in all cells analyzed. A higher magnification of individual cells reveals PCNA distribution in S-phase (upper panel showing punctate PCNA distribution) and in non S-phase cells (lower panel showing a more homogeneous distribution of PCNA outside of the nucleoli). γ H2AX is detected in laser micro-IR tracks in S-phase and non S-phase cells.

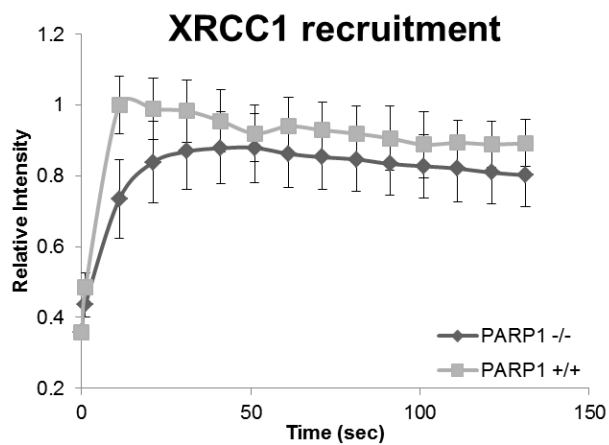
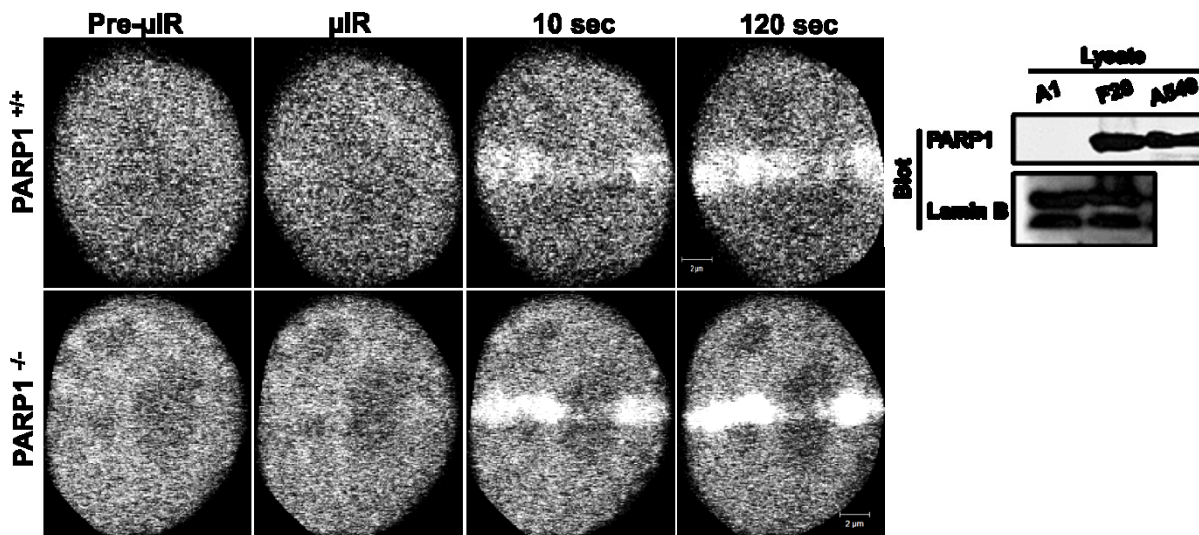
PARP1 mediated poly(ADP-ribosyl)ation accelerates the initial recruitment of SSBR core proteins (XRCC1, LIG3, and PNKP) to sites of DNA damage but is not required for retention

It is known that once PARP1 binds to damaged DNA it rapidly undergoes a conformational change that stimulates its catalytic activity¹⁶³, leading to the formation of PAR polymers that mediate the recruitment of downstream repair factors. To examine the effect of PARP1 on the accumulation of SSBR proteins, we studied the recruitment kinetics of XRCC1 and PNKP to sites of DNA damage in PARP1^{-/-} and PARP1^{+/+} MEFs (**Figure 18**). We observed that the extent of accumulation of both XRCC1 and PNKP in a PARP1^{-/-} background was comparable to that in PARP1^{+/+} MEFs (**Figures 18A and B**). We confirmed the results observed in the PARP1^{-/-} and PARP1^{+/+} MEFs by specific inhibition of PARP1 in HeLa cells. We made use of two chemically unrelated small molecule inhibitors of PARP, AG14361¹⁶⁴ and PJ-34¹⁶⁵, and tested their effects on the recruitment kinetics of SSBR core machinery. We observed that at concentrations of 1 and 2 μ M, AG14361 markedly inhibited the DNA damage-triggered poly(ADP-ribosyl)ation (**Figure 19A**). To delineate the site of damage, cells were also stained with anti- γ H2AX. We then tested the effect of the inhibitor, AG14361, on the recruitment profiles of XRCC1, PNKP and LIG3 in real time (**Figures 19B-D**). All three proteins showed only a briefly delayed recruitment to sites of DNA damage in response to PARP1 inhibition, but displayed a similar accumulation to untreated cells at later time points. We confirmed the results observed with AG14361 using PJ-34 (**Figure 19E**). Our results in PARP1^{-/-} MEFs and in cells treated with PARP1 inhibitors raise the

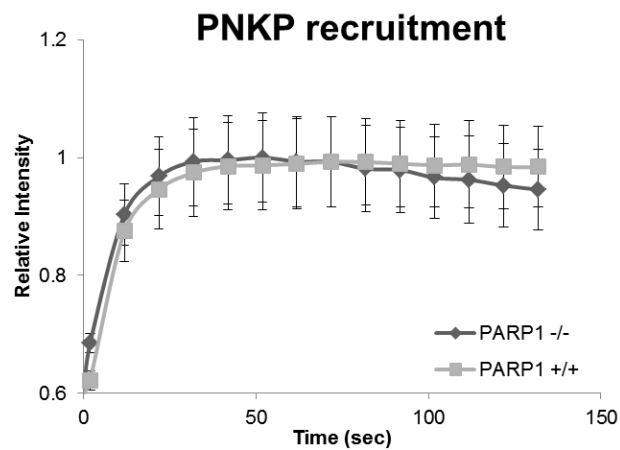
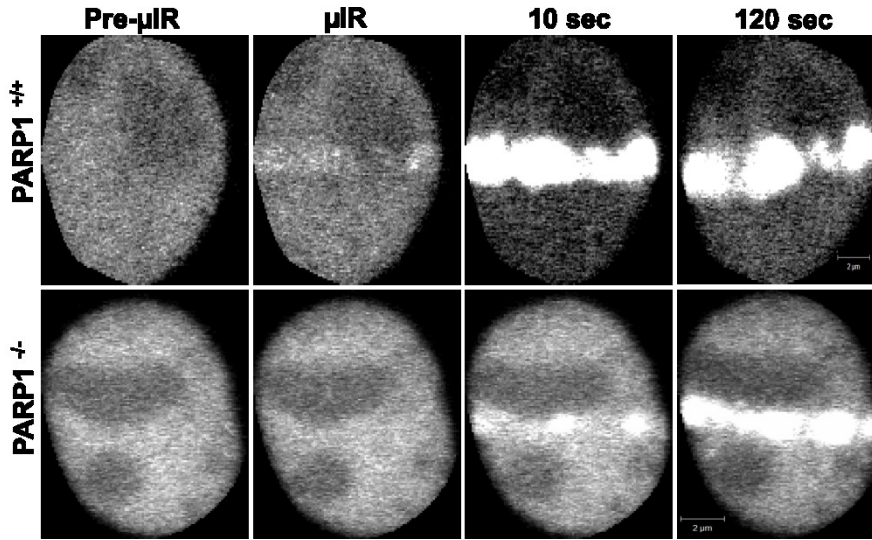
possibility of the presence of an additional sensor or sensors of DNA SSBs apart from PARP1. Therefore we tested the possibility of LIG3 in fulfilling such a role.

Figure 18: Recruitment of XRCC1 and PNKP in PARP1 WT and KO cells

A)



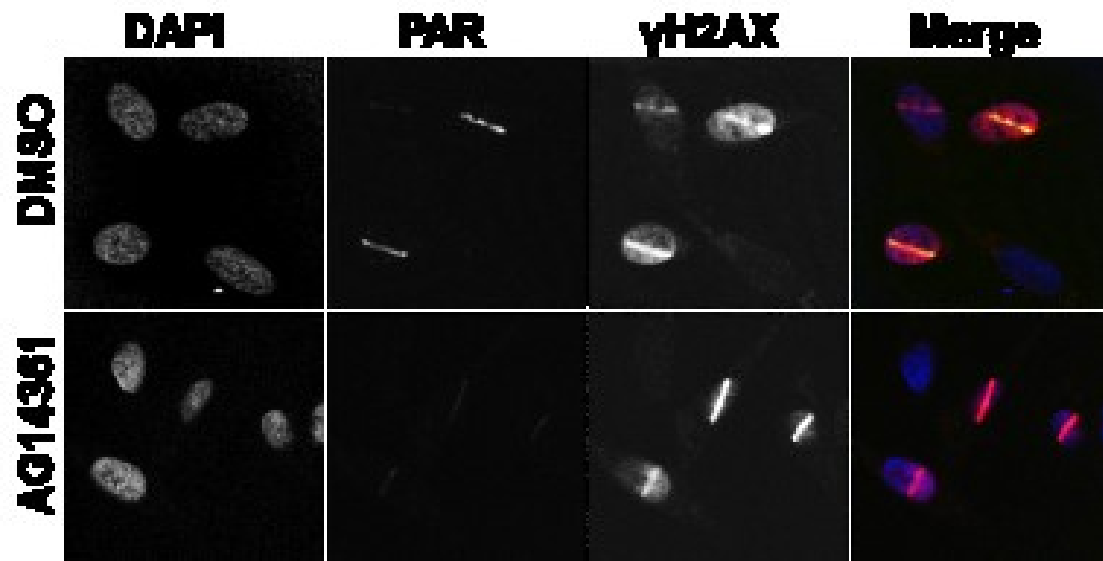
B)



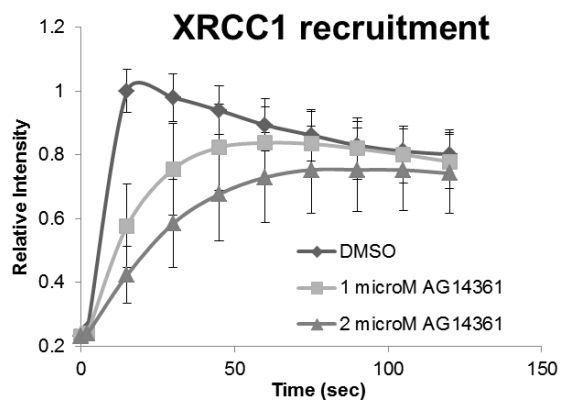
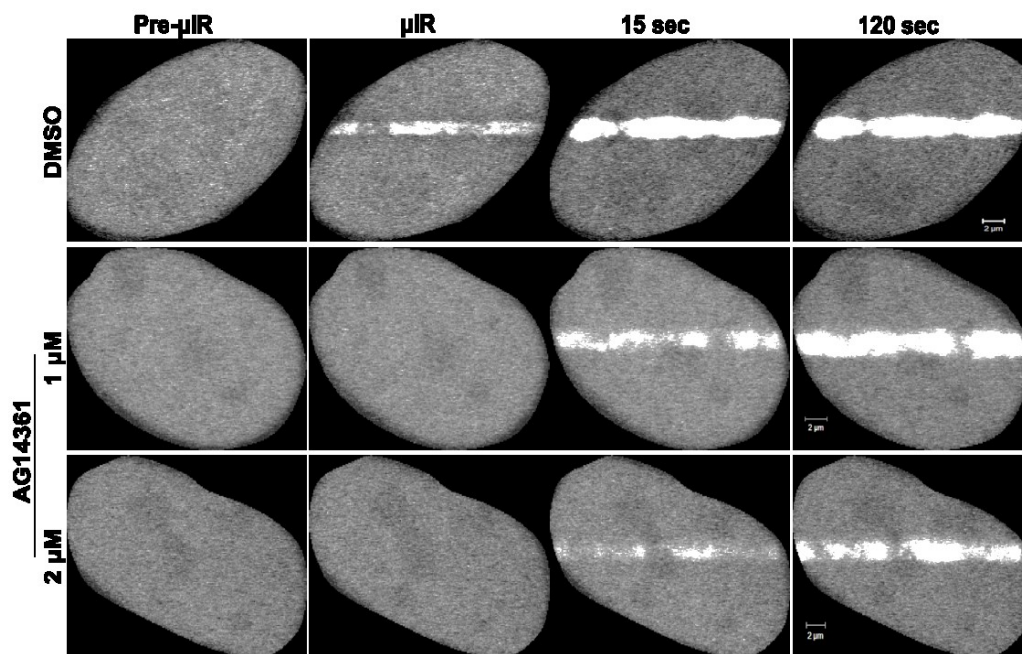
Recruitment of XRCC1 and PNKP in PARP1 WT and KO cells. The recruitment of SSBR proteins was monitored in PARP+/+ and PARP-/- MEFs expressing (A) XRCC1-mGFP (inset shows Western blot showing PARP1 levels in PARP1 WT (F20) and null (A1) MEFs, where A549 lysate was used as a positive control) and (B) PNKP-mGFP subjected to 750 nm multiphoton micro-irradiation. Error bars represent S.E.M from 3 independent experiments for a total of 36 individual cells.

Figure 19: PARP1 inhibition and the recruitment of SSBR proteins to sites of DNA damage

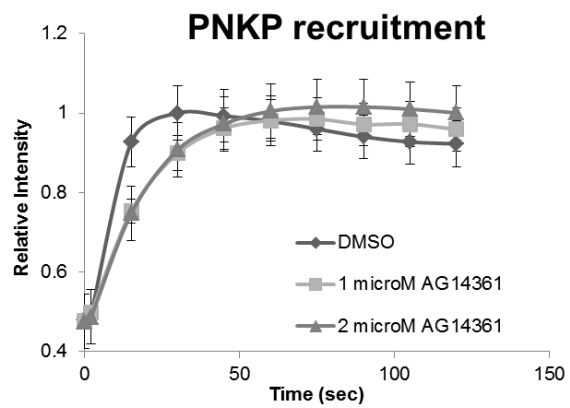
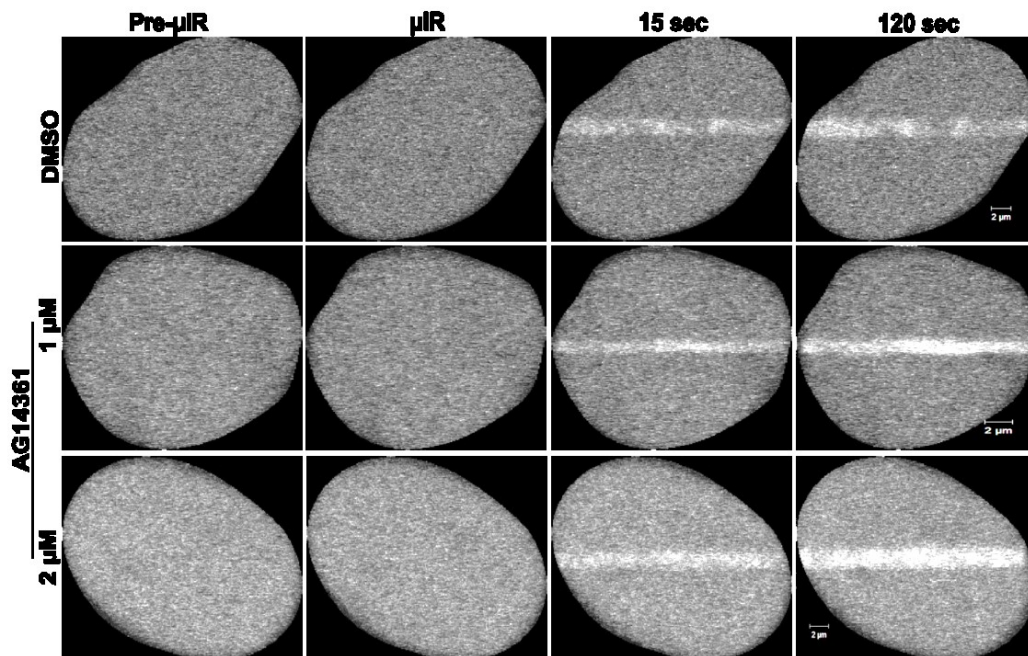
A)



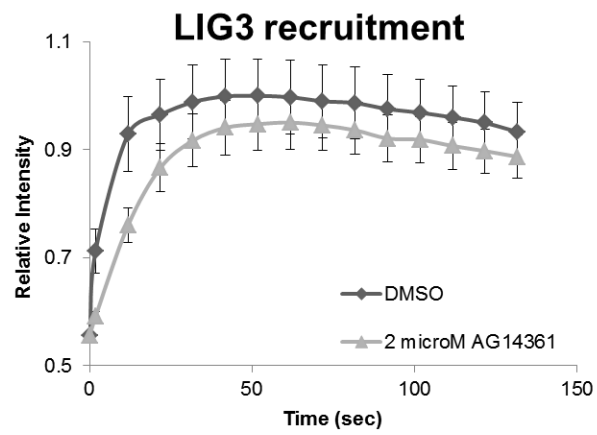
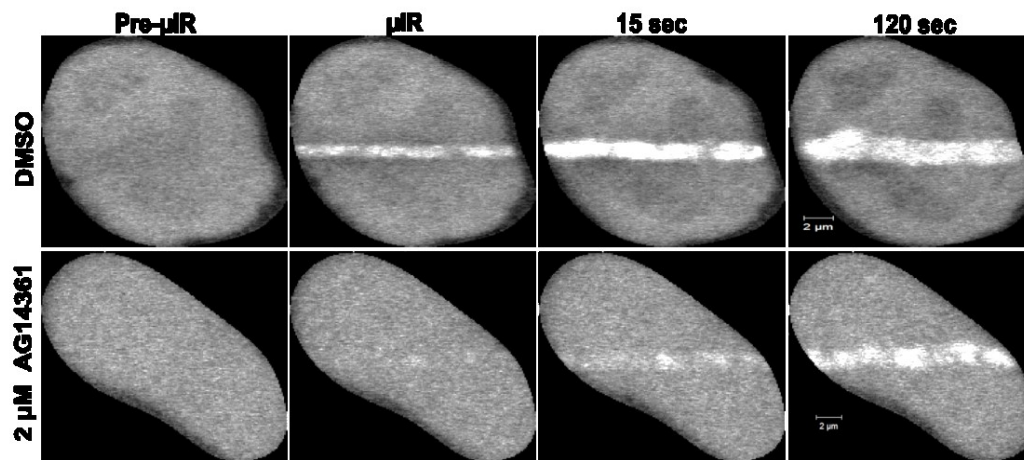
B)



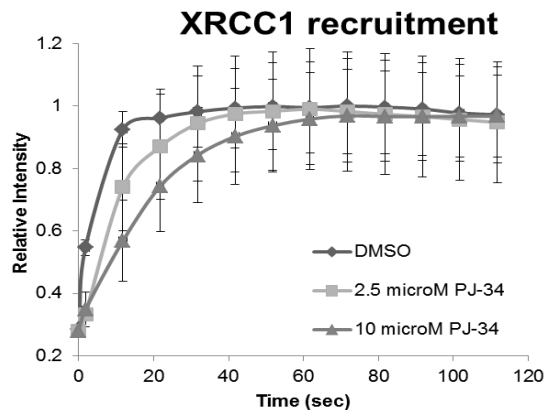
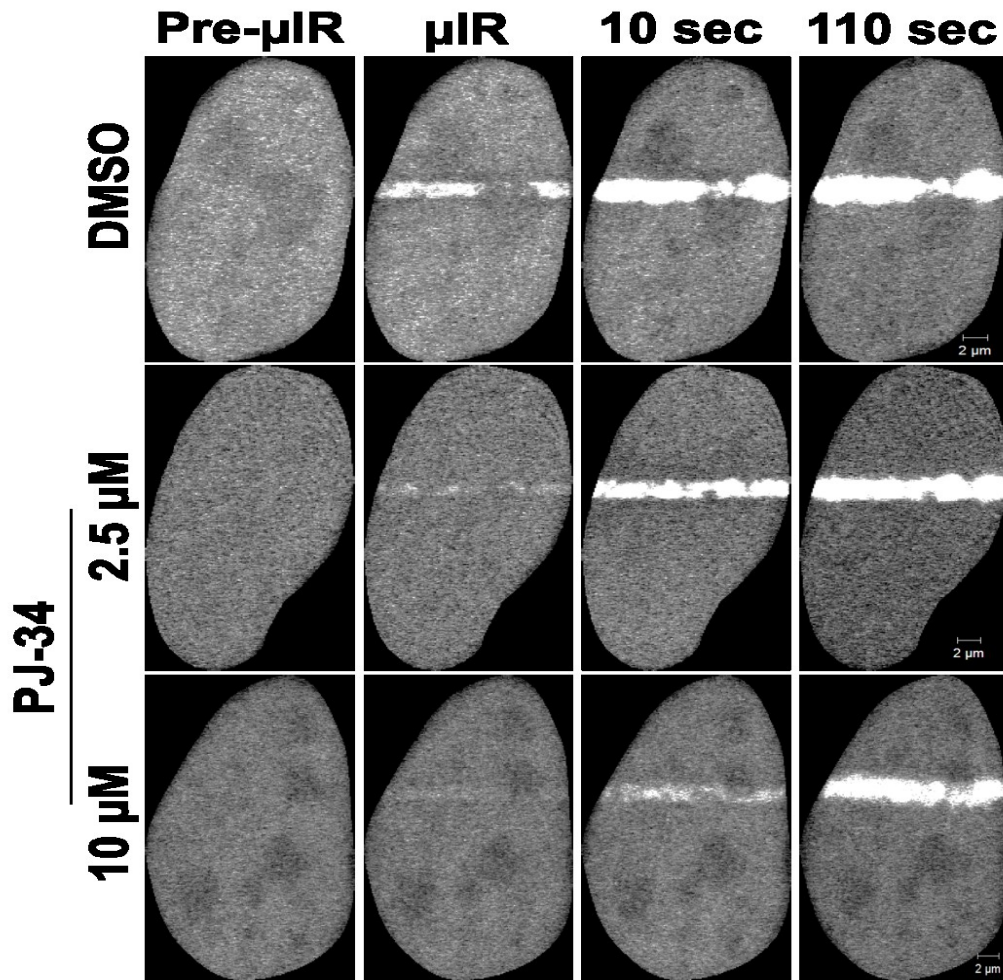
C)



D)



E)



PARP1 inhibition and the recruitment of SSBR proteins to sites of DNA damage. (A) Immunofluorescence staining, showing reduced formation of PAR following laser micro-irradiation in cells pretreated with AG14361. γ H2AX was used as a marker for DNA damage at laser tracks. HeLa cells expressing fluorescently tagged SSBR proteins were treated with the PARP inhibitor, AG14361, and then subjected to laser micro-irradiation. PARP inhibition only affected early recruitment events of (B) XRCC1, (C) PNKP and (D) LIG3 with almost no effect on the late events of accumulation of all the proteins at sites of DNA damage. For recruitment curves, error bars represent standard error of mean from 3 independent experiments for a total of 36 individual cells. (E) Confirmation of the PARP inhibition results using a different PARP inhibitor, PJ-34. For each recruitment curve, error bars represent S.E.M; $n= 24$

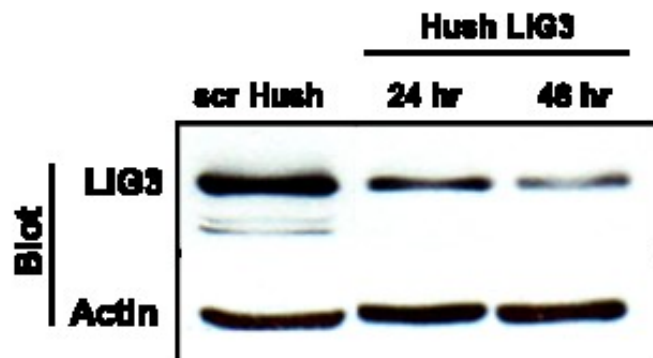
The influence of LIG3 on the recruitment of SSB core machinery

To test for the possible involvement of LIG3 in mediating the accumulation of other SSB proteins to DNA repair sites, we monitored the recruitment kinetics of PNKP and XRCC1 in response to DNA damage under conditions of reduced LIG3 expression (**Figure 20A**). To knock down LIG3, we made use of the shRNA plasmids that co-express a GFP reporter, facilitating the identification of knockdown cells within the population. In contrast to the effect of PARP1 inhibition, the transient knockdown of LIG3 decreased the level of PNKP and XRCC1 recruited to sites of DNA damage over the time frame examined (**Figures 20B and C**). We then determined if LIG3 and PARP1 are redundant SSB sensors by examining the effect of simultaneous inhibition of PARP1 and depletion of LIG3 on the accumulation of PNKP (**Figure 20D**). As noted above, PARP1 inhibition alone caused an initial deceleration in the recruitment of PNKP at sites of DNA damage while reduced LIG3 expression alone resulted in a sustained decrease of the level of PNKP that accumulated at sites of DNA damage. The simultaneous lack of PARP1 activity and lowered LIG3 expression had an additive effect on the observed decreased accumulation of PNKP. This indicates that PARP1 and LIG3 function in a non-redundant manner, possibly because they recognize different subsets of SSBs. To further confirm that there is no redundancy between PARP1 and LIG3, we monitored the accumulation of endogenous LIG3 at sites of DNA damage in response to PARP1 inhibition using two different DNA damage treatments, laser micro-irradiation and H₂O₂. Following laser micro-irradiation, endogenous LIG3 showed robust accumulation at tracks of induced DNA damage despite the substantial reduction in PAR production as a result of AG14361 treatment. Similarly, endogenous

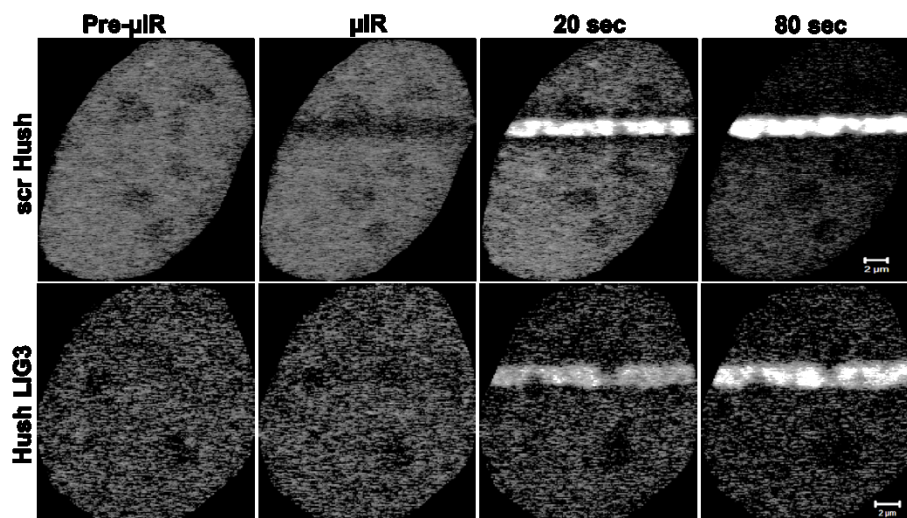
XRCC1 accumulated at tracks of DNA damage in AG14361 treated cells (**Figure 21A**). We were also able to demonstrate that in response to H₂O₂ induced DNA damage, LIG3 exhibited a unique pattern of distribution that was not affected by the efficient inhibition of PARP1 catalytic activity (**Figure 21B**). To rule out the possibility that this pattern of LIG3 might be attributed to its recently discovered role in DSB¹⁶⁶, we examined whether LIG3 would colocalize or not with the different DSB markers γ H2AX and 53BP1 under conditions of PARP1 inhibition. As shown in (**Figure 21C and D**), LIG3 did not colocalize with either γ H2AX or 53BP1 indicating that LIG3 distribution in response to H₂O₂ is mainly associated with response to SSBs.

Figure 20: LIG3 knockdown and the recruitment of XRCC1 and PNKP to sites of DNA damage

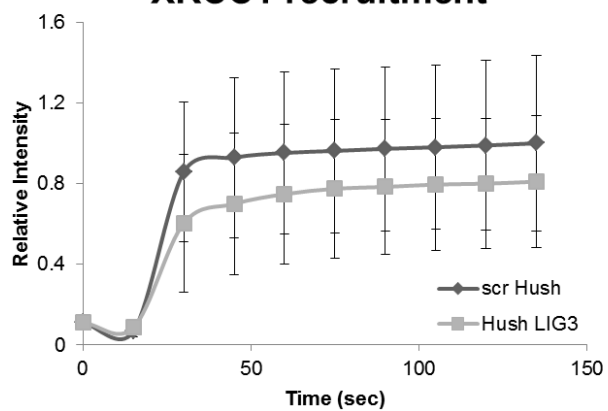
A)



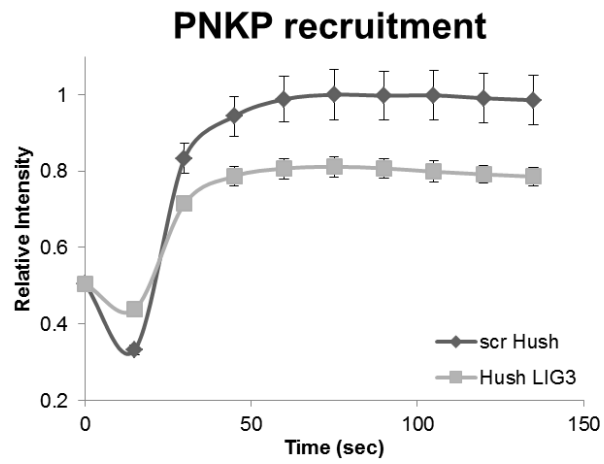
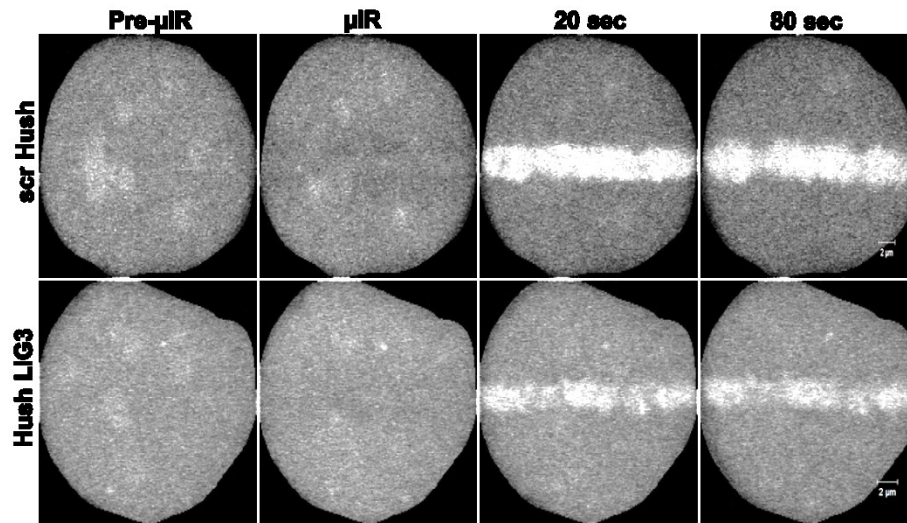
B)



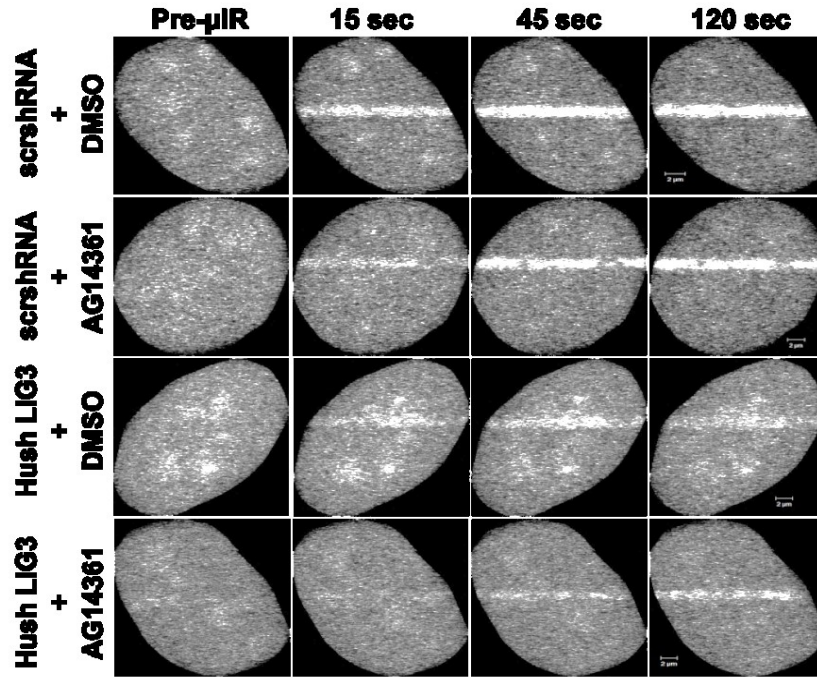
XRCC1 recruitment



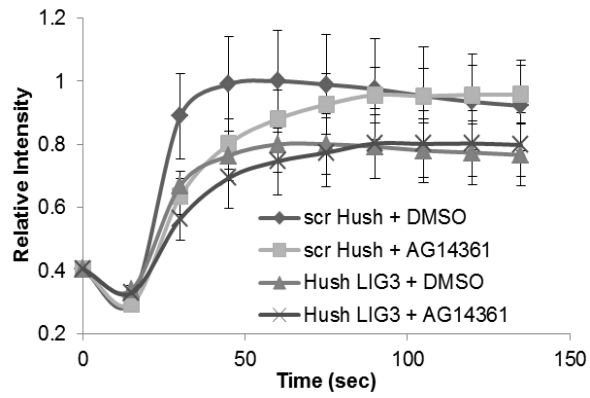
C)



D)

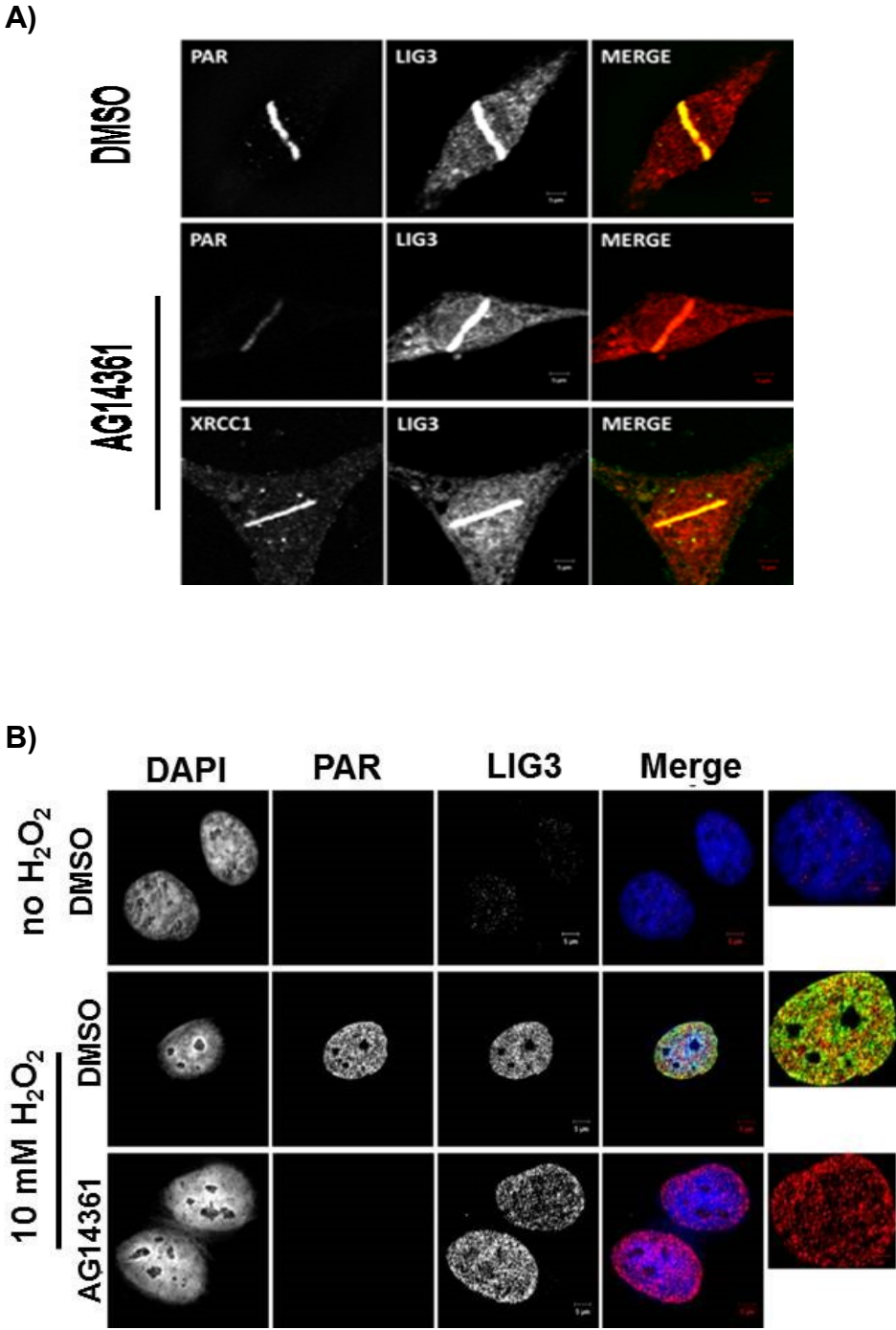


PNKP recruitment

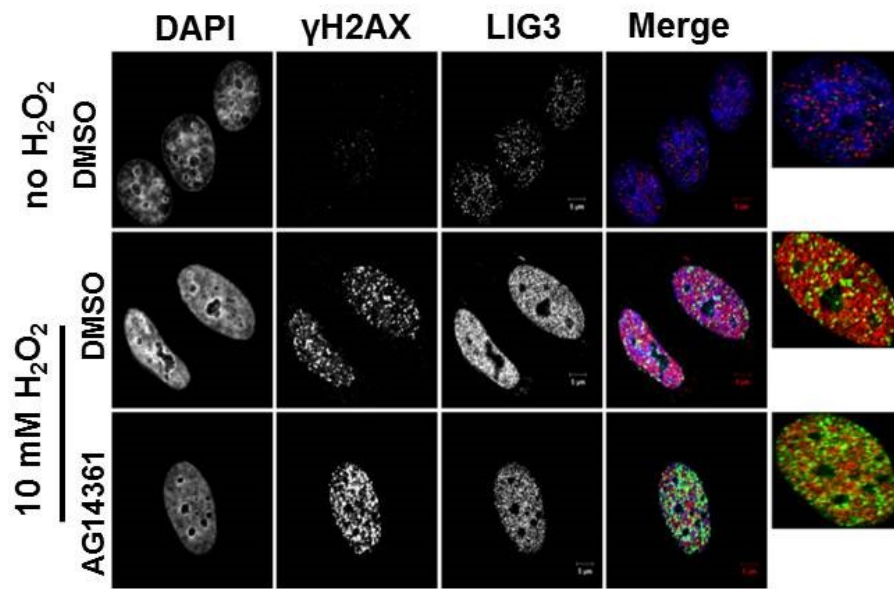


LIG3 knockdown and the recruitment of XRCC1 and PNKP to sites of DNA damage. Laser micro-irradiation was performed on HeLa cells expressing reduced levels of LIG3 (A) and (B) XRCC1-mRFP or (C) PNKP-mRFP. Reduced background levels of LIG3 lead to decreased overall recruitment of XRCC1 and PNKP to sites of DNA damage. (D) Simultaneous inhibition of PARP1 (using AG14361) and knockdown of LIG3 showed an additive effect on the reduction of the amount of PNKP recruited to sites of DNA damage. For recruitment curves, error bars represent S.E.M from 3 independent experiments for a total of 36 individual cells. Note that the mRFP photobleaches during laser micro-irradiation resulting in an initial loss of fluorescence at the damage sites.

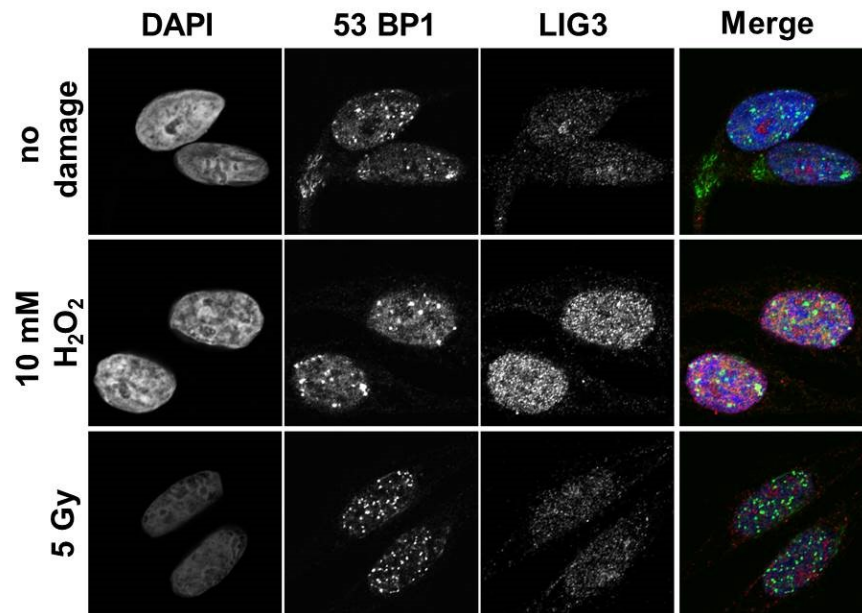
Figure 21: LIG3 and PARP1 are non-redundant damage sensors



C)



D)



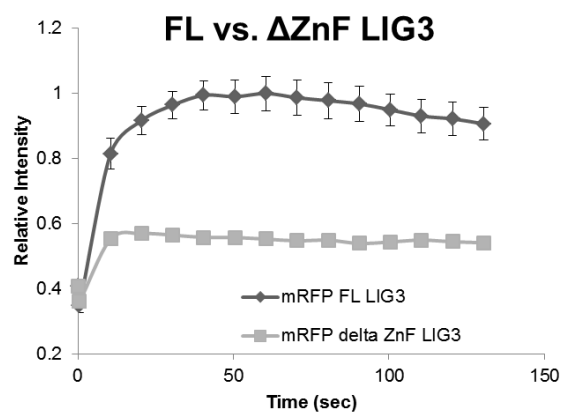
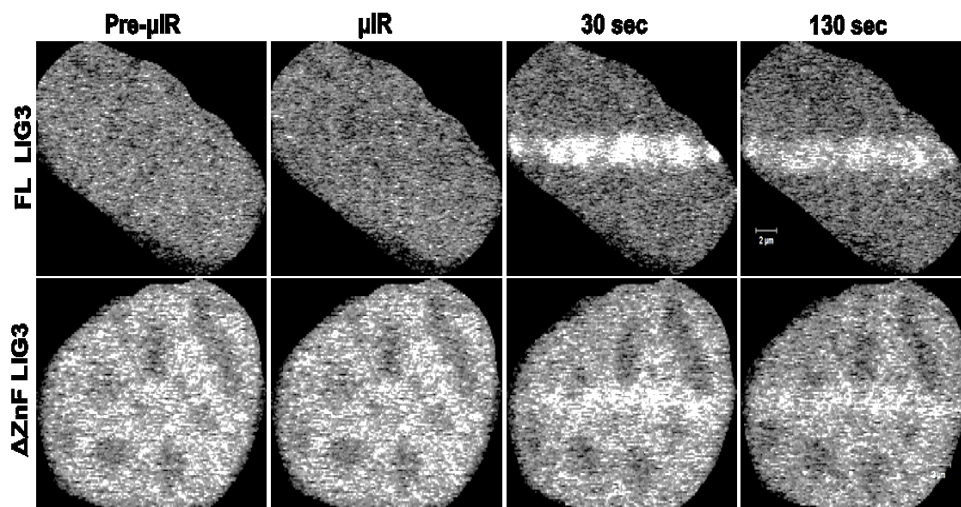
LIG3 and PARP1, distinct damage sensors. Endogenous LIG3 shows robust accumulation at sites of DNA damage created by either (A) laser micro-irradiation or (B) by 10 mM H₂O₂ even upon pre-treatment of cells with 1 and 2 μM AG14361. (C and D) LIG3 did not co-localize with γH2AX (universal DSB marker) or 53BP1 (NHEJ DSB marker). For AG14361 treatments, cells were incubated with either 1 or 2 μM drug at 37°C for 1-2 h, then cells were either subjected to laser micro-irradiation (see Materials and Methods), or treated with 10 mM H₂O₂ for 10 min, then fixed and stained for immunofluorescence.

ZnF domain, a nick sensor in LIG3

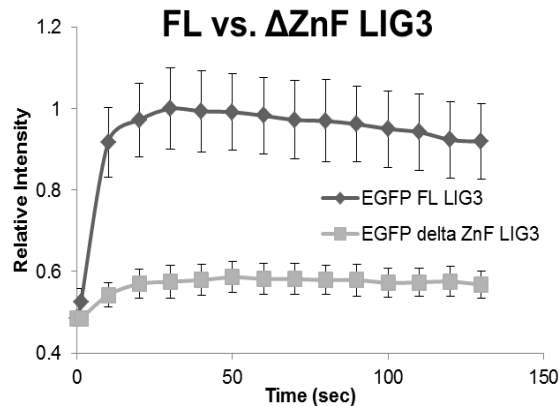
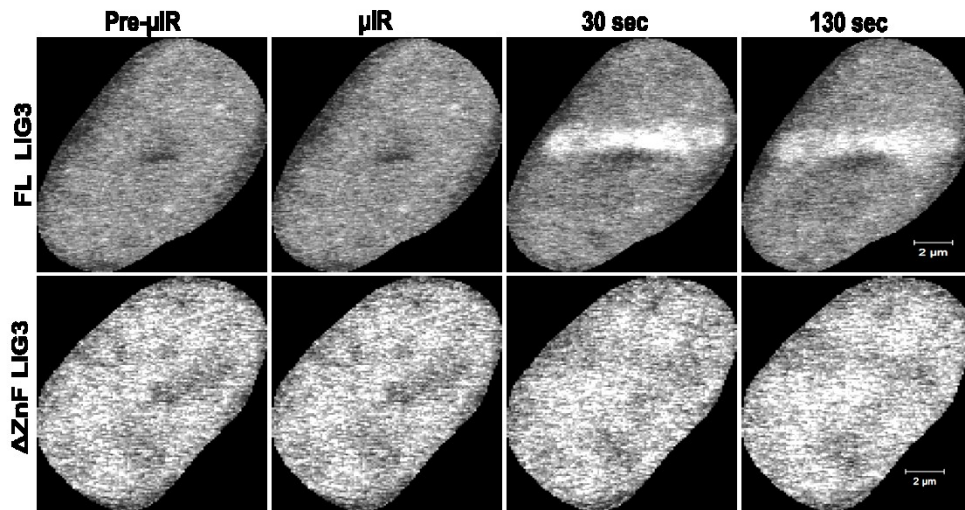
We extended our investigation of LIG3 to identify which domain(s) is required for its SSB sensor function. Previous biochemical studies have suggested that the N-terminal ZnF domain of LIG3 might be a candidate for this role ^{125,126}. To test the importance of this domain in the recruitment of LIG3 in live cells, we directly compared the recruitment kinetics of full length LIG3 and LIG3 lacking the ZnF domain (Δ ZnF-LIG3) to sites of DNA damage induced by laser micro-irradiation. In contrast to previous work that showed no difference in the recruitment to sites of DNA damage between both forms of LIG3 ¹²⁹, both fluorescent tagged versions (EGFP and mRFP) of Δ ZnF-LIG3 exhibited a significantly decreased level ($p < 0.05$) of recruitment compared to full length LIG3 (**Figure 22A**) under our experimental conditions. The residual recruitment of Δ ZnF-LIG3 to sites of DNA damage might reflect the BRCT domain-mediated interaction of LIG3 with XRCC1, which was observed to be required for the final nick sealing event in SSBR ¹⁶⁷. To test this, we expressed both full length LIG3 and Δ ZnF-LIG3 in EM9 cells (a CHO cell line devoid of XRCC1) and compared the recruitment profiles of both proteins in the absence of XRCC1. Consistent with our hypothesis, the Δ ZnF-LIG3 showed severely reduced recruitment at laser damaged DNA tracks (**Figure 22B**) while full length LIG3 accumulated at laser damaged tracks in the absence of XRCC1. The latter observation was surprising because it implies that recruitment of LIG3 to strand breaks can occur independently of XRCC1.

Figure 22: Comparison between the recruitment of full length LIG3 and LIG3 lacking the zinc finger to sites of DNA damage

A)



B)



Comparison between the recruitment of full length LIG3 and LIG3 lacking the zinc finger to sites of DNA damage. (A) HeLa cells or (B) EM9 cells expressing full length (FL) LIG3 or mutant Δ ZnF LIG3 were subjected to laser micro-irradiation. In HeLa cells FL LIG3 was robustly recruited to sites of DNA damage while Δ ZnF LIG3 was recruited less efficiently. Furthermore, FL-LIG3 was recruited to sites of DNA damage even in the absence of XRCC1 (EM9 cells) while Δ ZnF-LIG3 could not. For recruitment curves, error bars represent S.E.M.; $n=36$. Both cell lines were tested with mRFP and EGFP-tagged proteins and the tags were shown not to influence the result.

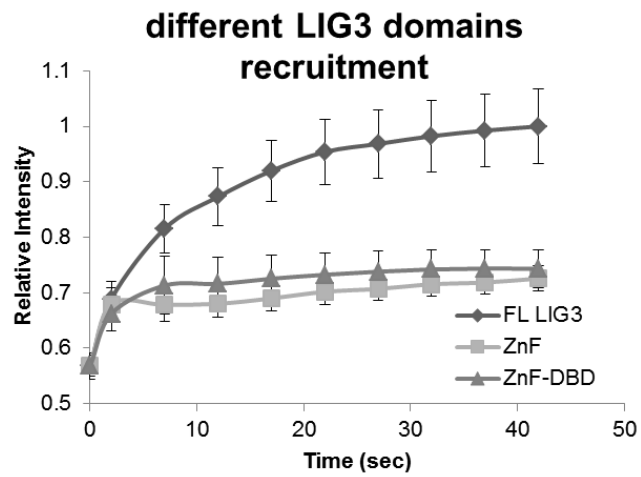
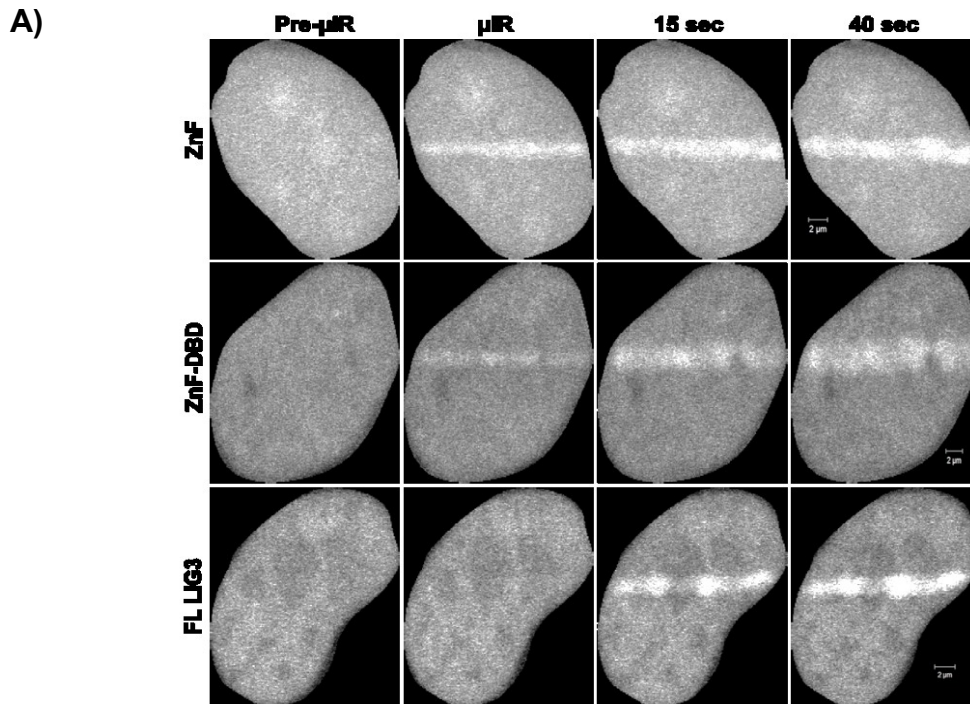
ZnF domain is sufficient for the initial rapid recruitment of LIG3 to sites of DNA damage

We next asked whether the ZnF domain is sufficient for recruitment to sites of DNA damage. Biochemical evidence indicated that LIG3 possesses two distinct SSB-sensing modules, the first of which mediates sensing distortions in the DNA backbone (early sensing function) and is comprised of the ZnF and a DNA binding domain (DBD). *In vitro*, these two domains within this module have been shown to function cooperatively to promote efficient SSB sensing/DNA binding and then the second SSB-sensing module (the catalytic core) mediates subsequent repair of SSBs¹²⁶. Therefore, we examined the behaviour of the domains of the early SSB-sensing function in live cells. Accordingly, we designed EGFP constructs encoding the ZnF and the ZnF-DBD (**Figure 23A**) and tested the recruitment of these domains to sites of DNA damage introduced by laser micro-irradiation. We observed that both ZnF alone as well as the tandem module ZnF-DBD are rapidly recruited to sites of DNA damage in live cells similar to that shown by full length LIG3, providing evidence that the *in vitro* SSB-sensing functions can also operate *in vivo*. However, the steady accumulation of the ZnF and ZnF-DBD domains after the initial response is considerably lower than full length LIG3. This is consistent with protein-protein interactions occurring outside the ZnF and DBD domains being responsible for generating most of the binding sites responsible for the retention of LIG3. Nonetheless, the results clearly indicate that the ZnF domain is capable of recognizing and binding the damage site independent of other domains within LIG3. To examine whether ZnF recruitment to damaged DNA is mediated by direct DNA binding or not, we examined the recruitment of a ZnF mutant

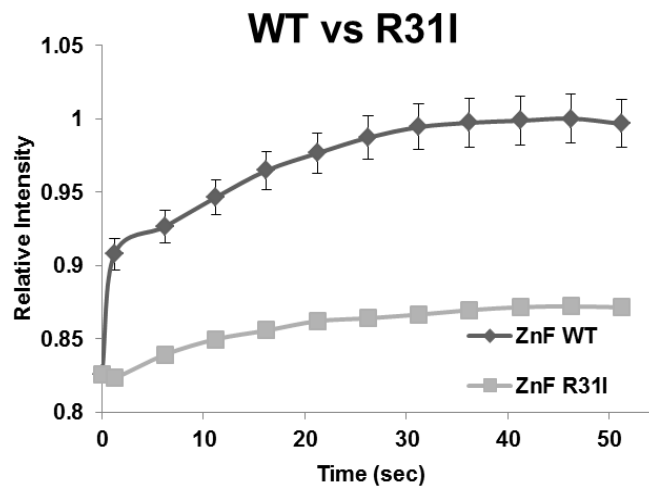
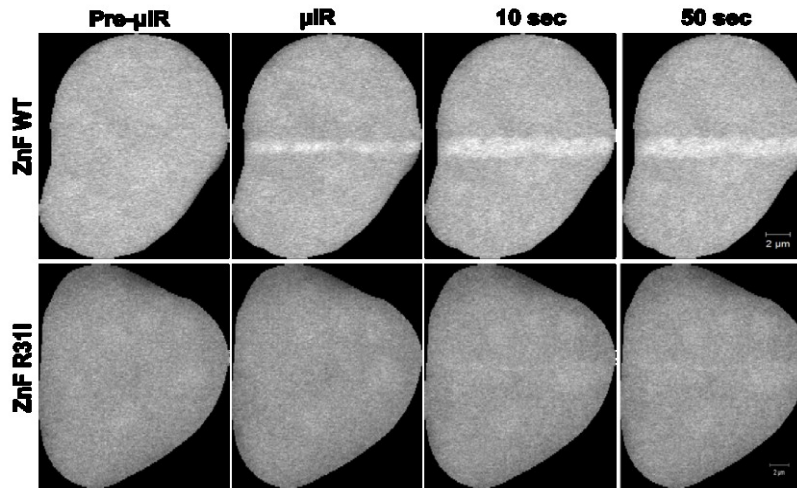
that was reported to lose its DNA binding without impacting the conformation of the ZnF, ZnF R31I¹⁶⁸. Compared to WT ZnF, the ZnF domain R31I mutant showed a significantly reduced recruitment ($p < 0.05$) to sites of DNA damage introduced by laser micro-irradiation (**Figure 23B**).

If the ZnF functions in damage sensing, then overexpression of this domain alone may slow the kinetics of SSBR by competing with the endogenous machinery without being able to support the protein-protein interactions necessary to repair the break. To test this, we carried out an alkaline comet assay on cells overexpressing GFP (control vector) or GFP-ZnF (**Figure 23C**). Control cells showed rapid repair after 1 h recovery after damage. Clearly, repair was impaired in cells overexpressing ZnF, as judged by the tail moments at 1- and 2-h recovery time points, indicating that this domain can function in a dominant negative manner to impede SSBR.

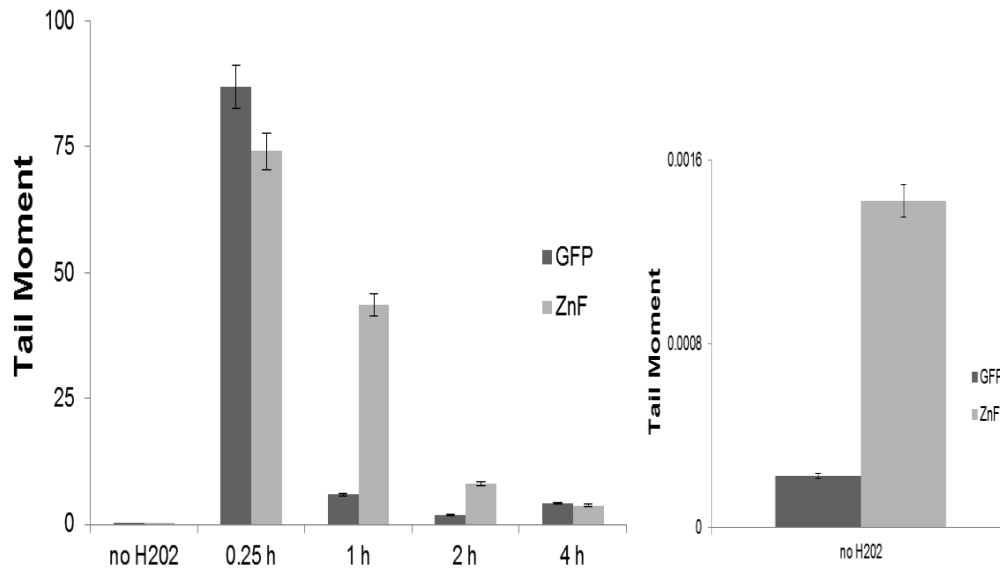
Figure 23: The ZnF domain is required and sufficient for the damage sensing function of LIG3



B)



C)



The ZnF domain is required for the damage sensing function of LIG3. (A)

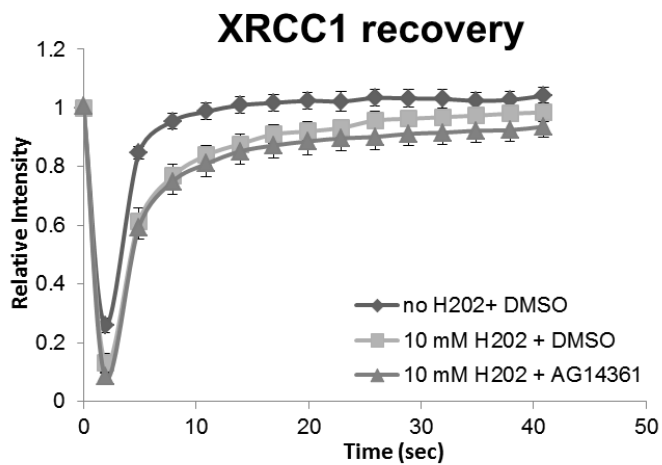
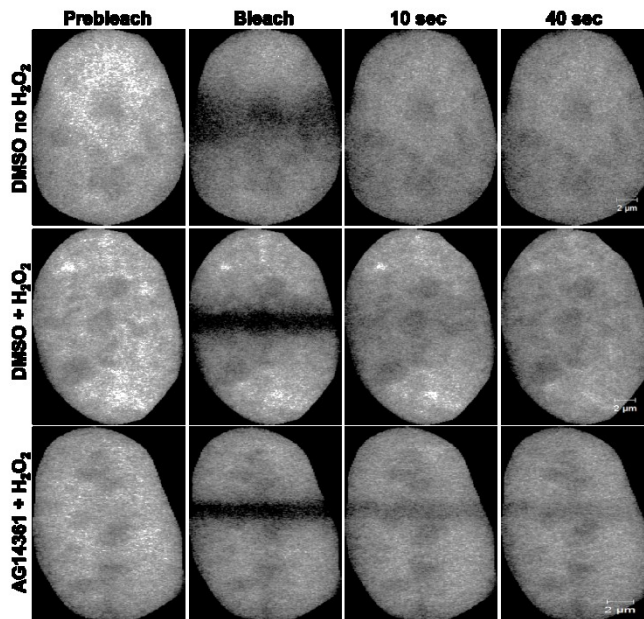
Comparison of the recruitment of fluorescently tagged full length (FL) LIG3 and the ZnF and ZnF-DBD domains of LIG3 to micro-irradiated DNA in HeLa cells. (B) Comparison of recruitment of wild-type (WT) and the DNA binding mutant of ZnF-R31I to micro-irradiated DNA in HeLa cells. For recruitment curves shown in A and B, bars represent S.E.M; $n=36$. (C) Expression of the ZnF domain of LIG3 retards single-strand break repair. HeLa cells expressing either the GFP-ZnF or GFP alone (control) were treated with 100 μ M hydrogen peroxide for 40 min on ice and then strand break repair was monitored by the alkaline comet assay and quantification of tail moments at the indicated time points as described in Materials and Methods. Expanding the ordinate (plot on the right hand side) showed that even in the absence of the hydrogen peroxide the ZnF expressing cells exhibit a slightly higher background level of damage.

Retention kinetics of SSB proteins at damaged DNA is PAR independent

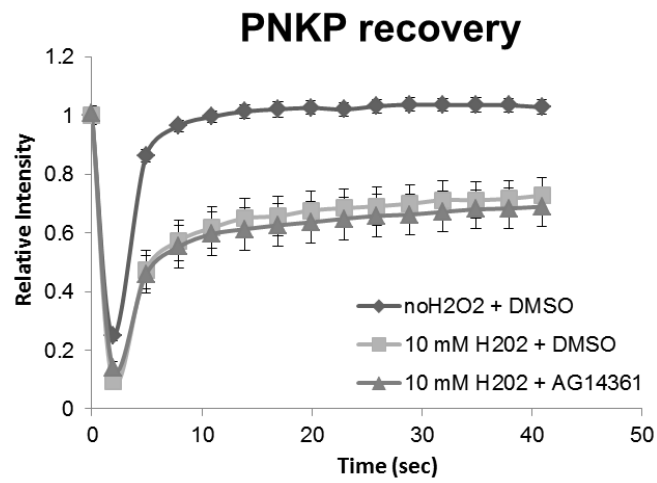
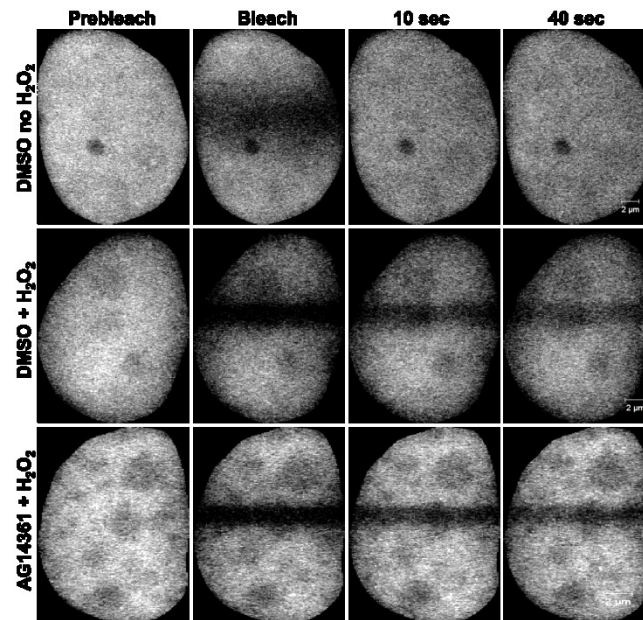
Having demonstrated that PARP1 catalytic activity is dispensable for the recruitment of SSB core machinery proteins to sites of DNA damage and that LIG3 appears to be an alternative SSB sensor, we asked if PARP1-mediated poly(ADP-ribosylation) (PARylation) might affect the binding kinetics of LIG3, PNKP, and XRCC1 to damaged DNA in live cells. We therefore carried out fluorescence recovery after photobleaching (FRAP) experiments to study the recovery kinetics of fluorescently-tagged versions of these proteins in cells treated with H₂O₂ in the absence and presence of 2 μM AG14361. Consistent with their roles in the SSB pathway, all three proteins showed a slower recovery in response to H₂O₂ treatment. In these experiments, a significant reduction ($p < 0.05$) in mobility arises when the fluorescent molecules bind to substrates that are essentially immobile on the time scale of min. Consequently, these experiments detect binding to damaged DNA. Surprisingly, inhibition of PARP1 catalytic activity using 2 μM AG14361 did not significantly impact (p -values > 0.05) on the recovery kinetics of the SSB factors during the ongoing repair process (**Figure 24A-C**). The latter observation implies that the core SSB proteins under study bind directly to the damaged DNA independent of the formation of PAR polymer. To further validate our hypothesis and previous results regarding the role of the ZnF domain of LIG3, we compared the recovery kinetics of full length LIG3 and Δ ZnF-LIG3. Both proteins showed reduced mobility in the presence of DNA damage, although Δ ZnF-LIG3 recovered more rapidly than that of full length LIG3 (**Figure 24D**). This result indicates that both the ZnF and domains outside of the ZnF contribute to the retention of LIG3 at SSBs.

Figure 24: PARP1 inhibition and the retention of SSBR proteins at sites of DNA damage

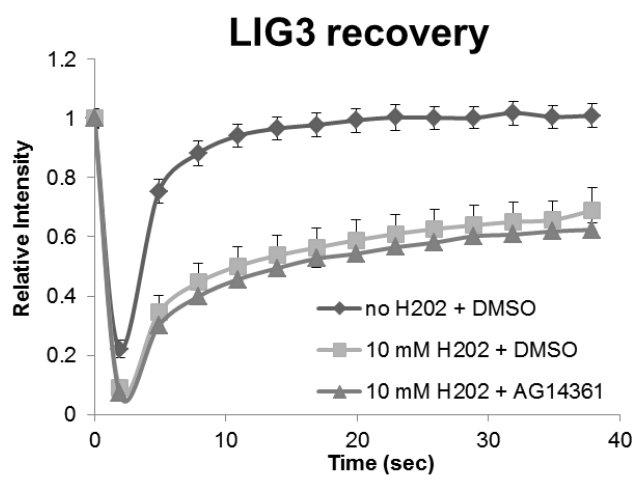
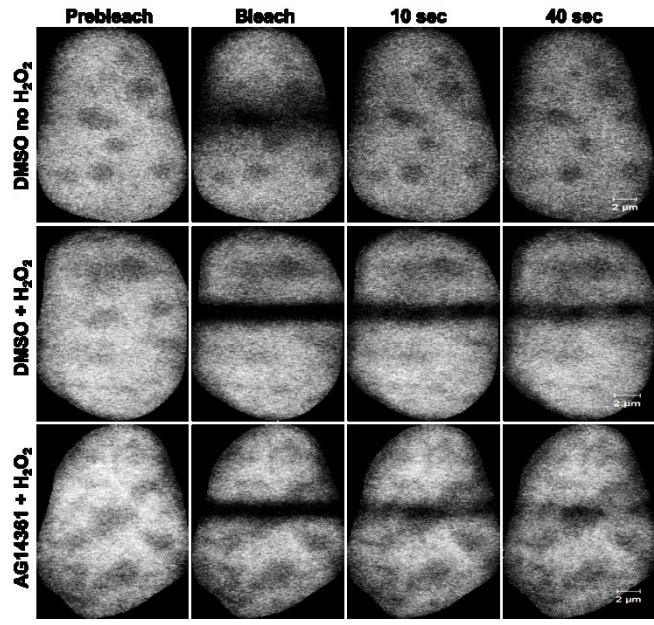
A)



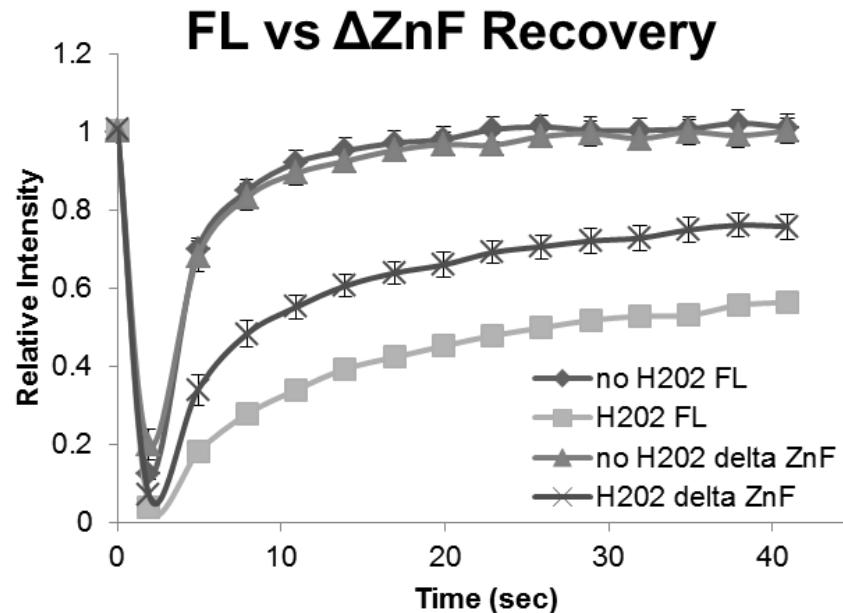
B)



C)



D)



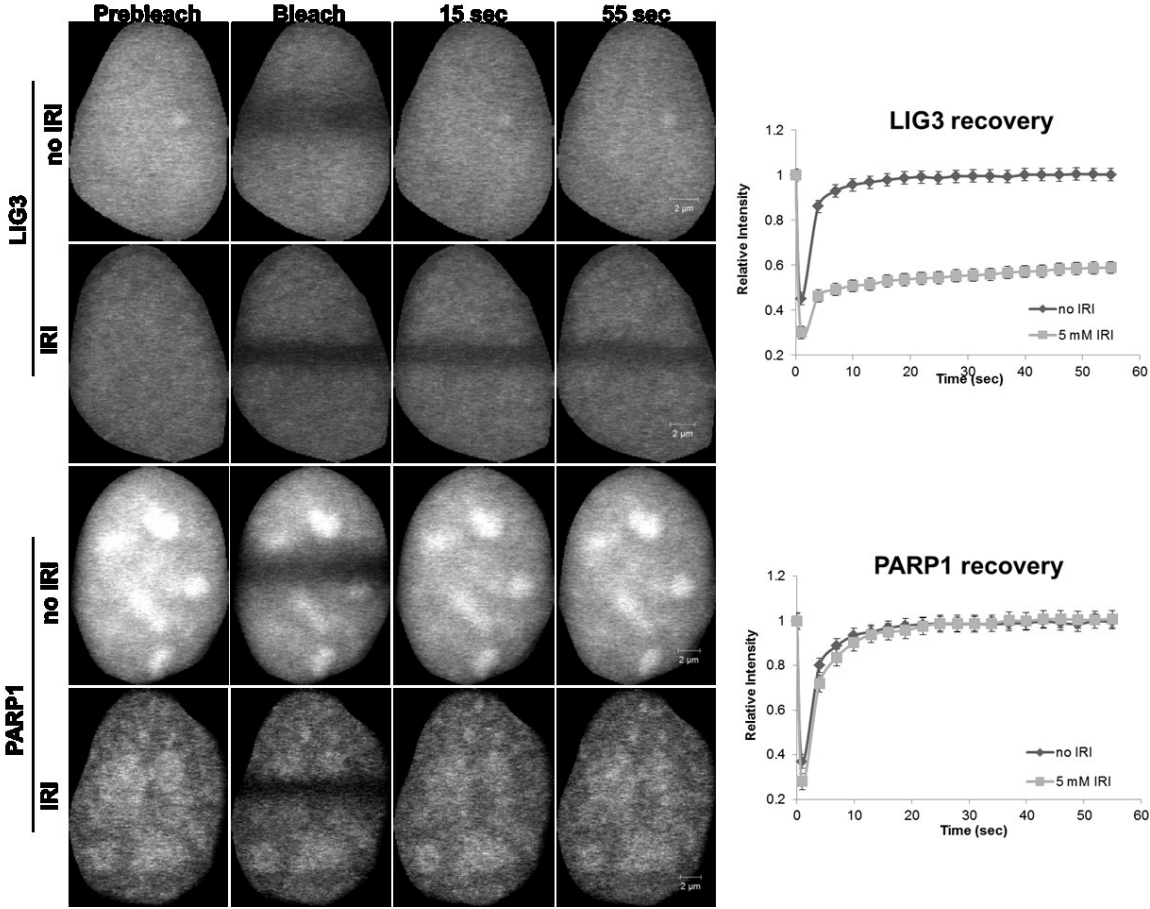
PARP1 inhibition and the retention of SSBR proteins at sites of DNA damage. FRAP analysis on HeLa cells expressing GFP tagged (A) XRCC1, (B) PNKP and (C) LIG3 respectively before and after DNA damage with 10 mM hydrogen peroxide in the absence and presence of 2 μ M AG14361 as described in experimental procedures. “Prebleach” indicates no photobleaching and “Bleach” is the 0 second time point. For recovery curves, error bars represent S.E.M; $n=24$. (D) FRAP analysis showing differences in binding kinetics in response to H₂O₂ damage between FL-LIG3 and Δ ZnF-LIG3. Error bars represent S.E.M; $n=24$.

LIG3 and not PARP1 functions as a nick sensor in live cells

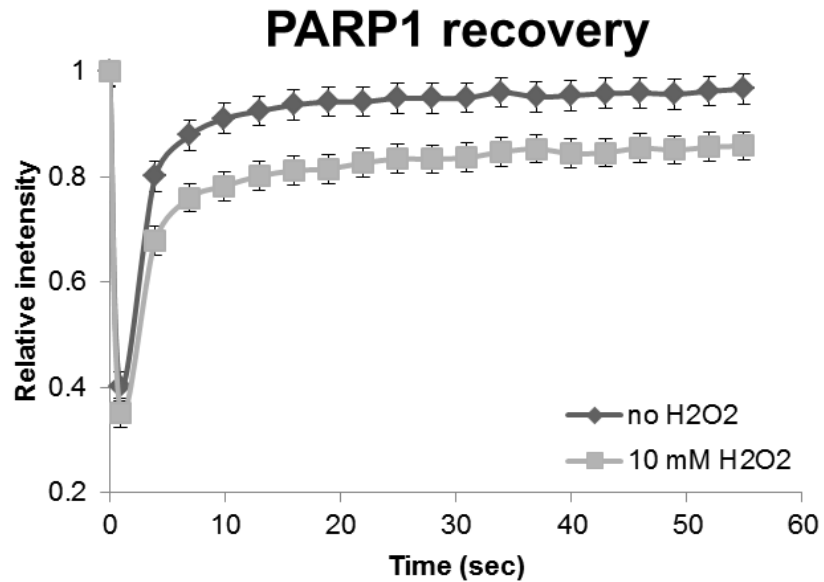
To generate SSB comprising only nicks, as opposed to gaps, cells were treated with irinotecan (IRI), a topoisomerase 1 poison, which generates abortive topoisomerase-1 cleavage complexes in the DNA. The resolution of such abortive complexes requires the action of TDP1, which removes the covalently bound topoisomerase from the DNA leaving nicks with 3'-phosphate and 5'-OH termini ⁸¹. Following exposure of the cells to IRI, we compared the recovery kinetics in photobleaching experiments of both PARP1 and LIG3. Surprisingly, PARP1 recovery was not significantly reduced ($p > 0.05$) in response to IRI treatment, but, LIG3 recovery was substantially retarded ($p < 0.05$) (**Figure 25A**). This result indicates that PARP1 may not recognize nicks but LIG3 clearly does, which is consistent with our prediction that LIG3 functions as a nick sensor in cells.

Figure 25: LIG3 is an *in vivo* nick sensor for irinotecan induced DNA damage

A)



B)



LIG3 is an *in vivo* nick sensor for irinotecan induced DNA damage. (A) FRAP analysis showing differences in binding kinetics after 5 mM irinotecan (IRI) treatment in HeLa cells expressing PARP1 and LIG3. “Prebleach” indicates no photobleaching and “Bleach” is the 0 second time point. Error bars represent S.E.M; $n=24$. (B) FRAP analysis showing the differences in binding kinetics of PARP1 in the presence and absence of DNA damage introduced by H₂O₂. Error bars represent S.E.M; $n=24$.

DISCUSSION

Indications of an alternative SSB sensor to PARP1

The purpose of this study was to elucidate the mechanisms of recruitment and retention of the SSB proteins, PARP1, XRCC1, PNKP and LIG3 to sites of SSBs in live cells using the combination of laser micro-irradiation and FRAP experiments. We initially established that the multi-photon excitation conditions we employed appeared to strongly activate SSBR but only weakly activate BER, as judged by the lack of production of one of the most abundant base lesions, 8-oxoguanine, and the minimal recruitment of OGG1, which is a DNA glycosylase that removes 8-oxoguanine, and the L360D mutant of XRCC1, which has a marked preference for BER over SSB¹⁰⁹. In agreement with Campalans et al.¹⁰⁹, we observed that 405 nm micro-irradiation in the presence of dye (in their case Ro-19-8022 and in our experiments Hoechst 33258) activated the BER pathway.

A large body of data has led to the current model of the SSBR pathway, in which PARP1 plays a leading role in sensing strand breaks and signaling their presence to enhance recruitment of the other SSB proteins^{103,104,158,159,169}. Surprisingly, we found that loss or inhibition of PARP1 led to only slightly delayed, rather than completely inhibited, recruitment of the other SSB proteins.

Previous *in vitro* biochemical studies have demonstrated that LIG3 binds with high affinity to model DNA substrates containing SSBs^{125,126}. Consequently, we examined the potential of LIG3 to contribute to the recruitment of the core SSBR machinery. We found that partial knockdown of LIG3, while not eliminating XRCC1 or PNKP

recruitment, did significantly reduce ($p < 0.05$) the accumulation of XRCC1 and PNKP at DNA damage sites. When an inhibitor of PARP1 was combined with shRNA directed against LIG3, we found that the recruitment was both delayed, which can be seen with PARP1 inhibition alone, and reduced in the total amount accumulated, which can be seen with LIG3 shRNA alone, suggesting that the two proteins act independently and additively as SSB sensors.

To further define the potential of LIG3 to act as a sensor for SSBs *in vivo*, we examined the ability of the LIG3 ZnF, which is homologous to ZnF2 of PARP1, and the LIG3 ZnF-DBD alone to recruit to sites of DNA damage. These have previously been shown to bind nicked DNA *in vitro*¹²⁶. We found that, despite being incapable of forming a complex with XRCC1, both the LIG3 ZnF and the LIG3 ZnF-DBD constructs rapidly localized to sites of DNA damage. Although both fragments of LIG3 were capable of being recruited with the same kinetics as the full-length protein, these domains did not accumulate to the same extent as the wild-type protein. This is consistent with two mechanisms involved in the recruitment of LIG3 to SSBs. The first mechanism, which is mediated through the ZnF or ZnF-DBD domains, is direct binding to damaged DNA^{125,126}. The second mechanism is likely through the established association with XRCC1. The latter mechanism seems not to play a major role in the initial recruitment of LIG3 at sites of DNA damage, as our results demonstrated that LIG3 is efficiently recruited to sites of DNA damage in EM9 cells, which lack the expression of XRCC1, but does play an important role in retention. Importantly, this result provides an explanation for how LIG3 can participate in the repair of mitochondrial DNA, which does not require XRCC1¹⁷⁰. To further validate the importance of LIG3 in SSBR, we

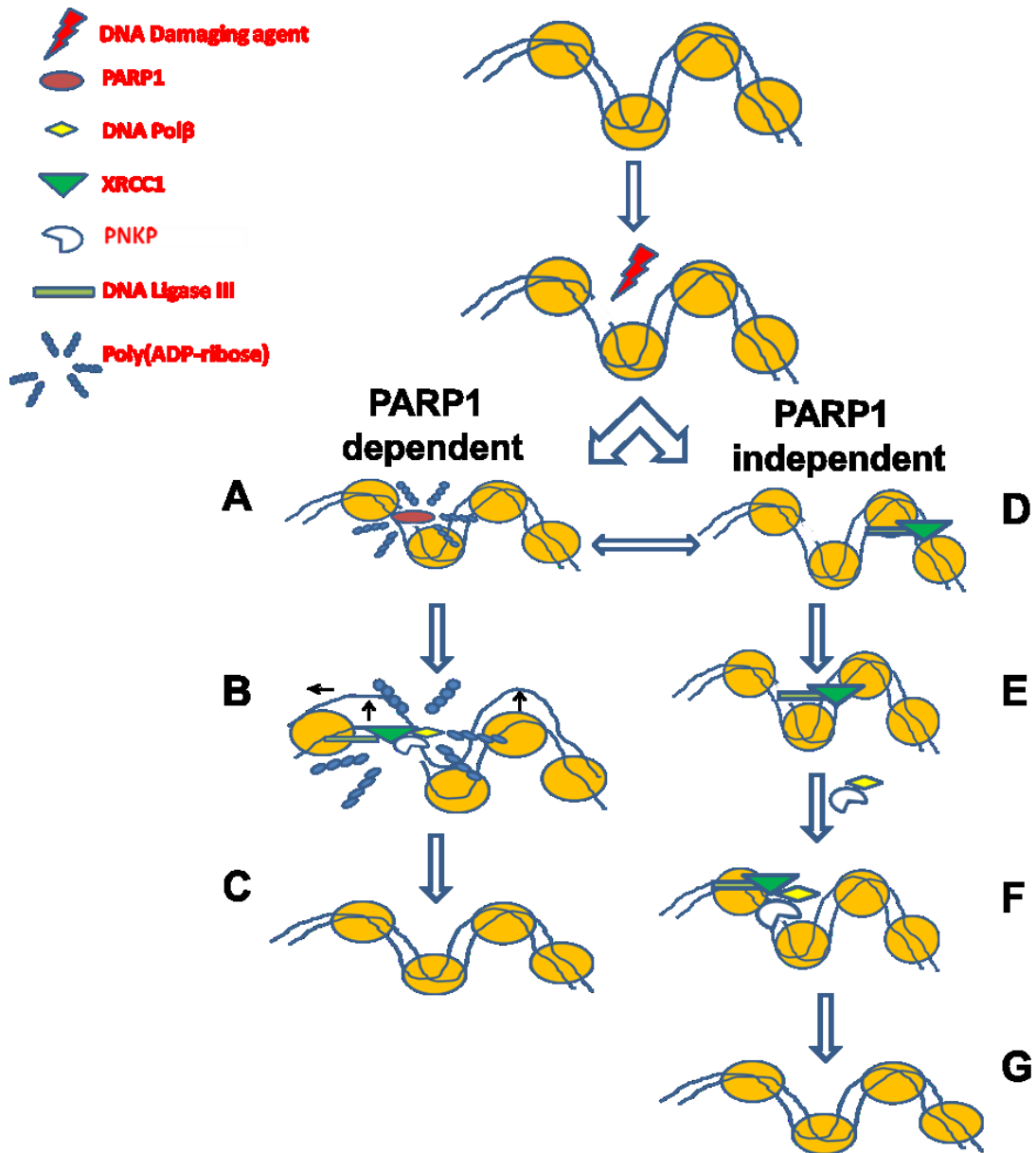
reasoned that the LIG3 ZnF should behave in a dominant negative fashion. When we overexpressed the LIG3 ZnF and then examined the rate of SSBR using the comet assay, we found that the rate of SSBR is significantly reduced. This is consistent with the ZnF binding to SSBs but not properly initiating the assembly of the SSBR machinery.

In vitro, the zinc finger domain of LIG3 shows a preference for nicks over gaps¹²⁶. We therefore tested the potential of LIG3 to directly sense nicks introduced by cellular treatment with IRI. Using FRAP, we found that LIG3 had dramatically reduced mobility following IRI treatment. Surprisingly, PARP1 showed no significant change in its mobility under the same conditions. This is in contrast to treatment with hydrogen peroxide, where both PARP1 and LIG3 showed reduced mobility (**Figure 25B and Figure 24C**). The observation that PARP1 is activated in response to topoisomerase 1 poisoning by camptothecin and its analogues has led to the expectation that this is mainly due to the binding of PARP1 to nicks. This was further supported by the finding that PARP1 inhibition sensitizes cells to camptothecin treatment¹⁷¹. Our findings suggest that PARP1 is not the nick sensor for breaks introduced by topoisomerase I inhibition. However, a plausible explanation for the increased sensitivity to topoisomerase I poisons upon PARP1 inhibition might lie in the finding that PARP1 null cells have lowered TDP1 activity compared to the wild-type cells¹⁷² and that PARP1 activity stabilizes TDP1 protein and enhances its accumulation at sites of DNA damage¹⁷³.

Collectively, our results reveal a direct role for LIG3 in SSB sensing and recruitment of the SSBR machinery and a surprisingly more limited role for PARP1 in these same

processes. When PARP1 is inhibited, the SSBR core machinery shows delayed recruitment but there is no observed reduction in recruitment once the break is detected. Because PARP1 stimulates the rate but not the abundance of SSBR proteins recruited to sites of DNA damage, the primary role of PARP1-mediated poly(ADP-ribos)ylation may be to decondense the chromatin rather than act as a scaffold for the assembly of SSBR proteins. It remains possible that binding to PAR is responsible for generating a large number of binding sites rapidly after DNA damage but that PAR binding plays a relatively minor role in the recruitment and retention of these proteins once the SSB response has been initiated. Instead our results indicate that binding sites established downstream of the recognition of breaks by LIG3 are a major mechanism responsible for the retention of SSB proteins. Partial knockdown of LIG3 resulted in a comparable reduction in recruitment of XRCC1 and PNKP. This residual recruitment was not sensitive to PARP1/2 inhibition. Thus, whether the remaining LIG3 was sufficient for the observed recruitment or whether another protein that has not yet been identified as a SSB sensor was responsible for this recruitment remains to be determined. In either case, our results reveal that the canonical SSB sensing pathway centered around PARP1 does not explain the recruitment of SSBR proteins that we observe in living cells. Rather, we find that LIG3 can function in place of PARP1 as a sensor for SSBs, especially nicks, that is capable of initiating signaling and assembly of the SSBR machinery¹⁷⁴ independent of PARP1 activity (**Figure 26**).

Figure 26: Two pathways exist for the short patch repair of SSBs



Two pathways exist for the short patch repair of SSBs. In the canonical pathway (PARP1 dependent) (A) PARP1 senses DNA damage and rapidly catalyzes the formation of PAR residues that allow for (B) chromatin expansion which in turn facilitates (C) the recruitment of downstream repair proteins. In the second pathway (PARP1 independent) (D) XRCC1-LIG3 complex continuously scan the DNA, upon sensing an interruption (via LIG3), (E) the complex is capable of causing a localized nucleosomal disruption (dependent on LIG3) ¹⁷⁴, and the scaffold XRCC1 is capable of (F) loading downstream repair factors, PNKP and Pol β , and then repair continues as previously described (G).

Chapter 4: Interaction between Polynucleotide Kinase/Phosphatase and the Scaffolding Protein XRCC1 is mediated through an N-terminal unstructured domain of XRCC1

Rajam S. Mani, Ismail Abdou, Inbal Mermershtain, Mesfin Fanta, Michael Hendzel, J.N.

Mark Glover, Michael Weinfeld

ABSTRACT

Polynucleotide kinase/phosphatase (PNKP) and the scaffold protein, XRCC1, are key proteins acting in the DNA single-strand break repair pathway. XRCC1 can stimulate PNKP by binding in its phosphorylated state to the FHA domain of PNKP. Additionally, non-phosphorylated XRCC1 stimulates PNKP by binding to its catalytic domain. Here, we have used XRCC1 fragments, as well as full-length protein, to further elucidate the interactions between these two proteins, as well as two variants of XRCC1 (Arg194Trp and Arg280His) arising from single nucleotide polymorphisms (SNPs) of the gene that have been associated with altered cancer risk. We observed that the interaction of the PNKP FHA domain with phosphorylated XRCC1 extends beyond the immediate phosphorylated region of XRCC1 (residues 515-526). We also found that a fragment of XRCC1 comprising residues 166-436 binds tightly to PNKP and DNA and efficiently activates the kinase activity of PNKP. However, the interaction of PNKP with the same fragment bearing either of the SNP-based variants is considerably weaker and their stimulation of PNKP is severely reduced, although the variant fragments still bind DNA effectively, but with slightly reduced affinity. This suggests that the stimulation of PNKP activity is mainly due to direct XRCC1- PNKP interactions and not due to a competition between PNKP and XRCC1 for product DNA. Laser micro-irradiation of DNA in cells revealed reduced recruitment of PNKP to the damaged DNA in the cells expressing either variant of XRCC1 in comparison to wild-type XRCC1 despite the equally efficient recruitment of wild-type and variant XRCC1 to the damaged DNA. This observation suggests that the elevated risk of cancer associated with these SNPs may be due in

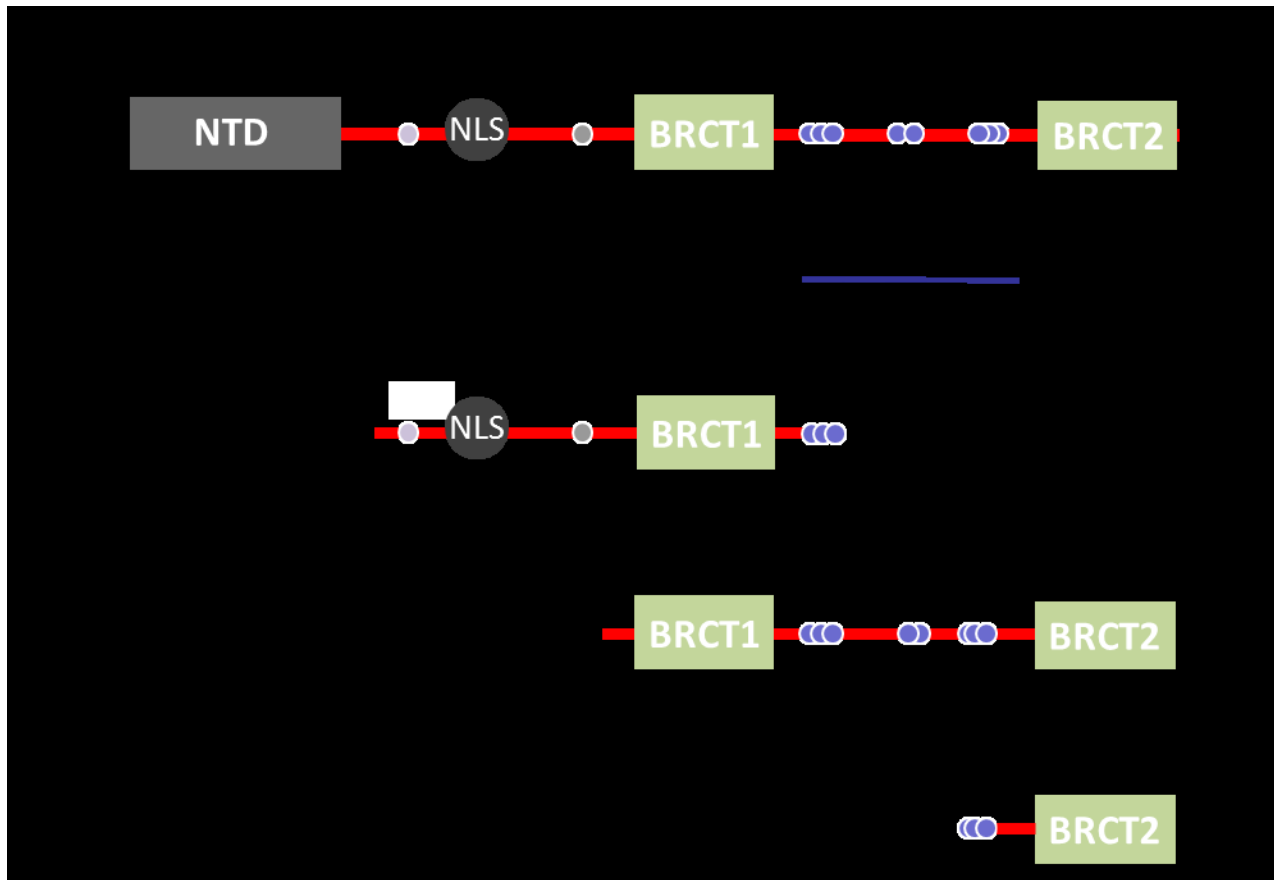
part to poorer recruitment of PNKP. It also indicates that the recruitment of PNKP to damaged DNA requires interaction of XRCC1 with the catalytic domain of PNKP.

INTRODUCTION

Human polynucleotide kinase/phosphatase (PNKP) is required to process unligatable strand break termini generated by many genotoxic agents or as intermediates in repair pathways and thus often participates in DNA single- and double-strand break repair as well as base excision repair^{9,140,175,176}. In its role in single-strand break repair and in the alternative non-homologous end joining pathway, PNKP is associated with the scaffolding protein XRCC1 and DNA ligase III^{177,178}. PNKP possesses 5'-DNA kinase and 3'-DNA phosphatase activities^{179,180}, both of which can be stimulated by XRCC1^{147,181,182}. It has been suggested that XRCC1 functions in a dual capacity to enhance PNKP kinase activity; first, XRCC1 enhances the capacity of PNKP to discriminate between strand breaks with 5'-OH termini and those with 5'-phosphate termini, and second, XRCC1 stimulates PNKP activity by displacing PNKP from the phosphorylated DNA product¹⁵¹. Although it is generally considered that interaction between PNKP and XRCC1 is mediated by the binding of CK2-phosphorylated XRCC1 protein to the FHA domain of PNKP^{137,177}, it is clear that XRCC1 in its non-phosphorylated form can interact with the catalytic domain of PNKP, thereby stimulating PNKP activity^{147,151,181}. In order to understand the mechanism of activation of PNKP by XRCC1, we initiated this study to look at the interactions between different regions of XRCC1 with PNKP and DNA. For this purpose, we utilized several XRCC1 fragments (**Figure 27**) including: (i) the extended BRCT2 domain of XRCC1 (EB2) from residues 511 to 633, since this region possesses a cluster of CK2 phosphorylation sites implicated in the interaction with the FHA domain¹⁷⁷; (ii) the BLB (BRCT1 Linked BRCT2) region of XRCC1 comprising residues 295 to 633; and (iii) the extended BRCT1 domain (EB1) comprising

the nuclear localization signal (NLS) and BRCT1 domain (residues 166-436), which is essential for the recruitment of XRCC1 to sites of DNA damage and DNA replication ¹⁵.

Figure 27: Schematic of human XRCC1. The diagram shows the major identified domains within XRCC1 and the protein fragments used for this study



XRCC1, a scaffold protein with multiple interaction modules. N-terminal domain (NTD, residues 1-160) has been shown to be a DNA binding domain as well as DNA Pol β interaction site. Extended BRCT1 (EB1, residues 166-436) domain, comprises the central BRCT1 domain and linker containing NLS. BRCT1-linked-BRCT2 (BLB, residues 295-633), comprises central and C-terminal BRCT domains with CK2 phosphorylation cluster in linker region. Extended BRCT2 (EB2, residues 511-633), comprises a part of the linker between two BRCT domains and BRCT2 domain

Hanssen-Bauer et al. ¹⁵ suggested a key role for the EB1 region in mediating DNA repair, but the mechanism by which it confers this property remains unclear. The EB1 domain also retains two of the most common amino acid variants of XRCC1, namely Arg194Trp and Arg280His. These variants have been linked with increased incidence of specific types of cancer and response to chemotherapy in defined populations ^{183–185}. Cells expressing these variants exhibit different repair profiles when treated with methyl methanesulfonate (MMS) or hydrogen peroxide and reduced DNA repair capacity compared to the wild-type protein ¹⁵. The observed differences in DNA repair profiles of the variants from the wild-type protein could be associated with either the affinity with which they bind DNA or their ability to interact with other DNA repair proteins such as PNKP.

The data presented here addresses the binding of phosphorylated XRCC1 to PNKP indicating that the interaction is more extensive than previously envisaged. We also show, by comparing the wild-type and variant EB1 fragments, that the stimulation of PNKP is primarily due to its direct interaction with XRCC1 rather than XRCC1 competition for substrate DNA. Finally, we provide evidence indicating that the reduced repair capacity associated with the variant XRCC1 species may be at least in part attributable to poorer stimulation of PNKP and reduced recruitment of PNKP to damaged DNA.

RESULTS

Overview of the fluorescence-based analytical approach for studying PNKP interaction with XRCC1 fragments

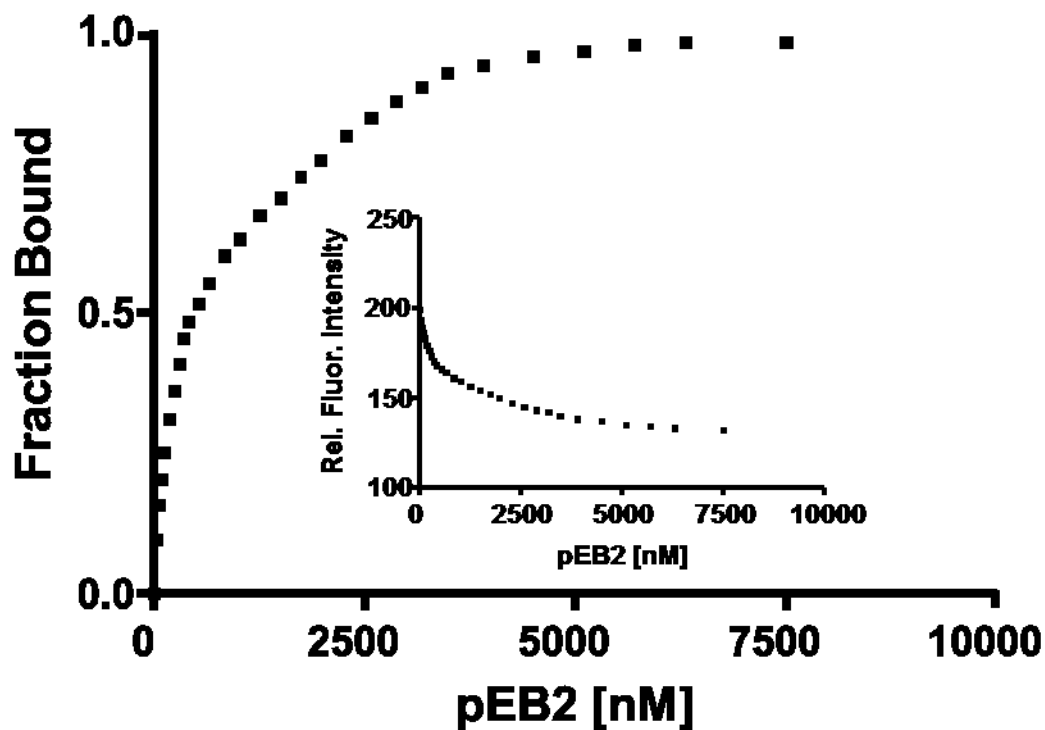
To study the interaction between XRCC1 fragments, DNA substrates and PNKP, we carried out a series of steady-state fluorescence measurements. Binding of protein to DNA substrates was examined by the change in intrinsic Trp fluorescence. To analyze the binding between XRCC1 fragments and PNKP, PNKP^{WFX402} (a mutated form of PNKP in which all the tryptophans except Trp402 have been replaced with phenylalanine) was labeled with acrylodan (AC), a sulfhydryl-specific covalent label, and the effect of XRCC1 fragment binding to PNKP^{WFX402-AC} was monitored by quenching of AC fluorescence around 490 nm following excitation at 380 nm^{186,187}. The AC-labeled PNKP was functionally active when tested for its kinase activity and retained ~85-90% of its activity compared with unlabeled PNKP. The degree of labeling of PNKP with AC was 1.3 ± 0.2 (mean \pm S.E., $n = 4$) mole of AC/mole of PNKP. PNKP^{WFX402-AC} when excited at 380 nm exhibits an emission maximum around 490 nm, suggesting that the environment of AC in PNKP has considerable hydrophobic character^{151,186}. In an earlier study we identified Cys409 as the Cys residue primarily labeled in PNKP^{151,186}.

Interaction between PNKP and the C-terminal domain of XRCC1

The C-terminal domain of XRCC1, which is known to contain several CK2 phosphorylation sites (**Figure 27**), is considered to be primarily responsible for binding to the FHA domain of PNKP¹⁷⁷. We first compared the interaction of full length PNKP with non-phosphorylated and phosphorylated C-terminal fragment EB2 of XRCC1 (residues 511-633). Phosphorylated XRCC1 was produced by co-expression of the

XRCC1 fragment together with CK2 in bacterial cells (Methods and Materials). Addition of pEB2 (where “p” denotes CK2 phosphorylated protein) resulted in quenching of the AC fluorescence of PNKP at 490 nm (**Figure 28**), and fluorescence titration as a function of pEB2 concentration yielded a K_d value of 500 ± 50 nM, while npEB2 (where “np” denotes non-phosphorylated peptide) did not induce any significant quenching in AC fluorescence, even at 5 μ M concentration, indicating that the non-phosphorylated protein does not bind to PNKP (Table 1).

Figure 28: Fluorescence titration of PNKPWF_X402-AC versus pEB2



Fluorescence titration of PNKP^{WFX402-AC} *versus* pEB2. Labeled protein (0.25 μ M) was excited at 380 nm, and the relative fluorescence (Rel.Fluor.) intensities were monitored at 490 nm (see inset). The fraction bound *versus* pEB2 concentration is plotted.

Table 1. Affinities of XRCC1 fragments for PNKP^{WFX402-AC} and PNKP^{FHA-AC}**(a) Binding to PNKP^{WFX402-AC}**

Sample	K _d (nM) ^a
pEB2 (residues 511-633)	500 ± 50
npEB2 (residues 511-633)	nd ^b
pBLB (residues 295-633)	110 ± 10
npBLB (residues 295-633)	450 ± 50
npEB1 (residues 166-436)	120 ± 10
npEB1 ^{R194W}	nd ^b
npEB1 ^{R280H}	nd ^b

(b) Binding to PNKP^{FHA-AC}

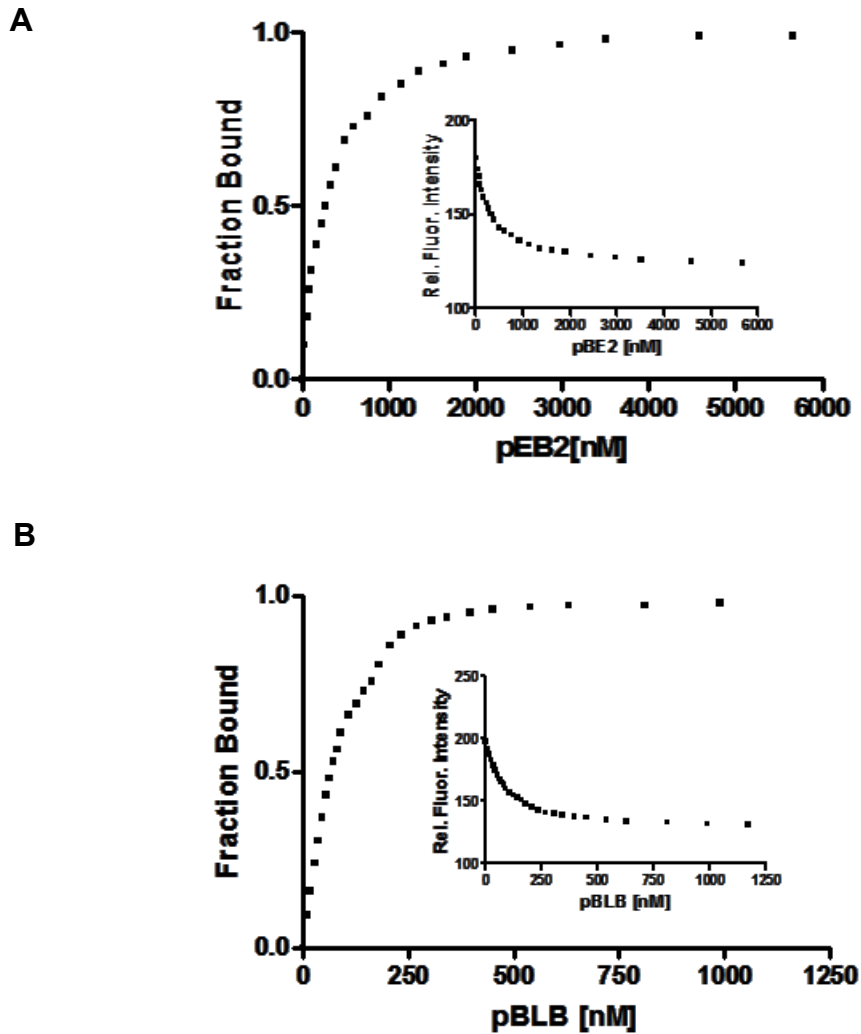
Sample	K _d (nM) ^a
pEB2 (residues 511-633)	270 ± 20
pBLB (residues 295-633)	65 ± 5

^aK_d values (mean ± S.E., n = 3) were determined by fluorescence titration.

^bnd – not determined

We then looked more directly at the interaction with the PNKP FHA domain. To obtain quantitative data for this interaction we labeled the single Cys residue (Cys46) in the FHA domain with AC^{147,151}. When the labeled protein was excited at 380 nm, the emission maximum occurred around 490 nm, and the addition of the pEB2 fragment resulted in AC fluorescence quenching (**Figure 29A**). Titration of PNKP^{FHA-AC} with pEB2 yielded a K_d of 270 ± 20 nM, i.e. slightly tighter binding than to full length PNKP. Extension of the C-terminal region to include the BRCT1 domain (i.e. the p295-633 fragment, pBLB) significantly increased the binding to either full-length PNKP (Table 1A, K_d 110 ± 10 nM) or the isolated FHA domain (**Figure 29B**, and Table 1B, K_d 65 ± 5 nM). We also examined the binding of the non-phosphorylated BLB fragment to PNKP^{WFX402-AC} and observed a K_d of ~ 450 nM. Taken together, these results suggest that regions of XRCC1 other than the CK2-phosphorylated region adjacent to BRCT2 contribute to the binding to PNKP.

Figure 29: Fluorescence titration of PNKP^{FHA-AC} versus pEB2 and pBLB



Fluorescence titration of PNKP^{FHA-AC} versus pEB2 and pBLB. Labeled PNKP^{FHA-AC} (0.3 μ M) was excited at 380 nm, and the relative fluorescence (Rel.Fluor.) intensities were monitored at 490 nm (see insets). (A) The fraction bound versus pEB2 concentration and (B) the fraction bound versus pBLB.

Interaction between PNKP and the extended BRCT1 domain of XRCC1

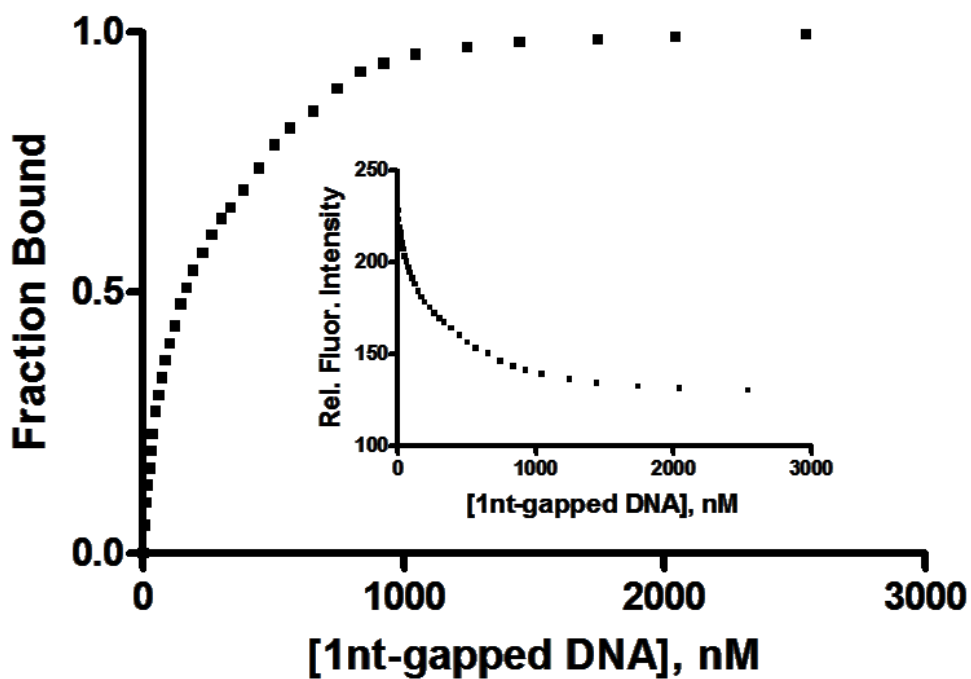
Others have shown that the extended BRCT1 domain, EB1 (residues 166-436), is required for the scaffolding function of XRCC1¹⁵. This fragment is also the location for two common XRCC1 variants, Arg194Trp and Arg280His, resulting from single nucleotide polymorphisms. We therefore examined the capacity of this XRCC1 fragment and the Arg194Trp and Arg280His variants to bind to PNKP. While the wild-type fragment bound PNKP^{WFX402-AC} tightly with a K_d of ~120 nM (Table 1), neither of the variant fragments caused sufficient fluorescence quenching (<6%) even at the saturating concentration of 3 μ M with the result that titration could not be carried out with these two variants to measure the K_d values. These findings suggest that the region from the NTD to past the BRCT1 in XRCC1 is involved in PNKP interactions. We also examined the binding of full length XRCC1 and the two variants to PNKP^{WFX402-AC}. XRCC1 exhibited tight binding to AC labeled PNKP resulting in nearly 30% quenching of AC fluorescence and the K_d value obtained from fluorescence titration was 55 ± 5 nM, while the two variants induced only ~5% AC quenching when the concentration of PNKP^{WFX402-AC} and the variants were 0.3 and 3 μ M, respectively, such that no binding affinity could be determined.

DNA binding to the extended BRCT1 domain of XRCC1

We have previously determined the binding affinities of full length wild-type XRCC1 for substrates that model DNA strand breaks¹⁵² by monitoring the effect of DNA binding on the intrinsic Trp fluorescence of XRCC1. Since the EB1 domain has been implicated in XRCC1 binding to damaged sites we examined the affinity of this domain for various

substrates that model DNA strand breaks by fluorescence titration (**Figure 30** and Table 2). The rank-order of affinities with which this fragment bound these ligands was 1 nt-gapped DNA > nicked DNA > intact duplex > single-stranded oligonucleotide, which is the same rank order we previously observed with full length XRCC1¹⁵². Interestingly, both the BLB and EB1 fragments, like full length XRCC1, preferentially bound a gapped DNA substrate over a single stranded substrate (Table 2), suggesting that a major DNA binding domain of XRCC1 lies between residues 295 and 436, which contains the BRCT1 domain. We also examined the EB1 Arg194Trp and Arg280His variant fragments for their DNA binding capacity and observed that they exhibited moderately lower binding affinities towards single-stranded DNA and 1 nt-gapped DNA than the wild-type fragment (Table 2).

Figure 30: Fluorescence titration of EB1 versus duplex DNA with a single nucleotide gap



Fluorescence titration of EB1 *versus* duplex DNA with a single nucleotide gap. The protein (0.3 μ M) was excited at 295 nm, and the fluorescence intensity was monitored at 340 nm (see inset). The fraction bound (i.e., relative fluorescence quenching) *versus* ligand concentration is plotted.

Table 2. Binding of XRCC1 fragments to substrates that model DNA strand breaks

Sample	Substrate	K_d (μM) ^a
EB1 (residues 166-436)	1 nt-gapped DNA ^b	0.14 ± 0.01
	Nicked DNA	0.26 ± 0.01
	Duplex (20-mer)	0.50 ± 0.05
	Single-stranded (24-mer)	0.75 ± 0.05
BLB (residues 295-633)	1 nt-gapped DNA	0.16 ± 0.01
	Single-stranded (24-mer)	0.65 ± 0.05
EB1 ^{R194W}	1 nt-gapped DNA	0.37 ± 0.01
	Single-stranded (24-mer)	1.70 ± 0.20
EB1 ^{R280H}	1 nt-gapped DNA	0.55 ± 0.02
	Single-stranded (24-mer)	3.30 ± 0.30

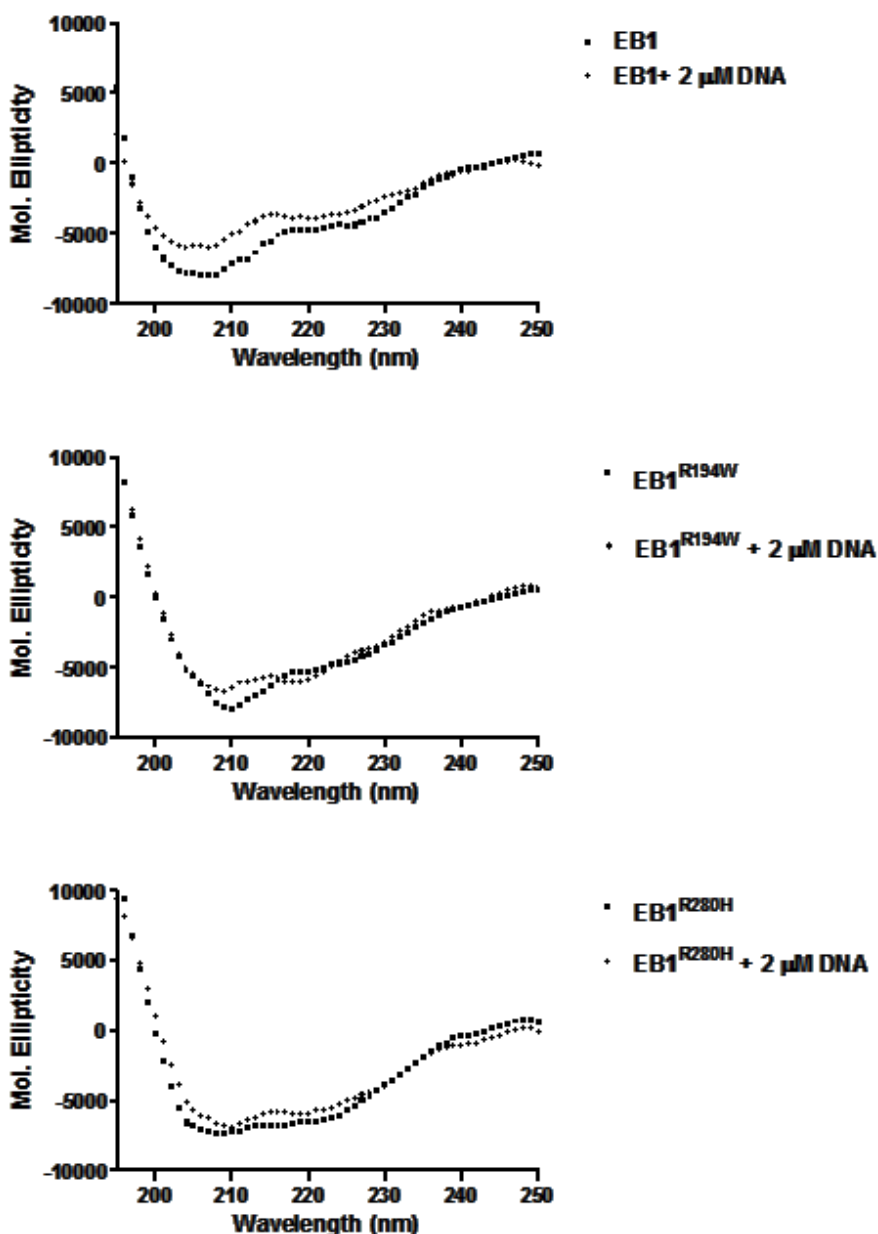
^a K_d values (means \pm S.E., $n = 3$) were determined by fluorescence titration

^b nt - nucleotide.

CD analysis of the extended BRCT1 domain of XRCC1 and interaction with DNA

Information concerning the secondary structure of EB1 and its two variants was obtained from far-UV-CD data (**Figure 31**). All the three EB1 fragments exhibited two negative CD bands around 209 and 222 nm, indicating the presence of α -helical organization. Secondary structure analysis suggested that the above two mutations in EB1 did not induce any major conformational change in EB1 (Table 3). However, the effect of DNA binding on these proteins was different, and the maximum change in protein conformation as a result of DNA binding was observed in EB1. Addition of 2 μ M 1-nt gapped DNA induced a conformational change in EB1; the molar ellipticity value $[\theta]_M$ at 209 nm was reduced from -7500 ± 300 to -5400 ± 300 deg cm² dmol⁻¹, upon binding DNA. The observed changes in $[\theta]_M$ at 209 nm for EB1^{R194W}, and EB1^{R280H} upon binding DNA were -7600 ± 300 to -6600 ± 300 , and -7350 ± 300 to -6800 ± 300 , respectively. The observed change with EB1^{R280H} was very small, only slightly above the experimental error and these results co-relate very well with the DNA binding ability of these proteins (Table 2).

Figure 31: CD analysis for WT and mutant EB1



CD analysis of the EB1 wild-type (A) and R194W (B) and R280H (C) fragments in the absence and presence of 1-nt gapped DNA substrate. Protein concentration used was 0.5 mg/ml in 50 mM Tris-HCl, pH 7.5, 100 mM NaCl, 5 mM MgCl₂, and 1 mM dithiothreitol.

Table 3: Secondary structural analysis of 166-436, R194W, R280 H, and 166-436-DNA complex

Protein	α -Helix ^a (%)	β -structure ^a (%)	Random ^a (%)
EB1	21 \pm 0.42	51 \pm 1.02	28 \pm 0.56
EB1 ^{R194W}	26 \pm 0.52	44 \pm 0.88	30 \pm 0.6
EB1 ^{R280H}	22 \pm 0.44	49 \pm 0.98	29 \pm 0.58
EB1 + DNA	16 \pm 0.32	49 \pm 0.98	35 \pm 0.7

^a Analysis of the CD spectra according to Provencher and Glöckner ¹⁵³

Effect of XRCC1 and its fragments on the DNA kinase activity of PNKP

To test whether XRCC1 and its fragments stimulate the 5'-kinase activity of PNKP, a single-stranded oligonucleotide (24-mer) was employed as the DNA substrate. DNA kinase reactions were carried out in the presence of [γ - 32 P]ATP. Under the conditions used, the 5'-kinase activity of PNKP increased ~4-fold in the presence of full length XRCC1 and the wild-type EB1 fragment was almost as effective (**Figure 32A**). In contrast, the R194W and R280H variants of EB1 showed a significantly diminished capacity to stimulate the PNKP kinase activity. The longer XRCC1 non-phosphorylated BLB fragment also had limited effect. Even though the BLB fragment comprises a larger portion of XRCC1, it was less effective in activating PNKP compared to the wild-type EB1 fragment, suggesting that the linker 1 in the N-terminal segment of XRCC1 plays an important role in activating PNKP. We also examined the effect of single point variants R194W and R280H of full length XRCC1 on the DNA kinase activity of PNKP (**Figure 32B**). These two single point variants induced limited activation of the kinase activity of PNKP.

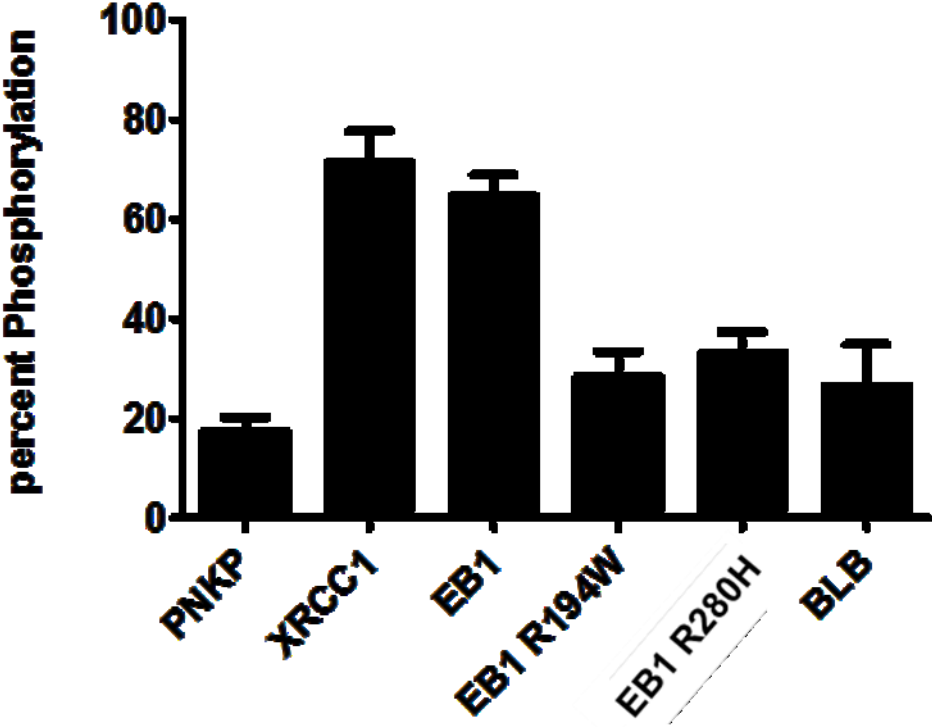
Influence of XRCC1 fragments on the turnover of PNKP

Full length XRCC1 is known to increase the turnover rate of PNKP based on measurement of its kinase activity^{147,151}. The kinase activity of PNKP was assayed using a limited concentration of the enzyme with 24-mer single-stranded oligonucleotide and [γ - 32 P] ATP (**Figure 32 C**). The rate of product accumulation decreased over the course of the assay and reached a plateau after ~10 min. Addition of full length XRCC1 at 20 min (i.e. in this plateau region) resulted in reactivation of PNKP kinase activity,

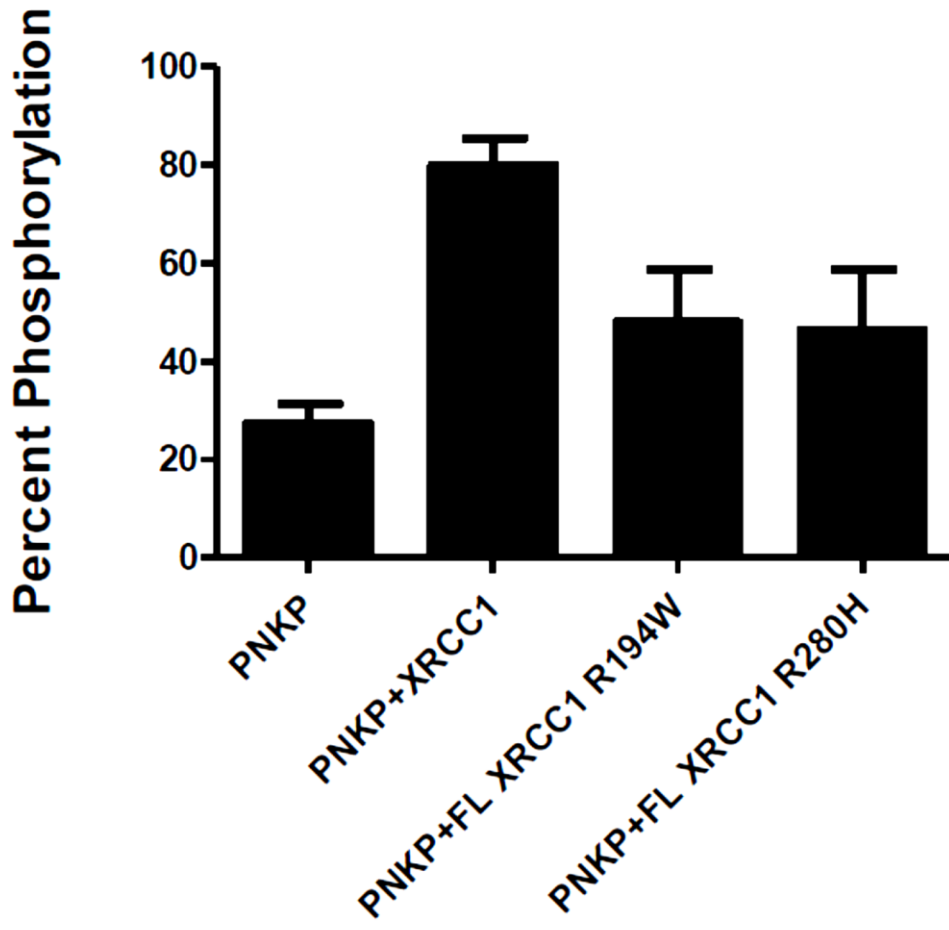
and the percent ^{32}P incorporated nearly doubled. The observed increase in kinase activity was due to PNKP, since XRCC1 has no kinase activity. Addition of wild-type EB1 though not as active as full length XRCC1 nonetheless showed a significant level of PNKP kinase reactivation. Neither the R194W nor the R280H EB1 variant when added to PNKP in the plateau region showed any appreciable effect, implying that these two variants were not able to reactivate PNKP's kinase activity. Similarly, the BLB fragment failed to significantly stimulate PNKP turnover (data not shown). Influence of single point variants R194W, and R280H in full length XRCC1 on the turnover rate of PNKP is shown in **Figure 32D**. Consistent with the result observed with EB1 R280H, the full length XRCC1 R280H failed to reactivate PNKP kinase activity. Of notice the full length version of R194W, in contrast to the truncated EB1 R194W, was able to reactivate PNKP kinase activity albeit to a lesser extent compared to WT XRCC1.

Figure 32: Activation of PNKP by full length XRCC1 and XRCC1 fragments

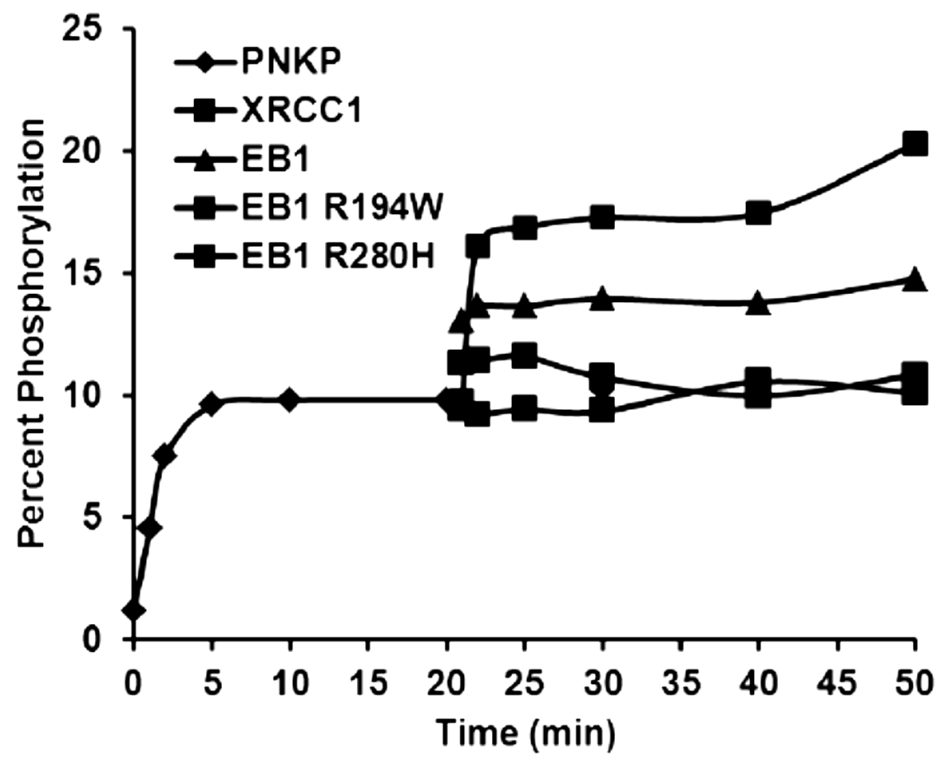
A



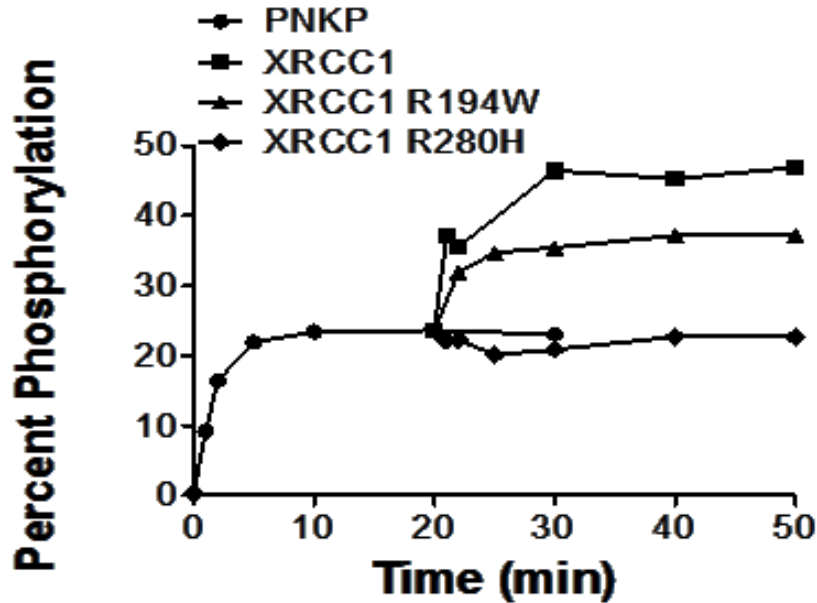
B



C



D

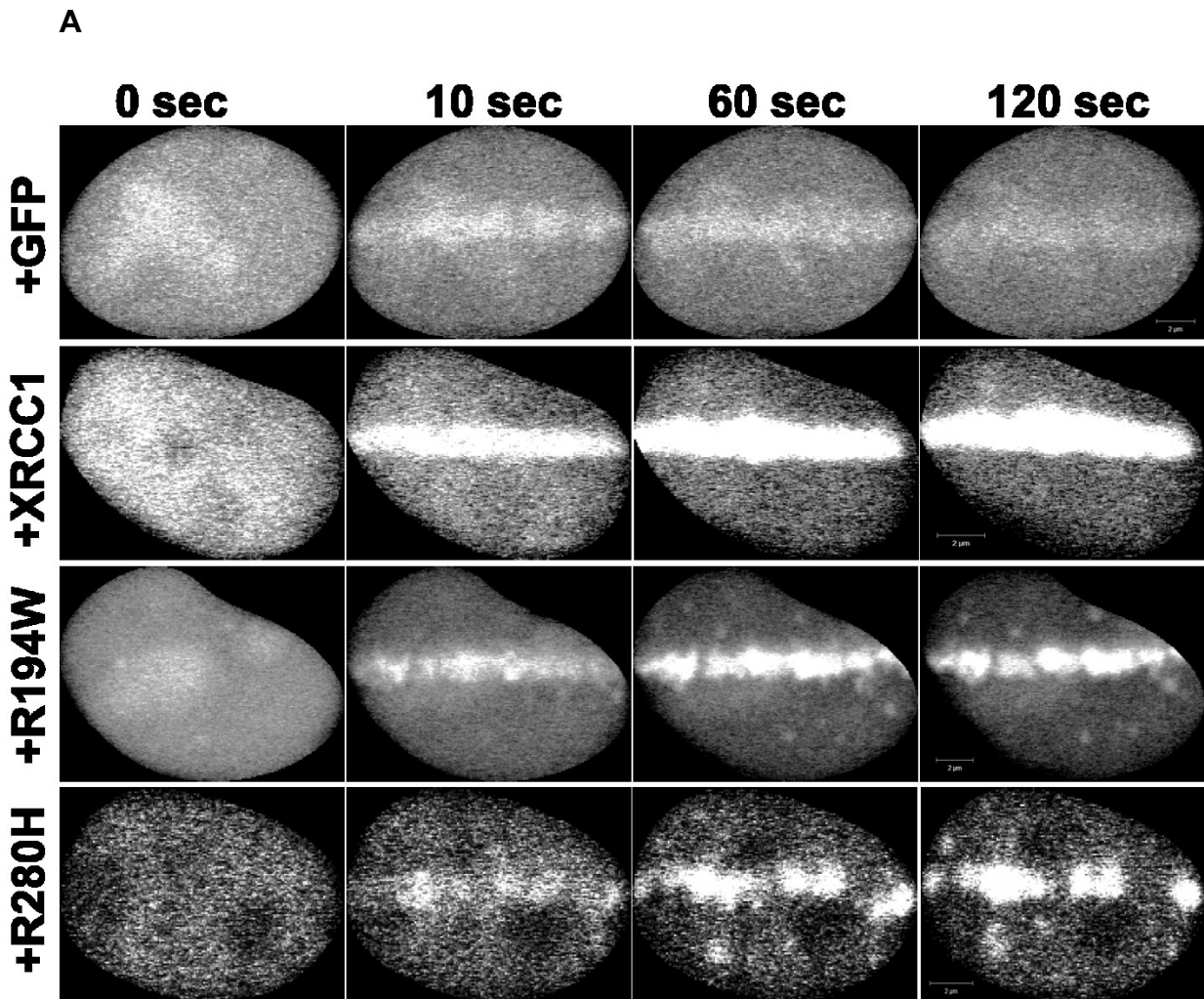


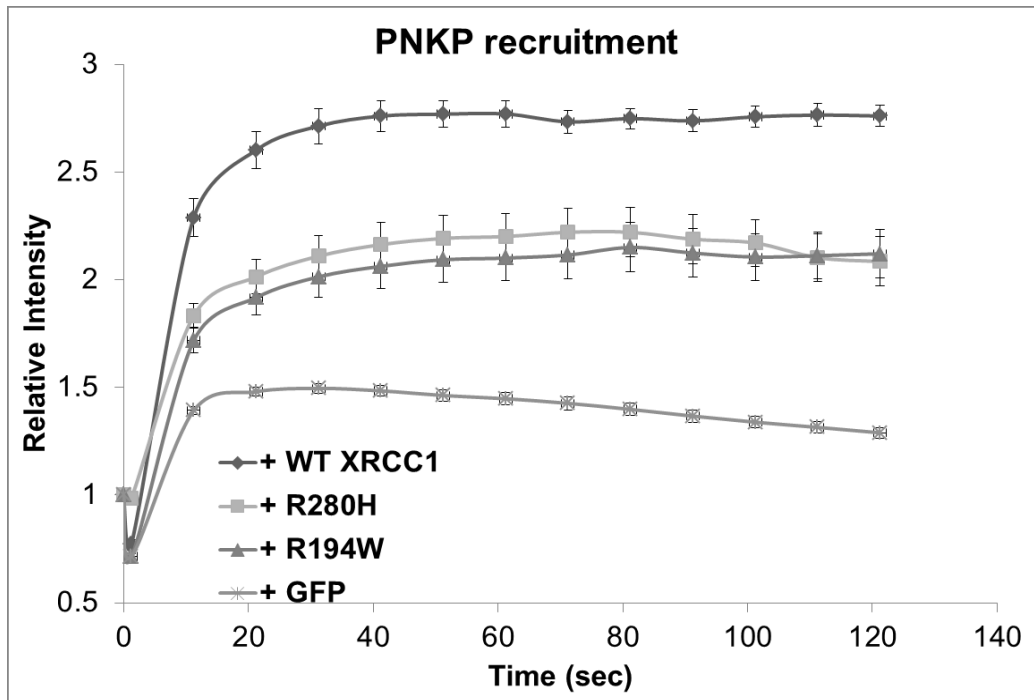
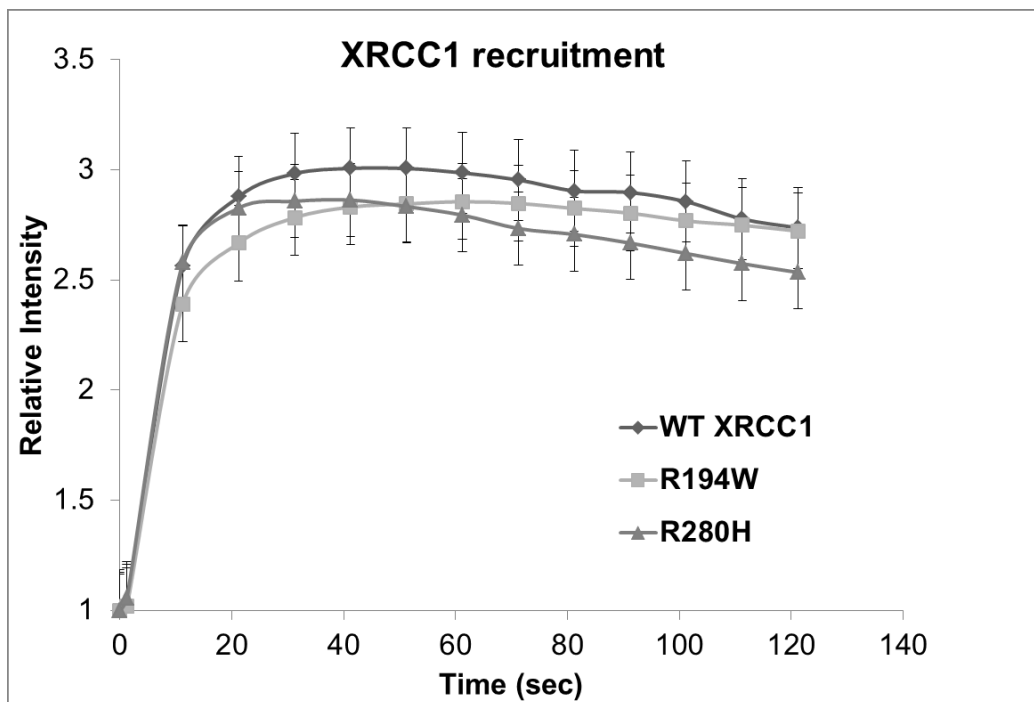
Activation of PNKP by full length XRCC1 and XRCC1 fragments. (A) Stimulation of PNKP kinase activity on single-stranded DNA by co-incubation with full length XRCC (XRCC1), EB1 (166-436), EB1^{W385A}, BLB (295-633), EB1^{R194W} and EB1^{R280H}. (B) Stimulation of PNKP kinase activity by co-incubation with wild-type and variant full length XRCC1. (C) Stimulation of PNKP kinase activity due to enzyme turnover by addition of full length XRCC1 (XRCC1), EB1 (166-436), EB1^{R194W} and EB1^{R280H} after 20 min incubation of PNKP with single-stranded DNA. (D) Stimulation of PNKP kinase activity due to enzyme turnover by addition of full length XRCC1 (XRCC1), XRCC1 R194W and XRCC1 R280H after 20 min incubation of PNKP with single-stranded DNA

Cellular interaction of wild-type and mutant XRCC1 with PNKP

To gain cellular insight into the impact of the XRCC1 variants, R280H and R194W, on the behavior of PNKP at damaged DNA, we transiently co-expressed mRFP-tagged PNKP with mGFP-tagged full length WT XRCC1, R280H, R194W and empty vector. To circumvent the effects of the interactions of mRFP-tagged PNKP with endogenous XRCC1, we used EM9 cells that lack the expression of any XRCC1. Then we carried out laser micro-irradiation experiments and followed the accumulation of PNKP at sites of DNA damage in real time. Consistent with previous observations, PNKP accumulated at sites of DNA damage in EM9 cells ³⁰ (**Figure 33A and B**). However, co-expressing wild-type XRCC1 further enhanced the recruitment of PNKP to DNA damaged sites, which is consistent with previous observations on the interaction between the two proteins. The two variants of XRCC1 (R280H and R194W) displayed a significantly reduced accumulation of PNKP to DNA damage sites compared to wild-type XRCC1. To rule out the possibility that this effect might be due to decreased recruitment of the XRCC1 variants in comparison to the wild-type protein, we followed and quantified their recruitment to DNA damage sites and observed minimal differences between the wild-type XRCC1 and the two variants (**Figure 33C**).

Figure 33: The effect of XRCC1 variants on the recruitment of PNKP to sites of DNA damage



B**C**

The effect of XRCC1 variants on the recruitment of PNKP to sites of DNA damage. EM9 cells were co-transfected with mRFP-PNKP, mGFP (vector only) and mGFP-tagged variants of XRCC1 (WT, R194W and R280H). Laser micro-irradiation was performed as described in Materials and Methods. (A) Examples showing the recruitment of mRFP-PNKP in cells cotransfected with mGFP, the R194W mutant and wild-type XRCC1. For each data set 12 cells were selected and we quantified the recruitment of mRFP-PNKP (B) and GFP-tagged XRCC1 proteins (C) to sites of DNA damage. Each line is based on three independent experiments, n=12, and error bars represent S.E.M.

Discussion

XRCC1 is regarded as a scaffolding protein capable of interacting with several proteins participating in SSB repair. It forms repair complexes with poly(ADP-ribose) polymerase 1^{158,188}, DNA polymerase β ^{84,115} and DNA ligase III¹²⁷. XRCC1 has been shown to interact with the PNKP FHA domain through a peptide sequence in XRCC1 phosphorylated by CK2 and stimulate the DNA kinase and DNA phosphatase activities at damaged DNA termini^{177,181}. More recently, we have shown that non-phosphorylated XRCC1 can interact with the catalytic domain of PNKP and stimulate PNKP activity as well^{147,151}. The purpose of this study was to examine in more detail the interactions between different regions of XRCC1 and PNKP in order to increase our understanding of the mechanism(s) of PNKP activation and their possible role in DNA repair.

Interactions of XRCC1 fragments with PNKP

Our earlier studies have clearly established a phosphorylation-independent interaction of XRCC1 with PNKP and also revealed that XRCC1 and CK2-phosphorylated XRCC1 (pXRCC1) bind to PNKP at different sites^{147,151}. These previous studies revealed that pXRCC1 binds with high affinity ($K_d = 4$ nM) to the FHA domain, while non-phosphorylated XRCC1 binds to the catalytic domain of PNKP with a K_d value of 43 nM. In XRCC1, the C-terminal domain contains the CK2 phosphorylation sites (residues 518, 519, 523 and 535)¹⁷⁷. The XRCC1 pEB2 fragment (residues 511-633), which encompasses the phosphorylation sites in addition to the BRCT2 domain of XRCC1, was capable of binding to the FHA domain as well as to full-length PNKP. The observed binding affinities of pEB2 to the FHA domain and full-length PNKP were distinctly lower than the affinities of the longer pBLB peptide (residues 295-633), suggesting that other

regions of XRCC1 (linker 1 and linker 2), though not involved in phosphorylation, can contribute to enhancing the interaction between phosphorylated XRCC1 and PNKP. Others¹⁸² have also come to a similar conclusion, i.e. that the interaction between XRCC1 and PNKP involves regions in XRCC1 that extend beyond the C-terminal domain containing the phosphopeptide (residues 515-526) and the FHA domain of PNKP. In this context, full length pXRCC1 exhibited very tight binding with an observed apparent K_d value of 4 nM¹⁴⁷ compared to the K_d value of 110 nM, obtained for the pBLB fragment. This suggests that the N-terminal region of XRCC1 also plays an important role in mediating interactions between phosphorylated XRCC1 and PNKP or that the protein conformation of the pBLB fragment does not completely mimic the conformation adopted by these residues within the full-length protein. However, the fact that the pBLB fragment bound the FHA domain with a similar affinity as it bound to full length PNKP suggests that the binding of this component of XRCC1 is confined to the FHA domain of PNKP.

The EB1 domain, comprising residues 166-436, is involved in the recruitment of XRCC1 to sites of damage and DNA replication¹⁵, implying that this region plays a major role in mediating DNA repair. Our data indicate that this region of XRCC1 contributes significantly to the binding of non-phosphorylated XRCC1 to PNKP, while the binding of the non-phosphorylated BLB fragment is considerably weaker. Nonetheless, the difference in K_d values for the interaction of full length XRCC1 and the EB1 fragment with PNKP (43 vs 140 nM) suggests that other residues enhance the binding of full length non-phosphorylated XRCC1 to PNKP.

The extended BRCT1 domain also harbours two common amino acid variants of XRCC1, namely Arg194Trp and Arg280His. These variants exhibited different repair profiles in comparison to the wild-type protein ¹⁵. Our data indicates that the amino acid changes have a profound effect on binding to PNKP, which will be discussed in further detail below. In the case of the R280H mutant, this could be related to the altered conformation revealed by CD (Table 3).

Interactions of XRCC1 fragments with DNA

Several lines of evidence indicate that the extended BRCT1 domain plays an important role in XRCC1 binding to DNA. A key observation is that the EB1 fragment like full length XRCC1 displays differential binding to various DNA substrates, with the tightest interactions occurring between the fragment and the 1 nt-gap and nicked DNA substrates, which mimic DNA single-strand breaks. The extended C-terminal domain BLB bound with similar affinity to DNA as EB1, suggesting that the overlapping region between the two fragments, i.e. residues 295-436, may be responsible for DNA binding.

The variant Arg194Trp and Arg280His EB1 fragments exhibited lower binding affinity for 24-mer single-stranded DNA and 1 nt-gapped DNA in comparison to wild-type EB1. The CD data showed that DNA binding to wild-type EB1 induced a conformational change in the protein fragment and its effect on the two variants was considerably less; in fact with EB1^{R280H} the observed change in ellipticity around 210 nm was only slightly above the experimental error. XRCC1 might serve as a strand break sensor in addition to its structural role as a scaffolding protein as it binds gapped and nicked SSB DNAs with higher affinities ^{152,189}. The observed differences in the DNA binding profile of these

XRCC1 variants may interfere in their ability to take part in DNA repair by affecting the sensor role and in turn their ability to direct the enzyme PNKP to the damaged site. However it should be noted that the full length XRCC1 proteins containing either of these mutations were recruited to sites of DNA damage induced by laser micro-irradiation with very similar kinetics as the wild-type protein (**Figure 33C**).

Effect of XRCC1 fragments on the kinase activity of PNKP

Full length XRCC1 and its wild-type extended BRCT1 fragment, EB1, were effective in markedly activating the kinase activity of PNKP (**Figure 32A**) and stimulating PNKP turnover (**Figure 32C**). However the non-phosphorylated BLB peptide had minimal effect on either the kinase activity or turnover of PNKP, clearly establishing the important role of Linker-1 in the N-terminal region of XRCC1 in its stimulatory interaction with PNKP. The R194W and R280H variants of EB1 also had a limited effect on the kinase activity or turnover of PNKP. However, since the non-phosphorylated BLB fragment, as well as the variant EB1 fragments, bound DNA reasonably tightly, we infer that the stimulation of PNKP activity is dependent on XRCC1 interaction with PNKP rather than displacement of PNKP due to competitive binding to DNA. Related to this, we found that the full length R194W and R280H XRCC1 variants were recruited to laser-induced DNA damage with similar kinetics as wild-type XRCC1, but showed a significantly reduced capacity to enhance PNKP recruitment (**Figure 33**). This raises the important possibility that the observed difference in DNA repair profiles of the SNP-derived variants compared to the wild-type protein ¹⁵ could be due to their poorer ability to bind and activate PNKP.

Finally, since full length non-phosphorylated XRCC1 binds only to the catalytic domain of PNKP and not to the FHA domain ¹⁴⁷, it would imply that EB1 also binds to the catalytic domain rather than the FHA domain. Therefore, the observation that the R194W and R280H XRCC1 variants have diminished capacity to recruit PNKP strongly suggests that interaction of XRCC1 with the catalytic domain of PNKP is required for the efficient recruitment of PNKP to DNA strand breaks in the nucleus.

In summary, in this study we have shown that the linker 1 in the N-terminal region of XRCC1 plays an important role in its interaction with PNKP. Phosphorylation of XRCC1 at its C-terminal end only strengthens its interaction with PNKP by virtue of its ability to bind to the FHA domain. Polymorphic variations, R194W and R280H, in the extended central BRCT domain disrupted its ability to interact with PNKP and our data suggest that this is potentially responsible for altering the DNA repair capability of cells carrying these changes to XRCC1.

Chapter 5: Discussion and perspectives

LIG3, a damage sensor in SSBR: Implications for cancer therapy

LIG3 and DDR

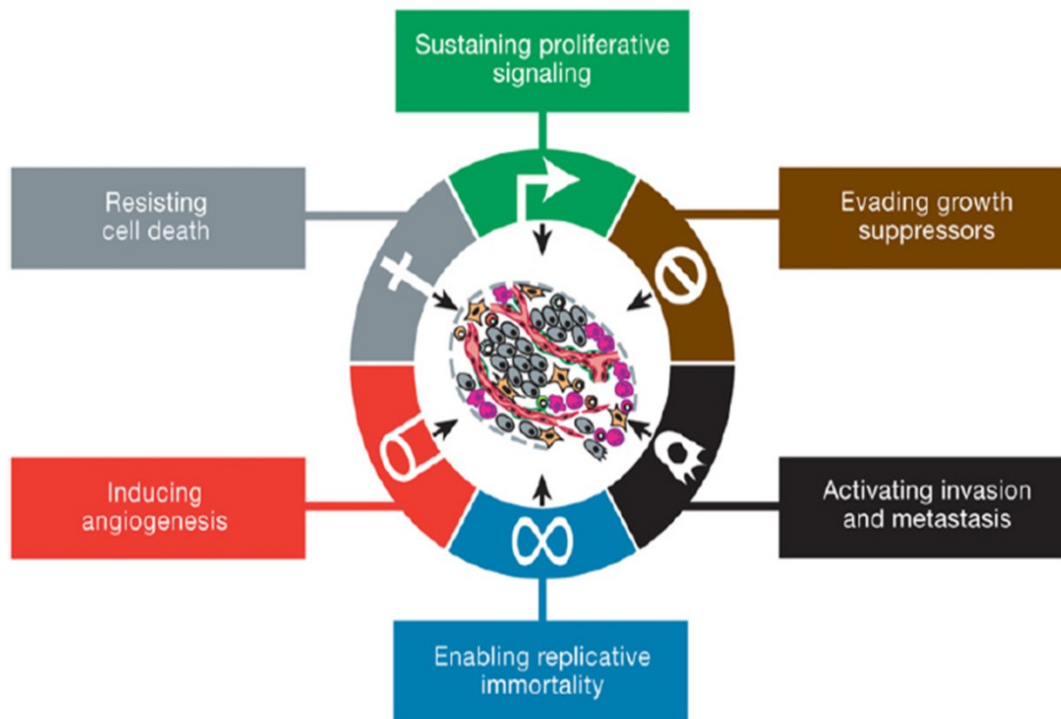
Contradicting views about the role of PARP1 function in being central to SSBR have pointed to the possibility of the existence of an alternative SSB sensing molecule (reviewed in Chapter 1). Based on previous biochemical studies^{114,125,126} and structural similarities between the PARP1 ZnF domain (damage sensing module) and that of LIG3¹²⁵, we hypothesized that LIG3 is an alternative sensor of SSBs. We have provided the first live cell data that supports the hypothesis that LIG3 fulfills such a role. Instead of relying on a single molecule for detecting SSBs, our finding provides us with a more dynamic view of the regulation of the robust SP-BER pathway in order to ensure the timely repair of the thousands of SSBs that occur daily^{12,19,25}. We have shown that LIG3 is required for the optimal recruitment of core SSBR proteins, XRCC1 and PNKP, to sites of DNA damage independent of PARP1 function. Notably, we have further shown that treatment of cells with the chemotherapeutic agent IRI significantly changes the binding kinetics of LIG3 but not PARP1. This result directly implicates LIG3 in the detection and binding of nicks generated by blocked topoisomerase I.

LIG3 and links to cancer initiation and progression

Replicative immortality is known to be one the “hallmarks of cancer” (**Figure 34**)¹⁹⁰. This characteristic is due to the ability of cancer cells to evade the telomere erosion processes, most frequently via acquiring mutations that enable overexpression of telomerase¹⁹⁰. On the other hand, increased genomic instability and mutations have been coined as “enabling characters” (**Figure 35**) to support driving cancer progression

¹⁹⁰. Recently, LIG3 has been shown to be essential to allow cells to 'escape telomere-driven crisis' associated with telomere shortening thus conferring a survival advantage to senescing cells ¹⁹¹. The process of telomere-driven crisis is characterized by growth arrest and fusion events that occur between telomeres and either regions of telomeric or non-telomeric DNA (DSBs) resulting in chromosomal translocations. The physiological consequences of such a process have been proposed to be dependent on the status of the tumor suppressor protein p53 ¹⁹². In the case of WT p53 background, the crisis serves as a strong activator for the G1/S check point leading to high rates of cell death¹⁹³. In a p53 null background, as is the case in many human cancers ¹⁹⁴, the check point is inactive and cells can evade the crisis. Importantly, cells escaping the crisis have been shown to require LIG3 and not LIG4 for this process ¹⁹¹. Consistent with a survival advantage escaping cells restore telomerase activity with a subsequent increase in telomere length ¹⁹¹ and have a payload of genomic instability that might contribute to mutagenesis and clonal evolution required during cancer progression ¹⁹¹. Indeed telomere-driven crisis in p53- lacking mouse models was shown to be a driver of tumorigenesis and subsequent metastatic potential ¹⁹³.

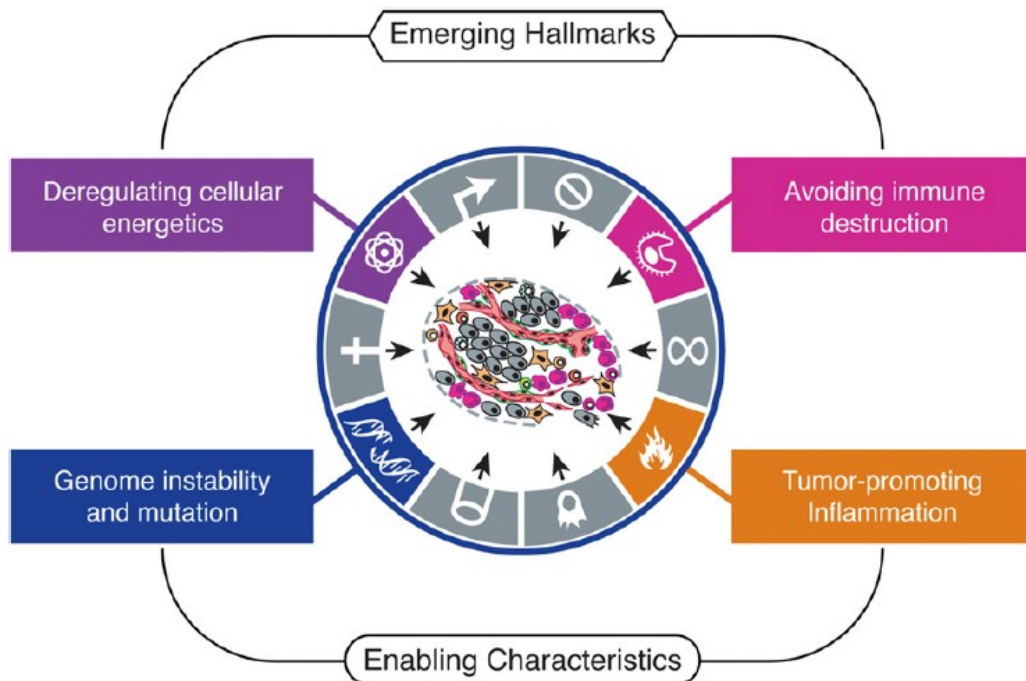
Figure 34: Hallmarks of Cancer



The Hallmarks of Cancer. The figure highlights the six fundamental hallmarks of cancer previously reviewed in 2000. Importantly enabling replicative immortality allows cancer cells to undergo unlimited growth-division cycles. One mechanism that confers replicative immortality is escaping telomere driven crisis, a process where LIG3 has been shown to play a pivotal role (discussed in above text). **Cell 144, Issue 5, p646–674, March 4, 2011**

Reproduced with permission from Elsevier. Copyright © 2011

Figure 35: Enabling characteristics that promote carcinogenesis



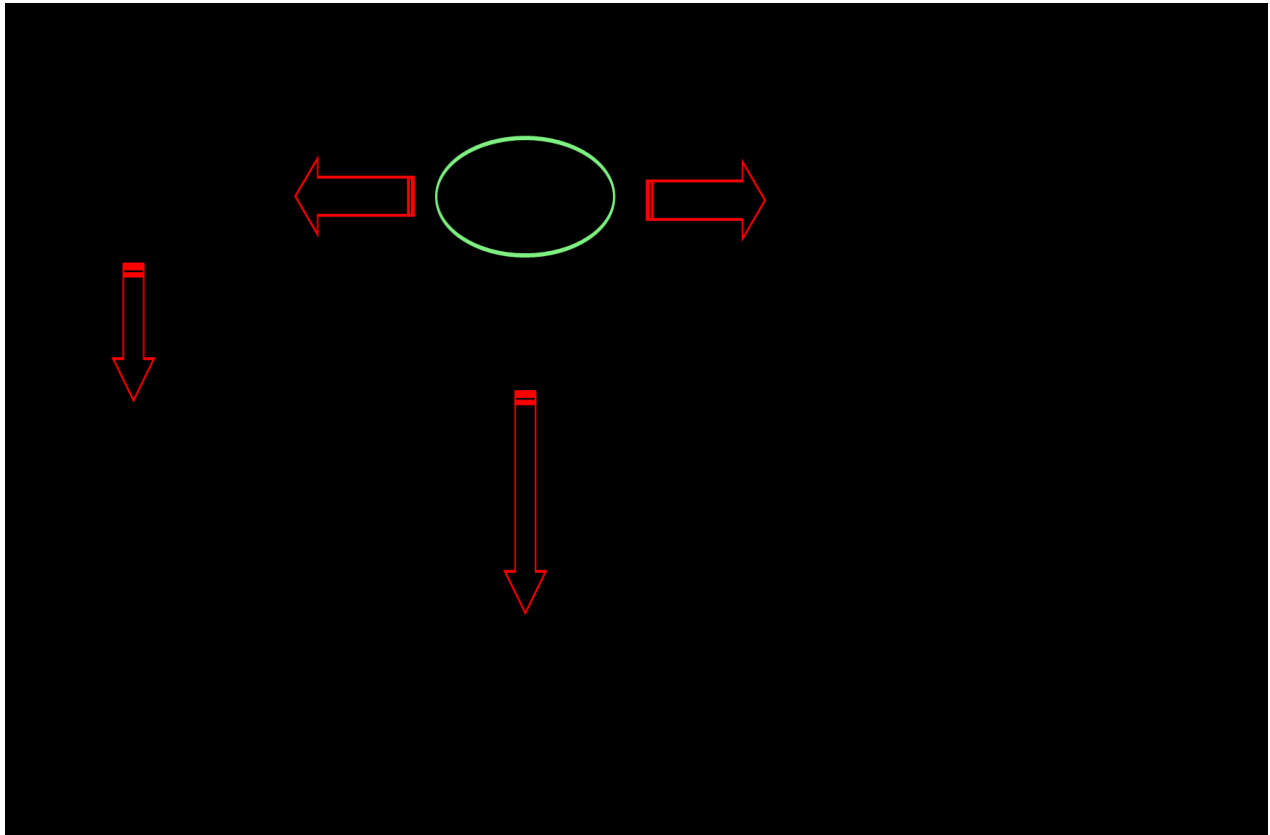
Emerging Hallmarks and Enabling Characteristics. Evidence has pointed to the possible existence of two additional hallmarks of cancer. First, cancer cells are able to modulate cellular metabolic pathways to support tumor growth. The second emerging hallmark is the ability of cancer cells to circumvent immunological responses and escape clearance by cells of the immune system. Generally, two enabling characteristics help support neoplasia and cancer progression. First, aberrant inflammatory responses have been linked to promote malignant transformation. Second, increasing pool of background mutations has been postulated to be a driver of carcinogenesis. In the latter process *LIG3* has been found to be overexpressed in different tumors and this finding has been linked to increased reliance of those tumor cells on an error prone DSB repair process, aNHEJ. **Cell 144, Issue 5, p646–674, March 4, 2011**

Reproduced with permission from Elsevier. Copyright © 2011

From a clinical perspective, LIG3 and PARP1 have been shown to be upregulated in CML cell lines that were found to be deficient in the core cNHEJ proteins, Artemis and LIG4^{195,196}. This finding was postulated to increase the reliance of those cells on the aNHEJ for the repair of DSBs¹⁹⁵. Indeed siRNA knockdown of LIG3 alone, or the combined inhibition of PARP1 and LIG3, in CML cells was associated with persistence of γ H2AX foci with or without exposure to IR^{195,196}. This is indicative of compromised repair of DSBs. Similar findings were reported in breast cancer cell lines¹⁹⁷. DSBR via aNHEJ is characterized by increased insertions, large deletions and microhomologies at repair sites⁵², conferring an inherent error prone nature to aNHEJ. The finding that different cancer cell lines rely on this pathway for DSBR can be theorized to help increase the pool of background mutations and chromosomal translocations thus promoting cancer progression.

Integrating these lines of evidence allows us to postulate multiple roles for LIG3 in supporting carcinogenesis (**Figure 36**). First, LIG3 would contribute to tumor initiation by permitting escape from telomere-driven crisis¹⁹¹, a process that has been linked in animal models to tumor progression and metastasis¹⁹³. Second, by promoting DSBR via aNHEJ in certain cancer types^{195,197,198}, LIG3 function would sustain tumor progression by increasing genomic instability within the population. Finally, being a sensor for SSBs, LIG3 would enhance SSBR, particularly upon treatment with DNA damaging agents such as IRI. Therefore development of LIG3 specific inhibitors would appear to be a viable option in chemotherapy. Indeed several studies indicated that targeting LIG3 specifically sensitizes cancer cells to chemotherapy and radiotherapy^{196,198,199} highlighting the importance of LIG3 to cancer cells.

Figure 36: Plausible roles of LIG3 at different stages of tumor evolution



LIG3 and links to carcinogenesis. LIG3 is a caretaker protein involved in the repair of nuclear and mitochondrial DNA via participating in SP-BER and DSBR. In a deregulated background such as cancer susceptible cells undergoing senescence, LIG3 promotes evasion of this crisis thereby enabling cellular survival. Cells that have escaped crisis have been shown to restore telomerase expression and increased chromosomal translocations, two characteristics that can promote tumor progression. Furthermore, LIG3 has been shown to be specifically overexpressed in certain tumors where it promotes DSBR via error prone aNHEJ thereby increasing the pool of background mutations. Finally, LIG3 through its damage sensing function allows detection and

subsequent repair of damage inflicted by specific types of chemotherapy such as IRI, thereby allowing cancer cell survival when challenged by DNA damaging agents.

An impediment towards development of specific inhibitors to LIG3 would be the structural overlap between the DNA binding domains and catalytic sites of LIG3 and other ligases, LIG1 and LIG4^{126,200}. Indeed most of the available DNA ligase inhibitors target two or more DNA ligases¹⁹⁹, with varying specificities. A unique structural feature of LIG3 is its N-terminal ZnF domain, which is absent in other DNA ligases²⁰¹. We have shown that this domain is required for SSB sensing function of LIG3 (Chapter 3), and that overexpression of this domain reduces the kinetics of SSBR. Additionally, the ZnF domain within LIG3 has been shown to be required for its role in binding double stranded DNA substrates¹⁶⁸ and therefore promoting aNHEJ¹⁶⁶. Indeed reconstitution of LIG3 deficient cells with Δ ZnF-LIG3 led to decreased reliance on aNHEJ as evidenced by lowered detection of aNHEJ signatures in these cells¹⁶⁶. We postulate that development of inhibitors that structurally mimic ZnF domain of LIG3 is an attractive therapeutic approach in chemotherapy, and would be of value particularly in LIG3 overexpressing tumors.

Mechanistic Insights on the Assembly of PNKP at sites of DNA damage

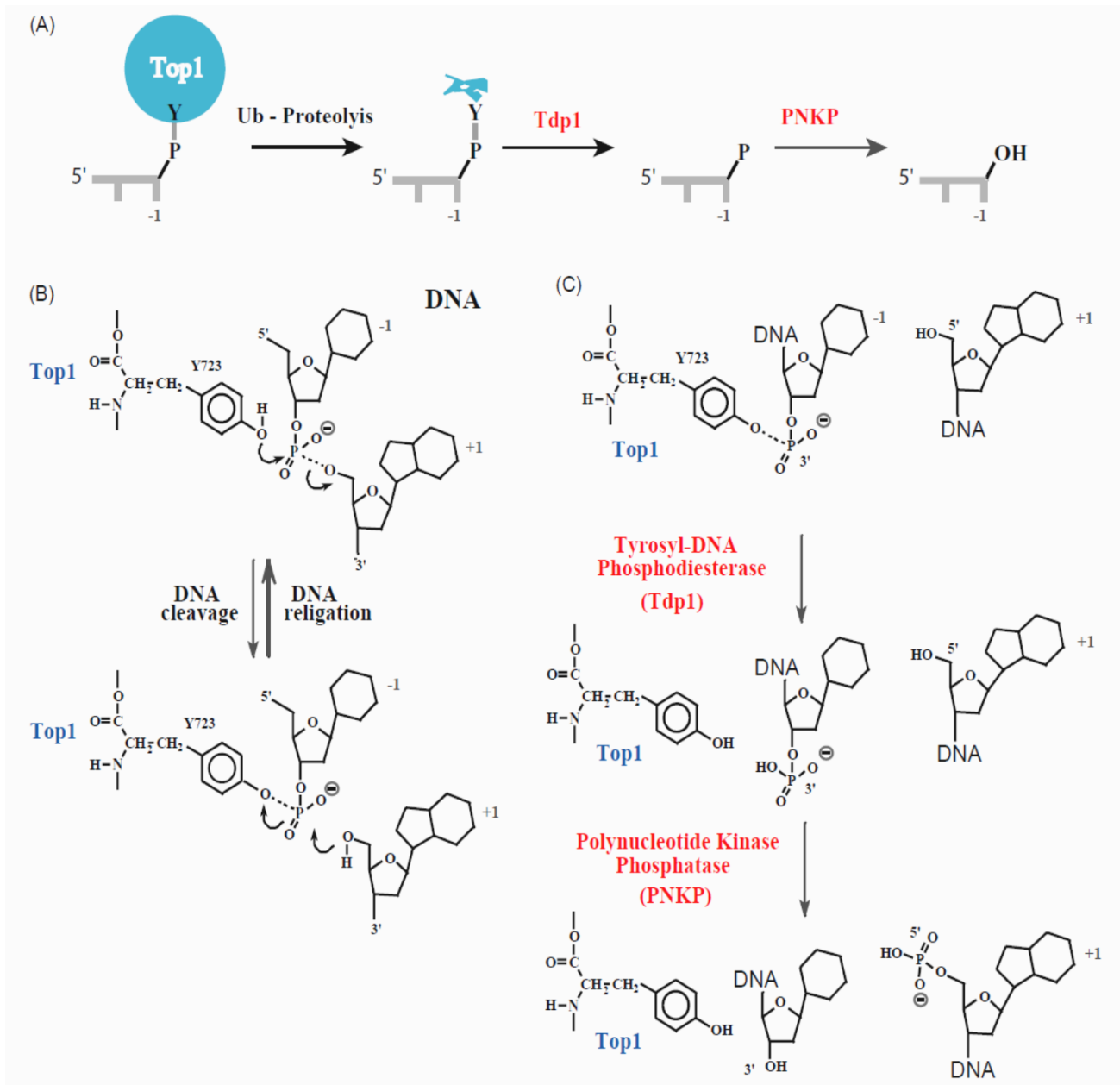
We have previously shown that the ATM/DNA-PKcs mediated phosphorylation of the linker domain in PNKP at residues S114 and S126 is required to ensure optimal levels of PNKP at sites of DNA damage ⁵⁵. Furthermore, blocking these phosphorylation sites impairs catalytic activity of PNKP at damaged DNA ends. We extended this work by studying the impact of such phosphorylation on the independent recruitment of different regions of PNKP to sites of DNA damage and explored the interplay between different PNKP domains to better elucidate how PNKP is assembled at damage sites. Our preliminary results indicate a competition between the FHA domain and full length PNKP for sites of DNA damage. We hypothesize a bimodal mechanism for the assembly of PNKP at sites of damage. First, the FHA domain via protein-protein and / or protein-DNA interactions binds to damaged DNA. Subsequently, the catalytic domain engages where the switch from FHA binding to catalytic domain binding might be facilitated via linker domain phosphorylation.

PNKP function and regulation

DNA damage is associated with DNA termini that are incompatible with gap filling and ligation because of '*dirty ends*' (**Figure 7**). These non-conventional ends arise either from a direct effect of the damaging agent or as repair intermediates as with the case of bifunctional glycosylases (described in chapter 1) ⁹. DNA end processors such as PNKP, TDP1 and APTX, play a pivotal role in multiple DNA repair pathways. The main function ascribed to this group of proteins is to restore proper DNA ends (5' P and 3' OH) to allow for subsequent gap filling and ligation by DNA polymerases and DNA

ligases respectively ^{14,200}. Consequently, defective functioning of DNA end processors leads to stalled repair intermediates such as abortive DNA ligation in the case of defects in APTX ²⁰² or abortive topoisomerase 1 complexes in the case of defects in TDP1 ²⁰³. This ultimately compromises cellular DNA repair capacity. Cooperation between different end processors for the repair of specific lesions is exemplified in the repair of topoisomerase 1 cleavage complexes ²⁰⁴ (**Figure 37**). Topoisomerase 1 forms a tyrosyl-phosphodiester bond with the DNA backbone, which is hydrolysed by TDP1 creating typical substrates for PNKP actions, 3'-P and 5'-OH. Finally, the nick is sealed by the XRCC1-LIG3 complex.

Figure 37: Formation of Topoisomerase 1 cleavage complexes and repair via TDP1/PNKP cooperation



Repair of Top1 covalent complexes by the Tdp1-PNKP pathway. (A) Stepwise reactions mediated by DNA end processors, TDP1 and PNKP, for the repair of Top1 DNA covalent complexes. Ubiquitin mediated degradation of Top1 is required for TDP1 stimulation. (B) Top1 cleaves DNA to reduce torsional stress and allow for metabolic processes to ensue. The cleavage reaction is initiated by nucleophilic attack of Y723 on sugar phosphate backbone of DNA forming a tyrosyl–phosphodiester bond. Then DNA religation (faster reaction indicated by bold arrow) occurs via the nucleophilic attack of 5'-OH end of cleaved DNA thereby releasing Top1. (C) In occasions where DNA religation cannot occur, TDP1 cleaves the tyrosyl–phosphodiester bond leaving a 3'-P ended DNA that is handed over to PNKP, which in turn restores the conventional 3'OH end. **Mutation Research 532 (2003) 173–203**

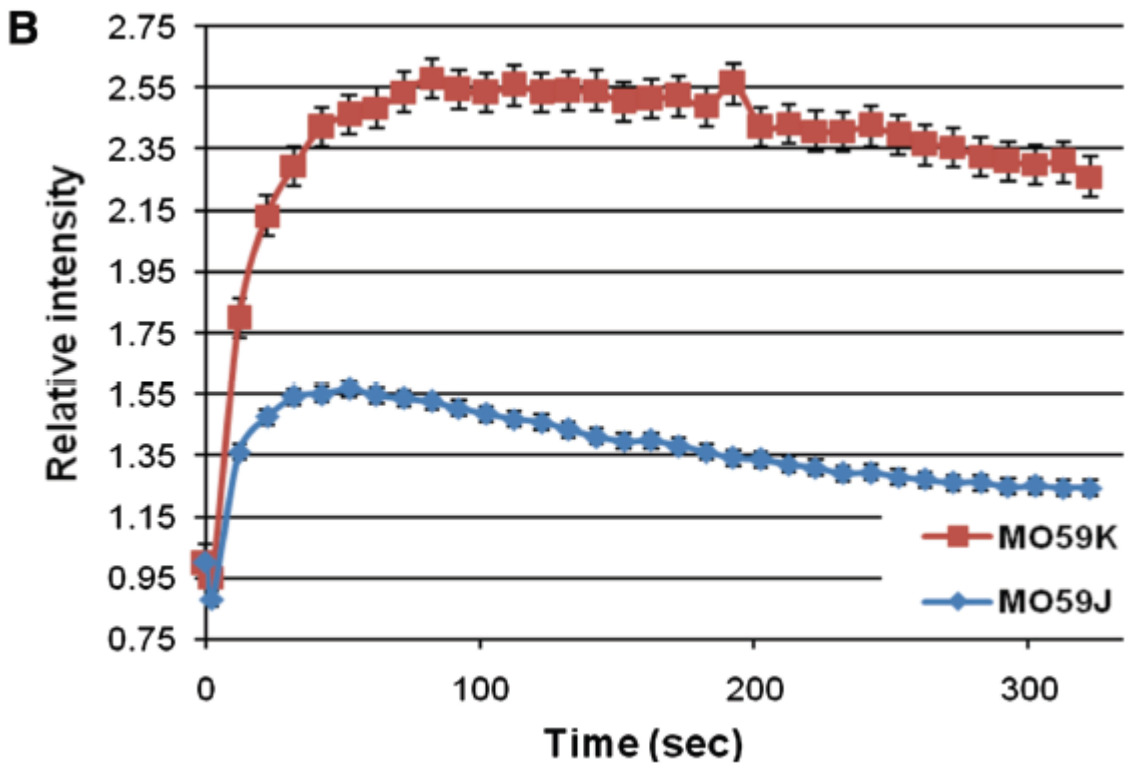
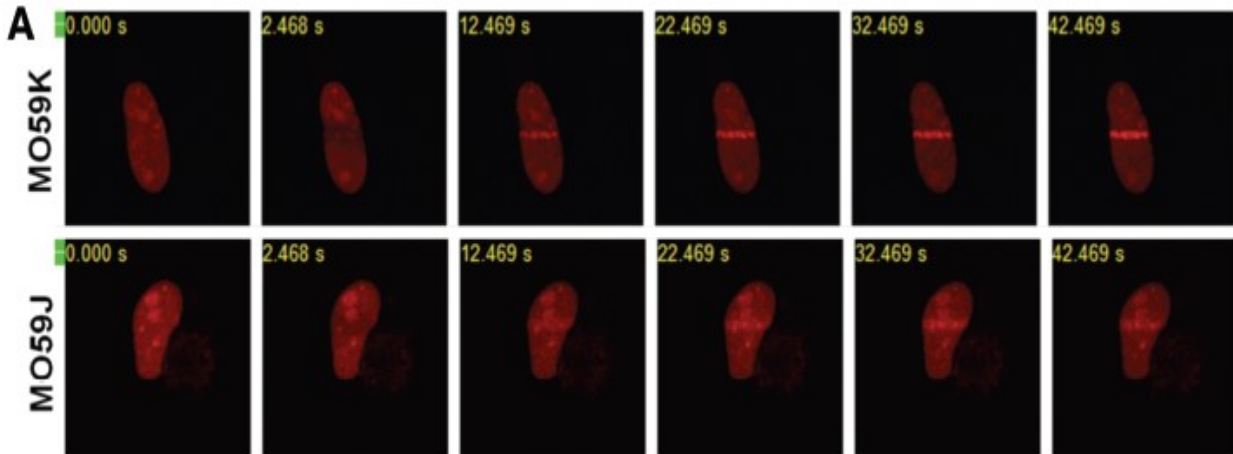
Reproduced with permission from Elsevier. Copyright © 2003

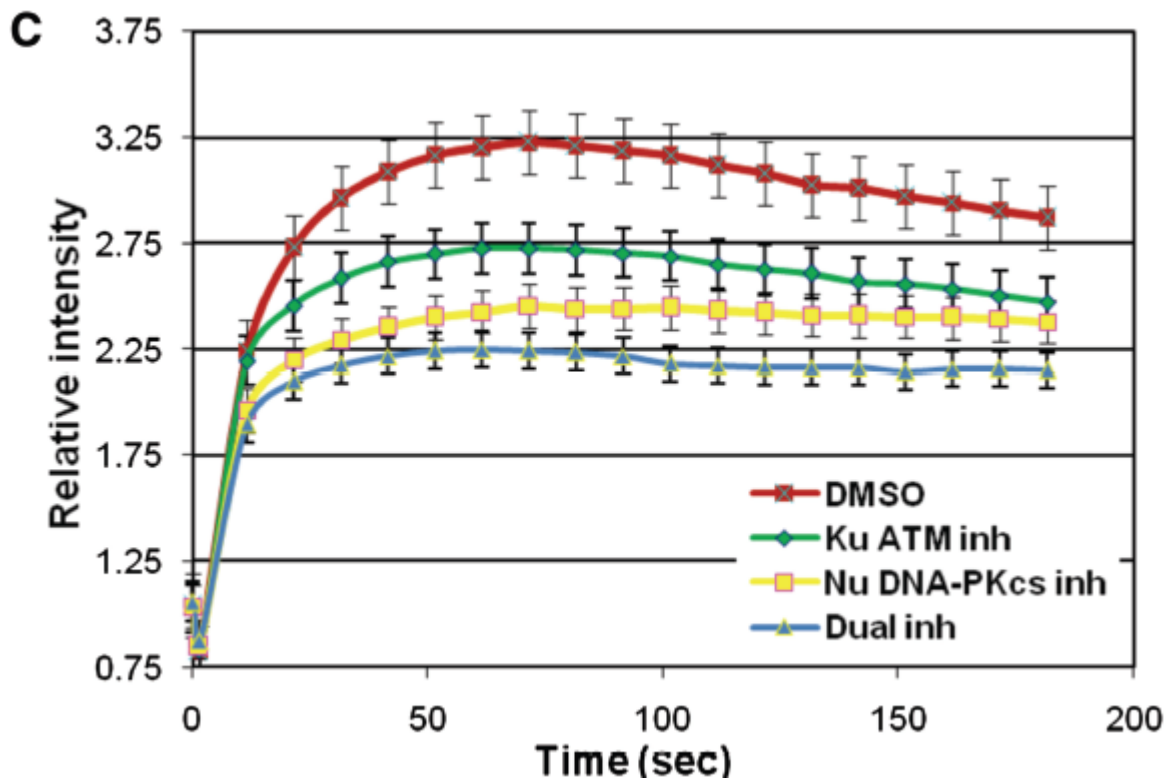
Importantly, genetic defects in three end processors PNKP, APTX and TDP1 have been linked to neurodegenerative disorders MCSZ, AOA1 and SCAN1^{6,205,206}. Additionally, targeting DNA end processors enhances cellular sensitivity to radiotherapy and topoisomerase I poisons^{149,207}. Therefore, better understanding of the mechanisms behind the recruitment of these proteins to sites of DNA damage is important.

Two mechanisms have been proposed to promote the accumulation of PNKP at sites of DNA damage. First, the accumulation of PNKP at SSBs has been attributed to its interaction with XRCC1. Phosphorylated and non-phosphorylated forms of XRCC1 interact with PNKP FHA and catalytic domains, respectively, although with different affinities, and stimulate the activities of PNKP by enhancing its turnover^{144,208}. XRCC1 is a well-established substrate of CK2¹⁷⁷ and XRCC1 is thought to be constitutively phosphorylated in the serine/threonine rich linker region between its two BRCT domains²⁰⁹. Several roles for these phosphorylation events of XRCC1 by CK2 have been described: (1) mobilization from chromatin to nuclear matrix thus facilitating repair²⁰⁹; (2) dissociation of XRCC1 from DNA thereby providing access to downstream proteins²¹⁰; (3) stabilization of XRCC1 protein²¹¹; and (4) promotion of the recruitment of downstream proteins to sites of DNA damage such as the recruitment of PNKP by interaction with the FHA domain of PNKP¹⁷⁷. Surprisingly, in laser μ IR experiments under conditions that don't induce DSBs, we and others^{15,30} have shown that PNKP recruits to sites of DNA damage in EM9 cells (cells devoid of XRCC1), albeit with lower efficiency than WT cells. Therefore, additional mechanism(s) might be responsible for the accumulation of PNKP at damaged DNA. We have previously shown that the linker domain of PNKP (between the FHA and catalytic domains) is phosphorylated in an

ATM/DNA-PKcs-dependent manner at S114/126 in response to DNA damage⁵⁵. These phosphorylation events are required for optimal functioning of PNKP on ssDNA substrates possibly due to compromised binding to damaged DNA. Consistently, recruitment of PNKP to tracks of laser induced DNA damage is decreased in MO59J cells (deficient in DNA-PKcs and ATM) compared to wild type counterparts MO59K cells (**Figure 38, A and B**). Results were confirmed in cells treated with small molecule inhibitors of ATM (KU55933) and DNA-PKcs (NU7741) (**Figure 38C**). Importantly, the phosphorylation of the linker region of PNKP is dispensable for its interaction with the cNHEJ protein, XRCC4⁵⁵. Therefore one might expect a role for these phosphorylation events in SSBR rather than DSBR.

Figure 38: Role of ATM/DNA-PKs in the recruitment of PNKP to laser induced damage tracks

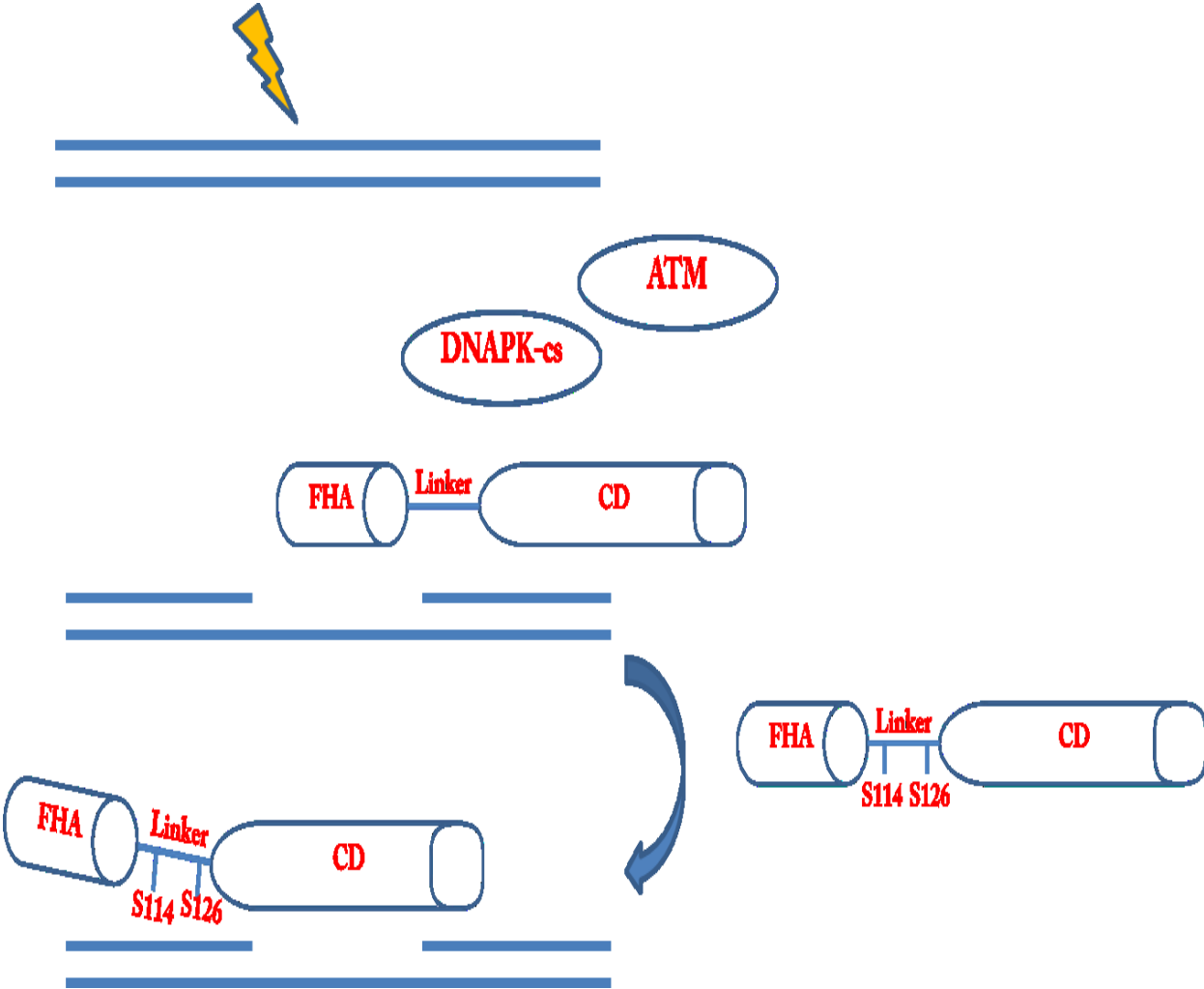




Recruitment of PNKP to sites of DNA damage induced by two-photon laser micro-irradiation is impaired in DNA-PK/ATM-deficient cells. (A) MO59K (DNA-PKcs/ATM WT) and MO59J (DNA-PKcs/ATM deficient) glioma cells transiently expressing PNKP-mRFP were subjected to laser micro-irradiation (as described in experimental procedures section). Recruitment kinetics of PNKP-mRFP at laser-induced DNA damage sites in individual cells was monitored in real time. (B) The amount of the fluorescently tagged protein at tracks of DNA damage was quantified (n=11 cells for each data set; error bars represent S.E.M.). The red line represents MO59K and the blue line represents MO59J cells. (C) HeLa cells expressing PNKP-mRFP were incubated with DMSO (red squares), ATM inhibitor KU55933, 10 μ M (green diamonds), DNA-PK inhibitor NU7741, 10 μ M (yellow squares) or both inhibitors together at 10 μ M each (blue triangles) for 2 h prior to micro-irradiation. Samples were quantified as in (A) and (B).

Based on this collection of observations, we hypothesize a sequential model for the accumulation of PNKP at sites of DNA damage (**Figure 39**). First, PNKP is recruited via its FHA domain binding to phosphorylated XRCC1, PAR or directly damaged DNA. Then, upon phosphorylation of the linker region by ATM/DNA-PKcs, the FHA binding to DNA is distorted allowing for the engagement of the catalytic domain.

Figure 39: Proposed model for the accumulation of PNKP at sites of DNA damage

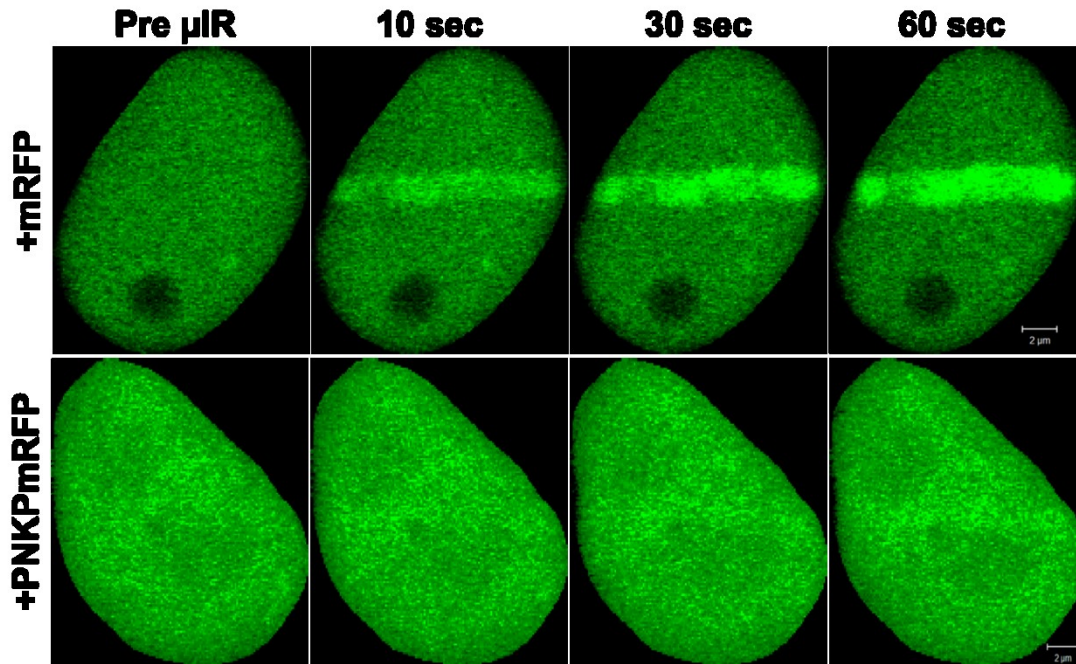


Sequential model for the assembly of PNKP at sites of DNA damage. DNA damage activates ATM and DNA-PKcs. PNKP is recruited via its FHA domain to sites of damage, primarily through interaction with XRCC1. ATM/DNA-PKcs phosphorylate many substrates including the linker domain of PNKP. This phosphorylation alters the conformation of PNKP and possibly reduces the affinity of the FHA domain to binding sites at damaged DNA allowing for the engagement of the catalytic domain with substrate DNA termini.

Preliminary results and future experiments

One way to explore the recruitment of individual domains within PNKP to sites of DNA damage is to express a fluorescent tagged version of each domain and compare the recruitment kinetics in laser μ IR experiments to full length PNKP. When I expressed a mGFP tagged version of the FHA domain fused to the linker (FHA-linker) domain in HeLa cells and tested its behaviour under laser μ IR, the hybrid protein recruits rapidly to sites of damage (**Figure 40**) and is similar to full length PNKP in that respect. To directly compare the recruitment kinetics of FHA-linker to full length PNKP, I co-expressed mGFP-FHA-linker and PNKP-mRFP and monitored the recruitment kinetics in real time. Surprisingly, full length PNKP suppressed the recruitment of FHA linker to laser induced tracks of DNA damage (**Figure 40**). This might reflect a higher affinity of the catalytic domain for binding sites on damaged DNA. To further test this, we will first examine the recruitment kinetics of the catalytic domain alone and compare it to full length PNKP. If our conjecture is correct we expect that the catalytic domain would act in a dominant negative fashion thereby suppressing the accumulation of full length PNKP at sites of DNA damage. However if the catalytic domain didn't suppress the recruitment of full length PNKP, then interactions with other proteins such as XRCC1 should be considered.

Figure 40: Recruitment of FHA-linker to sites of DNA damage



Accumulation of FHA-linker domain at sites of DNA damage in laser μ IR experiments. The upper panel shows the behaviour of FHA-linker in cells co-expressing mRFP vector only. The lower panel shows the recruitment of FHA linker in cells co-expressing PNKP-mRFP

Furthermore, differences in binding affinities between catalytic domain and FHA-linker domains of PNKP need to be assessed by live cell imaging experiments and biochemical assays. I would examine FRAP recovery kinetics of both modules and compare them in the presence and absence of DNA damaging treatment (e.g. hydrogen peroxide). If the catalytic domain of PNKP possesses a higher affinity for damaged DNA than FHA-linker, then a slower recovery of the former would be expected in response to DNA damage. Subsequently, I would express histidine tagged versions of these modules in bacteria. The binding constants of the purified proteins to DNA substrates could be measured by fluorescence quenching assays in response to increasing increments of substrate concentration either depending on acrylodan (AC) labelling (excitation/emission, 380/490 nm) or endogenous tryptophan residues (excitation/emission, 290/340 nm)^{55,139,208,212}.

To better elucidate the independent role(s) of each domain of PNKP in the accumulation of the protein at sites of DNA damage, the independent behaviour of the linker domain needs to be explored. Using site directed mutagenesis of the mGFP FHA-linker, the phosphorylation event on the two serine residues (S114/126) can be either ablated (S114/126A double-mutant) or mimicked (S114/126D double-mutant). Both alterations will be valuable tools. According to our previously published data⁵⁵, I would expect a decreased accumulation of the mutant FHA-linker (S114/126A) as compared to the WT version. To confirm this, we would generate fusion constructs for mammalian expression encoding for mGFP/mRFP tagged versions of WT and mutant linker domain. We would then assess whether the WT linker domain can recruit to sites of DNA damage independently. If this proved to be the case, then we would compare the

recruitment kinetics of both versions to sites of DNA damage using laser μ IR experiments.

Both versions of mutant FHA-linker will be of value in testing my hypothesis. If phosphorylation of the linker domain is responsible for the disengagement of the FHA domain from sites of DNA damage, then the alanine mutant FHA-linker (S114/126A) would be expected to have a slower recovery than either WT or phospho-mimic (S114/126D) FHA-linker under conditions of DNA damage. Analogous results would be expected in *in vitro* DNA binding experiments using purified proteins.

An important aspect to be tested is how our proposed model can reflect the actual behaviour of PNKP and affect its enzymatic function. Our previous results with full length PNKP indicated that the phosphorylation events at these sites (using S114/126D) reduces the affinity of PNKP to damaged substrates thereby reducing its enzymatic activities⁵⁵. I would like to provide a clearer explanation for this observation. I would test the ability of FHA-linker and CD domains of PNKP to reconstitute the enzymatic function of PNKP *in vitro*. The ability to phosphorylate 5'-OH termini on DNA substrates (kinase assay) will be tested. Using different versions of purified FHA-linker + catalytic domain proteins, we will carry out the DNA kinase assay where purified full length PNKP will be used as a reference control. I expect a higher activity of the catalytic domain using the mutant FHA-linker (S114/126D) possibly due to reduced affinity to DNA.

Significance

This proposed work aims to provide deeper insights into the regulation of the DNA end processor enzyme, PNKP. My hypothesis provides a model of how post translational modifications of the linker domain might regulate PNKP binding and activities at damaged substrates.

Importantly, this model would provide a novel role for DSBR proteins, ATM/DNA-PKcs, in the regulation of SSBR. Previous evidence alluded to the possibility of ATM being involved in cell cycle regulation of SSBR²¹³. In the absence of DNA damage, LIG3 is phosphorylated at Ser123 during S-phase by Cdk2. This modification is hypothesized to control the switch between SP-BER to LP-BER during S-phase. However, in the presence of DNA damage, ATM inactivates Cdk2 and activates protein-phosphatase 1 thus driving the dephosphorylation of Ser123 on LIG3. The authors claim that this dephosphorylation might permit the interaction of LIG3 with other SP-BER proteins and increase the overall SSBR capacity of cells under conditions of DNA damage by having both SP-BER and LP-BER functioning²¹³. I have not investigated the impact of cell cycle regulation on the ATM/DNA-PKcs phosphorylation of the linker domain of PNKP, however, my model would provide a novel interface where DSBR and SSBR proteins cooperate to handle the continuing threat to the integrity of DNA.

References

1. Hoeijmakers, J. H. Genome maintenance mechanisms for preventing cancer. *Nature* **411**, 366–74 (2001).
2. Giglia-Mari, G., Zotter, A. & Vermeulen, W. DNA damage response. *Cold Spring Harb. Perspect. Biol.* **3**, a000745 (2011).
3. Reynolds, J. J. & Stewart, G. S. A nervous predisposition to unrepaired DNA double strand breaks. *DNA Repair (Amst)*. **12**, 588–99 (2013).
4. el-Khamisy, S. F. & Caldecott, K. W. DNA single-strand break repair and spinocerebellar ataxia with axonal neuropathy-1. *Neuroscience* **145**, 1260–6 (2007).
5. Reynolds, J. J. *et al.* Defective DNA ligation during short-patch single-strand break repair in ataxia oculomotor apraxia 1. *Mol. Cell. Biol.* **29**, 1354–62 (2009).
6. Shen, J. *et al.* Mutations in PNKP cause microcephaly, seizures and defects in DNA repair. *Nat. Genet.* **42**, 245–9 (2010).
7. Hoeijmakers, J. H. J. DNA damage, aging, and cancer. *N. Engl. J. Med.* **361**, 1475–85 (2009).
8. Karimi-busheri, F. *et al.* Molecular Characterization of a Human DNA Kinase *. **274**, 24187–24194 (1999).
9. Weinfeld, M., Mani, R. S., Abdou, I., Aceytuno, R. D. & Glover, J. N. M. Tidying up loose ends: the role of polynucleotide kinase/phosphatase in DNA strand break repair. *Trends Biochem. Sci.* **36**, 262–71 (2011).
10. Chatterjee, A. *et al.* The role of the mammalian DNA end-processing enzyme polynucleotide kinase 3'-phosphatase in spinocerebellar ataxia type 3 pathogenesis. *PLoS Genet.* **11**, e1004749 (2015).
11. Gao, R. *et al.* Inactivation of PNKP by mutant ATXN3 triggers apoptosis by activating the DNA damage-response pathway in SCA3. *PLoS Genet.* **11**, e1004834 (2015).
12. McKinnon, P. J. & Caldecott, K. W. DNA strand break repair and human genetic disease. *Annu. Rev. Genomics Hum. Genet.* **8**, 37–55 (2007).
13. Caldecott, K. Single-strand break repair and genetic disease. *Nat. Rev. Genet.* **9**, 619–31 (2008).

14. El-Khamisy, S. F. To live or to die: a matter of processing damaged DNA termini in neurons. *EMBO Mol. Med.* **3**, 78–88 (2011).
15. Hanssen-Bauer, A. *et al.* The region of XRCC1 which harbours the three most common nonsynonymous polymorphic variants, is essential for the scaffolding function of XRCC1. *DNA Repair (Amst)*. **11**, 357–66 (2012).
16. Sobol, R. W. Genome instability caused by a germline mutation in the human DNA repair gene POLB. *PLoS Genet.* **8**, e1003086 (2012).
17. Schanst, G. P. V. A. N. D. E. R. DNA strand break and rejoining in cultured human fibroblasts exposed to fast neutrons or gamma rays. 75–85 (1983).
18. Dianov, G. L. & Hübscher, U. Mammalian base excision repair: the forgotten archangel. *Nucleic Acids Res.* **41**, 3483–90 (2013).
19. Hegde, M. L., Hazra, T. K. & Mitra, S. Early steps in the DNA base excision/single-strand interruption repair pathway in mammalian cells. *Cell Res.* **18**, 27–47 (2008).
20. Robertson, a B., Klungland, a, Rognes, T. & Leiros, I. DNA repair in mammalian cells: Base excision repair: the long and short of it. *Cell. Mol. Life Sci.* **66**, 981–93 (2009).
21. Bouziane, M. *et al.* Repair of DNA alkylation damage. *Acta Biochim. Pol.* **45**, 191–202 (1998).
22. Jacobs, A. L. & Schär, P. DNA glycosylases: in DNA repair and beyond. *Chromosoma* **121**, 1–20 (2012).
23. Duncan, B. K. & Miller, J. H. Mutagenic deamination of cytosine residues in DNA. *Nature* **287**, 560–1 (1980).
24. Michaels, M. L. & Miller, J. H. The GO system protects organisms from the mutagenic effect of the spontaneous lesion 8-hydroxyguanine (7,8-dihydro-8-oxoguanine). *J. Bacteriol.* **174**, 6321–5 (1992).
25. Almeida, K. H. & Sobol, R. W. A unified view of base excision repair: lesion-dependent protein complexes regulated by post-translational modification. *DNA Repair (Amst)*. **6**, 695–711 (2007).
26. Horton, J. K. *et al.* XRCC1 and DNA polymerase beta in cellular protection against cytotoxic DNA single-strand breaks. *Cell Res.* **18**, 48–63 (2008).

27. Fortini, P. & Dogliotti, E. Base damage and single-strand break repair: mechanisms and functional significance of short- and long-patch repair subpathways. *DNA Repair (Amst)*. **6**, 398–409 (2007).
28. Lan, L. *et al.* In situ analysis of repair processes for oxidative DNA damage in mammalian cells. (2004).
29. Mortusewicz, O. & Leonhardt, H. XRCC1 and PCNA are loading platforms with distinct kinetic properties and different capacities to respond to multiple DNA lesions. *BMC Mol. Biol.* **8**, 81 (2007).
30. Hanssen-Bauer, A. *et al.* XRCC1 coordinates disparate responses and multiprotein repair complexes depending on the nature and context of the DNA damage. *Environ. Mol. Mutagen.* **52**, 623–35 (2011).
31. Petermann, E., Keil, C. & Oei, S. L. Roles of DNA ligase III and XRCC1 in regulating the switch between short patch and long patch BER. *DNA Repair (Amst)*. **5**, 544–55 (2006).
32. Rouleau, M., Patel, A., Hendzel, M. J., Kaufmann, S. H. & Poirier, G. G. PARP inhibition: PARP1 and beyond. *Nat. Rev. Cancer* **10**, 293–301 (2010).
33. Pardo, B., Gómez-González, B. & Aguilera, a. DNA repair in mammalian cells: DNA double-strand break repair: how to fix a broken relationship. *Cell. Mol. Life Sci.* **66**, 1039–56 (2009).
34. Mahaney, B. L., Meek, K. & Lees-Miller, S. P. Repair of ionizing radiation-induced DNA double-strand breaks by non-homologous end-joining. *Biochem. J.* **417**, 639–50 (2009).
35. Downs, J. A. Chromatin structure and DNA double-strand break responses in cancer progression and therapy. *Oncogene* **26**, 7765–72 (2007).
36. Keeney, S. & Neale, M. J. Initiation of meiotic recombination by formation of DNA double-strand breaks: mechanism and regulation. *Biochem. Soc. Trans.* **34**, 523–5 (2006).
37. Dudley, D. D., Chaudhuri, J., Bassing, C. H. & Alt, F. W. Mechanism and control of V(D)J recombination versus class switch recombination: similarities and differences. *Adv. Immunol.* **86**, 43–112 (2005).
38. JUNG, D. Unraveling V(D)J Recombination Insights into Gene Regulation. *Cell* **116**, 299–311 (2004).
39. Krejci, L., Altmannova, V., Spirek, M. & Zhao, X. Homologous recombination and its regulation. *Nucleic Acids Res.* **40**, 5795–818 (2012).

40. Chapman, J. R., Taylor, M. R. G. & Boulton, S. J. Playing the end game: DNA double-strand break repair pathway choice. *Mol. Cell* **47**, 497–510 (2012).
41. Iyama, T. & Wilson, D. M. DNA repair mechanisms in dividing and non-dividing cells. *DNA Repair (Amst)*. **12**, 620–36 (2013).
42. Stucki, M. & Jackson, S. P. gammaH2AX and MDC1: anchoring the DNA-damage-response machinery to broken chromosomes. *DNA Repair (Amst)*. **5**, 534–43 (2006).
43. Savic, V. *et al.* Formation of dynamic gamma-H2AX domains along broken DNA strands is distinctly regulated by ATM and MDC1 and dependent upon H2AX densities in chromatin. *Mol. Cell* **34**, 298–310 (2009).
44. Caestecker, K. W. & Van de Walle, G. R. The role of BRCA1 in DNA double-strand repair: past and present. *Exp. Cell Res.* **319**, 575–87 (2013).
45. Sugiyama, T. & Kowalczykowski, S. C. Rad52 protein associates with replication protein A (RPA)-single-stranded DNA to accelerate Rad51-mediated displacement of RPA and presynaptic complex formation. *J. Biol. Chem.* **277**, 31663–72 (2002).
46. Jensen, R. B., Carreira, A. & Kowalczykowski, S. C. Purified human BRCA2 stimulates RAD51-mediated recombination. *Nature* **467**, 678–83 (2010).
47. McIlwraith, M. J. *et al.* Reconstitution of the strand invasion step of double-strand break repair using human Rad51 Rad52 and RPA proteins. *J. Mol. Biol.* **304**, 151–64 (2000).
48. McIlwraith, M. J. *et al.* Human DNA polymerase eta promotes DNA synthesis from strand invasion intermediates of homologous recombination. *Mol. Cell* **20**, 783–92 (2005).
49. Daley, J. M. & Sung, P. 53BP1, BRCA1, and the choice between recombination and end joining at DNA double-strand breaks. *Mol. Cell. Biol.* **34**, 1380–8 (2014).
50. Lieber, M. R. The mechanism of double-strand DNA break repair by the nonhomologous DNA end-joining pathway. *Annu. Rev. Biochem.* **79**, 181–211 (2010).
51. Chatterjee, P. *et al.* Defective chromatin recruitment and retention of NHEJ core components in human tumor cells expressing a Cyclin E fragment. *Nucleic Acids Res.* **41**, 10157–69 (2013).

52. Deriano, L. & Roth, D. B. Modernizing the nonhomologous end-joining repertoire: alternative and classical NHEJ share the stage. *Annu. Rev. Genet.* **47**, 433–55 (2013).
53. Ma, Y. *et al.* A biochemically defined system for mammalian nonhomologous DNA end joining. *Mol. Cell* **16**, 701–13 (2004).
54. Drouet, J. *et al.* DNA-dependent protein kinase and XRCC4-DNA ligase IV mobilization in the cell in response to DNA double strand breaks. *J. Biol. Chem.* **280**, 7060–9 (2005).
55. Zolner, A. E. *et al.* Phosphorylation of polynucleotide kinase/ phosphatase by DNA-dependent protein kinase and ataxia-telangiectasia mutated regulates its association with sites of DNA damage. *Nucleic Acids Res.* **39**, 9224–37 (2011).
56. Ma, Y., Pannicke, U., Schwarz, K. & Lieber, M. R. Hairpin Opening and Overhang Processing by an Artemis/DNA-Dependent Protein Kinase Complex in Nonhomologous End Joining and V(D)J Recombination. *Cell* **108**, 781–794 (2002).
57. Neal, J. a & Meek, K. Choosing the right path: does DNA-PK help make the decision? *Mutat. Res.* **711**, 73–86 (2011).
58. Reynolds, P. *et al.* The dynamics of Ku70/80 and DNA-PKcs at DSBs induced by ionizing radiation is dependent on the complexity of damage. *Nucleic Acids Res.* **40**, 10821–31 (2012).
59. Ma, Y., Schwarz, K. & Lieber, M. R. The Artemis:DNA-PKcs endonuclease cleaves DNA loops, flaps, and gaps. *DNA Repair (Amst)*. **4**, 845–51 (2005).
60. Karimi-Busheri, F., Rasouli-Nia, A., Allalunis-Turner, J. & Weinfeld, M. Human polynucleotide kinase participates in repair of DNA double-strand breaks by nonhomologous end joining but not homologous recombination. *Cancer Res.* **67**, 6619–25 (2007).
61. Panier, S. & Boulton, S. J. Double-strand break repair: 53BP1 comes into focus. *Nat. Rev. Mol. Cell Biol.* **15**, 7–18 (2014).
62. Mouw, K. W. & D’Andrea, A. D. Crosstalk between the nucleotide excision repair and Fanconi anemia/BRCA pathways. *DNA Repair (Amst)*. **19**, 130–4 (2014).
63. Helleday, T., Petermann, E., Lundin, C., Hodgson, B. & Sharma, R. A. DNA repair pathways as targets for cancer therapy. *Nat. Rev. Cancer* **8**, 193–204 (2008).
64. Wang, H. *et al.* Biochemical evidence for Ku-independent backup pathways of NHEJ. *Nucleic Acids Res.* **31**, 5377–88 (2003).

65. Nussenzweig, A. & Nussenzweig, M. C. A backup DNA repair pathway moves to the forefront. *Cell* **131**, 223–5 (2007).
66. Wang, H. *et al.* DNA ligase III as a candidate component of backup pathways of nonhomologous end joining. *Cancer Res.* **65**, 4020–30 (2005).
67. Soni, A. *et al.* Requirement for Parp-1 and DNA ligases 1 or 3 but not of Xrcc1 in chromosomal translocation formation by backup end joining. *Nucleic Acids Res.* **42**, 6380–92 (2014).
68. Caldecott, K. W., Tucker, J. D., Stanker, L. H. & Thompson, L. H. Characterization of the XRCC1-DNA ligase III complex *in vitro* and its absence from mutant hamster cells. *Nucleic Acids Res.* **23**, 4836–43 (1995).
69. Boboila, C. *et al.* Robust chromosomal DNA repair via alternative end-joining in the absence of X-ray repair cross-complementing protein 1 (XRCC1). *Proc. Natl. Acad. Sci. U. S. A.* **109**, 2473–8 (2012).
70. Audebert, M., Salles, B. & Calsou, P. Involvement of poly(ADP-ribose) polymerase-1 and XRCC1/DNA ligase III in an alternative route for DNA double-strand breaks rejoining. *J. Biol. Chem.* **279**, 55117–26 (2004).
71. Wang, M. *et al.* PARP-1 and Ku compete for repair of DNA double strand breaks by distinct NHEJ pathways. *Nucleic Acids Res.* **34**, 6170–82 (2006).
72. Cheng, Q. *et al.* Ku counteracts mobilization of PARP1 and MRN in chromatin damaged with DNA double-strand breaks. *Nucleic Acids Res.* **39**, 9605–19 (2011).
73. Wray, J. *et al.* PARP1 is required for chromosomal translocations. *Blood* **121**, 4359–65 (2013).
74. Haince, J.-F. *et al.* PARP1-dependent kinetics of recruitment of MRE11 and NBS1 proteins to multiple DNA damage sites. *J. Biol. Chem.* **283**, 1197–208 (2008).
75. Dueva, R. & Iliakis, G. Alternative pathways of non-homologous end joining (NHEJ) in genomic instability and cancer. **2**, 163–177 (2013).
76. Saß, C. & Alberti, W. Comparison of biological effects of DNA damage induced by ionizing radiation and hydrogen peroxide in CHO cells. **76**, (2000).
77. Ward, J. F., Evans, J. W., Limoli, C. L. & Calabro-Jones, P. M. Radiation and hydrogen peroxide induced free radical damage to DNA. *Br. J. Cancer. Suppl.* **8**, 105–12 (1987).

78. Powell, S. & McMillan, T. J. DNA damage and repair following treatment with ionizing radiation. *Radiother. Oncol.* **19**, 95–108 (1990).
79. Lundin, C. *et al.* Methyl methanesulfonate (MMS) produces heat-labile DNA damage but no detectable *in vivo* DNA double-strand breaks. *Nucleic Acids Res.* **33**, 3799–811 (2005).
80. Deweese, J. E., Osheroff, M. A. & Osheroff, N. DNA Topology and Topoisomerases: Teaching a ‘Knotty’ Subject. *Biochem. Mol. Biol. Educ.* **37**, 2–10 (2008).
81. Pommier, Y. DNA topoisomerase I inhibitors: chemistry, biology, and interfacial inhibition. *Chem. Rev.* **109**, 2894–902 (2009).
82. Feuerhahn, S. & Egly, J.-M. Tools to study DNA repair: what’s in the box? *Trends Genet.* **24**, 467–74 (2008).
83. Pastwa, E., Somiari, R. I., Malinowski, M., Somiari, S. B. & Winters, T. A. *In vitro* non-homologous DNA end joining assays--the 20th anniversary. *Int. J. Biochem. Cell Biol.* **41**, 1254–60 (2009).
84. Kubota, Y. *et al.* Reconstitution of DNA base excision-repair with purified human proteins: interaction between DNA polymerase beta and the XRCC1 protein. *EMBO J.* **15**, 6662–70 (1996).
85. Klungland, A. & Lindahl, T. Second pathway for completion of human DNA base excision-repair: reconstitution with purified proteins and requirement for DNase IV (FEN1). *EMBO J.* **16**, 3341–8 (1997).
86. Cremer, C. *et al.* UV micro-irradiation of the Chinese hamster cell nucleus and caffeine post-treatment immunocytochemical localization of DNA photolesions in cells with partial and generalized chromosome shattering. *Mutat. Res. Mol. Mech. Mutagen.* **107**, 465–476 (1983).
87. Zorn, C., Cremer, T., Cremer, C. & Zimmer, J. Laser UV microirradiation of interphase nuclei and post-treatment with caffeine. *Hum. Genet.* **35**, 83–89 (1976).
88. Nagy, Z. & Soutoglou, E. DNA repair: easy to visualize, difficult to elucidate. *Trends Cell Biol.* **19**, 617–29 (2009).
89. Dinant, C. *et al.* Activation of multiple DNA repair pathways by sub-nuclear damage induction methods. *J. Cell Sci.* **120**, 2731–40 (2007).

90. Kong, X. *et al.* Comparative analysis of different laser systems to study cellular responses to DNA damage in mammalian cells. *Nucleic Acids Res.* **37**, e68 (2009).
91. Ishikawa-Ankerhold, H. C., Ankerhold, R. & Drummen, G. P. C. Advanced fluorescence microscopy techniques--FRAP, FLIP, FLAP, FRET and FLIM. *Molecules* **17**, 4047–132 (2012).
92. McNally, J. G. Quantitative FRAP in analysis of molecular binding dynamics *in vivo*. *Methods Cell Biol.* **85**, 329–51 (2008).
93. Mueller, F., Mazza, D., Stasevich, T. J. & McNally, J. G. FRAP and kinetic modeling in the analysis of nuclear protein dynamics: what do we really know? *Curr. Opin. Cell Biol.* **22**, 403–11 (2010).
94. Young, L. C. & Hendzel, M. J. The oncogenic potential of Jumonji D2 (JMJD2/KDM4) histone demethylase overexpression. *Biochem. Cell Biol.* **91**, 369–77 (2013).
95. Wilson, S. H. & Kunkel, T. A. Passing the baton in base excision repair. *Nat. Struct. Biol.* **7**, 176–8 (2000).
96. Prasad, R., Shock, D. D., Beard, W. A. & Wilson, S. H. Substrate channeling in mammalian base excision repair pathways: passing the baton. *J. Biol. Chem.* **285**, 40479–88 (2010).
97. Parsons, J. L. & Dianov, G. L. Co-ordination of base excision repair and genome stability. *DNA Repair (Amst)*. **12**, 326–33 (2013).
98. Eustermann, S. *et al.* The DNA-binding domain of human PARP-1 interacts with DNA single-strand breaks as a monomer through its second zinc finger. *J. Mol. Biol.* **407**, 149–70 (2011).
99. Coquelle, N. & Glover, J. N. M. PARP pairs up to PARsylate. *Nat. Struct. Mol. Biol.* **19**, 660–1 (2012).
100. Langelier, M.-F., Planck, J. L., Roy, S. & Pascal, J. M. Structural basis for DNA damage-dependent poly(ADP-ribosylation) by human PARP-1. *Science* **336**, 728–32 (2012).
101. Ali, A. a E. *et al.* The zinc-finger domains of PARP1 cooperate to recognize DNA strand breaks. *Nat. Struct. Mol. Biol.* **19**, 685–92 (2012).
102. Kim, M. Y., Zhang, T. & Kraus, W. L. Poly(ADP-ribosylation) by PARP-1: 'PAR-laying' NAD⁺ into a nuclear signal. *Genes Dev.* **19**, 1951–67 (2005).

103. Godon, C. *et al.* PARP inhibition versus PARP-1 silencing: different outcomes in terms of single-strand break repair and radiation susceptibility. *Nucleic Acids Res.* **36**, 4454–64 (2008).
104. Mortusewicz, O., Amé, J.-C., Schreiber, V. & Leonhardt, H. Feedback-regulated poly(ADP-ribosyl)ation by PARP-1 is required for rapid response to DNA damage in living cells. *Nucleic Acids Res.* **35**, 7665–75 (2007).
105. Act, A. B. Requirement of poly (ADP-ribose) polymerase in recovery from DNA damage in mice and in cells. **94**, 7303–7307 (1997).
106. Dantzer, F. *et al.* Involvement of poly(ADP-ribose) polymerase in base excision repair. *Biochimie* **81**, 69–75 (1999).
107. Abdou, I., Poirier, G. G., Hendzel, M. J. & Weinfeld, M. DNA ligase III acts as a DNA strand break sensor in the cellular orchestration of DNA strand break repair. *Nucleic Acids Res.* 1–18 (2014). doi:10.1093/nar/gku1307
108. El-Khamisy, S. F. A requirement for PARP-1 for the assembly or stability of XRCC1 nuclear foci at sites of oxidative DNA damage. *Nucleic Acids Res.* **31**, 5526–5533 (2003).
109. Campalans, A. *et al.* Distinct spatiotemporal patterns and PARP dependence of XRCC1 recruitment to single-strand break and base excision repair. *Nucleic Acids Res.* **41**, 3115–29 (2013).
110. Rouleau, M., Aubin, R. a & Poirier, G. G. Poly(ADP-ribosyl)ated chromatin domains: access granted. *J. Cell Sci.* **117**, 815–25 (2004).
111. Smeenk, G. *et al.* Poly(ADP-ribosyl)ation links the chromatin remodeler SMARCA5/SNF2H to RNF168-dependent DNA damage signaling. *J. Cell Sci.* **126**, 889–903 (2013).
112. Jakob, B. *et al.* DNA double-strand breaks in heterochromatin elicit fast repair protein recruitment, histone H2AX phosphorylation and relocation to euchromatin. *Nucleic Acids Res.* **39**, 6489–99 (2011).
113. Pleschke, J. M., Kleczkowska, H. E., Strohm, M. & Althaus, F. R. Poly(ADP-ribose) binds to specific domains in DNA damage checkpoint proteins. *J. Biol. Chem.* **275**, 40974–80 (2000).
114. Leppard, J. B., Dong, Z., Mackey, Z. B. & Tomkinson, A. E. Physical and Functional Interaction between DNA Ligase III α and Poly (ADP-Ribose) Polymerase 1 in DNA Single-Strand Break Repair Physical and Functional Interaction between DNA Ligase III β and Poly (ADP-Ribose) Polymerase 1 in DNA Single-Strand Brea. (2003). doi:10.1128/MCB.23.16.5919

115. Caldecott, K. W., Aoufouchi, S., Johnson, P. & Shall, S. XRCC1 polypeptide interacts with DNA polymerase beta and possibly poly (ADP-ribose) polymerase, and DNA ligase III is a novel molecular 'nick-sensor' *in vitro*. *Nucleic Acids Res.* **24**, 4387–94 (1996).
116. Noren Hooten, N., Kompaniez, K., Barnes, J., Lohani, A. & Evans, M. K. Poly(ADP-ribose) polymerase 1 (PARP-1) binds to 8-oxoguanine-DNA glycosylase (OGG1). *J. Biol. Chem.* **286**, 44679–90 (2011).
117. Bryant, H. E. *et al.* Specific killing of BRCA2-deficient tumours with inhibitors of poly(ADP-ribose) polymerase. *Nature* **434**, 913–7 (2005).
118. Farmer, H. *et al.* Targeting the DNA repair defect in BRCA mutant cells as a therapeutic strategy. *Nature* **434**, 917–21 (2005).
119. Patel, A. G., Sarkaria, J. N. & Kaufmann, S. H. Nonhomologous end joining drives poly (ADP-ribose) polymerase (PARP) inhibitor lethality in homologous recombination-deficient cells. (2011). doi:10.1073/pnas.1013715108/-/DCSupplemental.www.pnas.org/cgi/doi/10.1073/pnas.1013715108
120. Wang, Z. Q. *et al.* Mice lacking ADPRT and poly(ADP-ribosyl)ation develop normally but are susceptible to skin disease. *Genes Dev.* **9**, 509–20 (1995).
121. Vodenicharov, M. D., Sallmann, F. R., Satoh, M. S. & Poirier, G. G. Base excision repair is efficient in cells lacking poly(ADP-ribose) polymerase 1. *Nucleic Acids Res.* **28**, 3887–96 (2000).
122. Ström, C. E. *et al.* Poly (ADP-ribose) polymerase (PARP) is not involved in base excision repair but PARP inhibition traps a single-strand intermediate. *Nucleic Acids Res.* **39**, 3166–75 (2011).
123. Parsons, J. L., Dianova, I. I., Boswell, E., Weinfeld, M. & Dianov, G. L. End-damage-specific proteins facilitate recruitment or stability of X-ray cross-complementing protein 1 at the sites of DNA single-strand break repair. **272**, 5753–5763 (2005).
124. Petrucco, S. Sensing DNA damage by PARP-like fingers. *Nucleic Acids Res.* **31**, 6689–6699 (2003).
125. Mackey, Z. B. DNA Ligase III Is Recruited to DNA Strand Breaks by a Zinc Finger Motif Homologous to That of Poly(ADP-ribose) Polymerase. IDENTIFICATION OF TWO FUNCTIONALLY DISTINCT DNA BINDING REGIONS WITHIN DNA LIGASE III. *J. Biol. Chem.* **274**, 21679–21687 (1999).

126. Cotner-Gohara, E., Kim, I.-K., Tomkinson, A. E. & Ellenberger, T. Two DNA-binding and nick recognition modules in human DNA ligase III. *J. Biol. Chem.* **283**, 10764–72 (2008).
127. Thompson, L. H. An Interaction between the Mammalian DNA Repair Protein XRCC1 and DNA Ligase III. **14**, (1994).
128. Caldecott, K. W., Aoufouchi, S., Johnson, P. & Shall, S. XRCC1 Polypeptide Interacts with DNA Polymerase and Possibly Poly (ADP-Ribose) Polymerase, and DNA Ligase III Is a Novel Molecular ‘Nick-Sensor’ *In vitro*. *Nucleic Acids Res.* **24**, 4387–4394 (1996).
129. Mortusewicz, O., Rothbauer, U., Cardoso, M. C. & Leonhardt, H. Differential recruitment of DNA Ligase I and III to DNA repair sites. *Nucleic Acids Res.* **34**, 3523–32 (2006).
130. Zhang, L. *et al.* The XRCC1 Arg194Trp polymorphism is not a risk factor for glioma: A meta-analysis involving 1,440 cases and 2,562 controls. *Exp. Ther. Med.* **4**, 1057–1062 (2012).
131. Qian, Y. *et al.* [Relationship between polymorphisms of X-ray repair cross-complementing group 1 gene Arg194Trp, Arg399Gln and susceptibility of breast cancer]. *Zhonghua Yu Fang Yi Xue Za Zhi* **44**, 242–6 (2010).
132. Hu, Z., Ma, H., Chen, F., Wei, Q. & Shen, H. XRCC1 polymorphisms and cancer risk: a meta-analysis of 38 case-control studies. *Cancer Epidemiol. Biomarkers Prev.* **14**, 1810–8 (2005).
133. De Ruyck, K. *et al.* Polymorphisms in base-excision repair and nucleotide-excision repair genes in relation to lung cancer risk. *Mutat. Res.* **631**, 101–10 (2007).
134. Wang, J.-Y. & Cai, Y. X-ray repair cross-complementing group 1 codon 399 polymorphism and lung cancer risk: an updated meta-analysis. *Tumour Biol.* **35**, 411–8 (2014).
135. Huang, J. *et al.* The Arg194Trp polymorphism in the XRCC1 gene and cancer risk in Chinese Mainland population: a meta-analysis. *Mol. Biol. Rep.* **38**, 4565–73 (2011).
136. Bao, Y. *et al.* XRCC1 gene polymorphisms and the risk of differentiated thyroid carcinoma (DTC): a meta-analysis of case-control studies. *PLoS One* **8**, e64851 (2013).

137. Breslin, C. & Caldecott, K. W. DNA 3'-phosphatase activity is critical for rapid global rates of single-strand break repair following oxidative stress. *Mol. Cell. Biol.* **29**, 4653–62 (2009).
138. Bernstein, N. K. *et al.* The molecular architecture of the mammalian DNA repair enzyme, polynucleotide kinase. *Mol. Cell* **17**, 657–70 (2005).
139. Lu, M. *et al.* Independent mechanisms of stimulation of polynucleotide kinase / phosphatase by phosphorylated and non-phosphorylated XRCC1. 1–12 (2009). doi:10.1093/nar/gkp1023
140. Bernstein, N. K. *et al.* Polynucleotide kinase as a potential target for enhancing cytotoxicity by ionizing radiation and topoisomerase I inhibitors. *Anticancer. Agents Med. Chem.* **8**, 358–67 (2008).
141. Bernstein, N. K. *et al.* Mechanism of DNA substrate recognition by the mammalian DNA repair enzyme, Polynucleotide Kinase. *Nucleic Acids Res.* **37**, 6161–73 (2009).
142. Parsons, J. L. *et al.* Phosphorylation of PNKP by ATM prevents its proteasomal degradation and enhances resistance to oxidative stress. *Nucleic Acids Res.* **40**, 11404–15 (2012).
143. Segal-Raz, H. *et al.* ATM-mediated phosphorylation of polynucleotide kinase/phosphatase is required for effective DNA double-strand break repair. *EMBO Rep.* **12**, 713–9 (2011).
144. Lu, M. *et al.* Independent mechanisms of stimulation of polynucleotide kinase/phosphatase by phosphorylated and non-phosphorylated XRCC1. *Nucleic Acids Res.* **38**, 510–21 (2010).
145. Ali, A. A. E., Jukes, R. M., Pearl, L. H. & Oliver, A. W. Specific recognition of a multiply phosphorylated motif in the DNA repair scaffold XRCC1 by the FHA domain of human PNK. *Nucleic Acids Res.* **37**, 1701–12 (2009).
146. Li, M., Lu, L.-Y., Yang, C.-Y., Wang, S. & Yu, X. The FHA and BRCT domains recognize ADP-ribosylation during DNA damage response. *Genes Dev.* **27**, 1752–68 (2013).
147. Lu, M. *et al.* Independent mechanisms of stimulation of polynucleotide kinase/phosphatase by phosphorylated and non-phosphorylated XRCC1. *Nucleic Acids Res.* **38**, 510–21 (2010).
148. Mani, R. S., Karimi-Busheri, F., Fanta, M., Cass, C. E. & Weinfeld, M. Spectroscopic studies of DNA and ATP binding to human polynucleotide kinase: evidence for a ternary complex. *Biochemistry* **42**, 12077–84 (2003).

149. Freschauf, G. K. *et al.* Mechanism of action of an imidopiperidine inhibitor of human polynucleotide kinase/phosphatase. *J. Biol. Chem.* **285**, 2351–60 (2010).
150. Unger, T., Jacobovitch, Y., Dantes, A., Bernheim, R. & Peleg, Y. Applications of the Restriction Free (RF) cloning procedure for molecular manipulations and protein expression. *J. Struct. Biol.* **172**, 34–44 (2010).
151. Mani, R. S. *et al.* XRCC1 stimulates polynucleotide kinase by enhancing its damage discrimination and displacement from DNA repair intermediates. *J. Biol. Chem.* **282**, 28004–13 (2007).
152. Mani, R. S. *et al.* Biophysical Characterization of Human XRCC1 and Its Binding to Damaged and Undamaged DNA †. *Biochemistry* **43**, 16505–16514 (2004).
153. Provencher, S. W. & Gloeckner, J. Estimation of globular protein secondary structure from circular dichroism. *Biochemistry* **20**, 33–37 (1981).
154. Carrero, G., McDonald, D., Crawford, E., de Vries, G. & Hendzel, M. J. Using FRAP and mathematical modeling to determine the *in vivo* kinetics of nuclear proteins. *Methods* **29**, 14–28 (2003).
155. Wilson, S. H. *et al.* Base excision repair and design of small molecule inhibitors of human DNA polymerase β . *Cell. Mol. Life Sci.* **67**, 3633–47 (2010).
156. Cappelli, E. *et al.* Involvement of XRCC1 and DNA Ligase III Gene Products in DNA Base Excision Repair. *J. Biol. Chem.* **272**, 23970–23975 (1997).
157. Horton, J., Watson, M. & Stefanick, D. XRCC1 and DNA polymerase β in cellular protection against cytotoxic DNA single-strand breaks. *Cell Res.* **18**, 48–63 (2008).
158. El-Khamisy, S. F. A requirement for PARP-1 for the assembly or stability of XRCC1 nuclear foci at sites of oxidative DNA damage. *Nucleic Acids Res.* **31**, 5526–5533 (2003).
159. Campalans, A. & Kortulewski, T. Distinct spatiotemporal patterns and PARP dependence of XRCC1 recruitment to single-strand break and base excision repair. *Nucleic acids ...* **41**, 3115–29 (2013).
160. Van der Schans, G. P., Paterson, M. C. & Cross, W. G. DNA strand break and rejoining in cultured human fibroblasts exposed to fast neutrons or gamma rays. *Int. J. Radiat. Biol. Relat. Stud. Phys. Chem. Med.* **44**, 75–85 (1983).
161. Della-Maria, J. *et al.* The interaction between polynucleotide kinase phosphatase and the DNA repair protein XRCC1 is critical for repair of DNA alkylation damage

- and stable association at DNA damage sites. *J. Biol. Chem.* **287**, 39233–44 (2012).
162. Jakob, B. *et al.* DNA double-strand breaks in heterochromatin elicit fast repair protein recruitment, histone H2AX phosphorylation and relocation to euchromatin. *Nucleic Acids Res.* **39**, 6489–99 (2011).
 163. Malanga, M. & Althaus, F. R. The role of poly (ADP-ribose) in the DNA damage signaling network 1. (2005). doi:10.1139/O05-038
 164. Veuger, S. J., Curtin, N. J., Smith, G. C. M. & Durkacz, B. W. Effects of novel inhibitors of poly(ADP-ribose) polymerase-1 and the DNA-dependent protein kinase on enzyme activities and DNA repair. *Oncogene* **23**, 7322–9 (2004).
 165. Mabley, J. G. *et al.* Anti-inflammatory effects of a novel, potent inhibitor of poly (ADP-ribose) polymerase. *Inflamm. Res.* **50**, 561–9 (2001).
 166. Simsek, D. *et al.* DNA ligase III promotes alternative nonhomologous end-joining during chromosomal translocation formation. *PLoS Genet.* **7**, e1002080 (2011).
 167. Taylor, R. M., Wickstead, B., Cronin, S. & Caldecott, K. W. Role of a BRCT domain in the interaction of DNA ligase III-alpha with the DNA repair protein XRCC1. *Curr. Biol.* **8**, 877–80 (1998).
 168. Taylor, R. M., Whitehouse, C. J. & Caldecott, K. W. The DNA ligase III zinc finger stimulates binding to DNA secondary structure and promotes end joining. *Nucleic Acids Res.* **28**, 3558–63 (2000).
 169. Caldecott, K. W. Protein ADP-ribosylation and the cellular response to DNA strand breaks. *DNA Repair (Amst)*. **19**, 108–13 (2014).
 170. Katyal, S. & McKinnon, P. J. Disconnecting XRCC1 and DNA ligase III. *Cell Cycle* **10**, 2269–2275 (2011).
 171. Zhang, Y.-W. *et al.* Poly(ADP-ribose) polymerase and XPF-ERCC1 participate in distinct pathways for the repair of topoisomerase I-induced DNA damage in mammalian cells. *Nucleic Acids Res.* **39**, 3607–20 (2011).
 172. Pommier, Y. *et al.* Repair of Topoisomerase I-Mediated DNA Damage. **6603**, 1–37 (2008).
 173. Das, B. B. *et al.* PARP1-TDP1 coupling for the repair of topoisomerase I-induced DNA damage. *Nucleic Acids Res.* **42**, 4435–49 (2014).
 174. Odell, I. D. *et al.* Nucleosome disruption by DNA ligase III-XRCC1 promotes efficient base excision repair. *Mol. Cell. Biol.* **31**, 4623–32 (2011).

175. Allinson, S. L. DNA end-processing enzyme polynucleotide kinase as a potential target in the treatment of cancer. *Future Oncol.* **6**, 1031–1042 (2010).
176. Wiederhold, L. *et al.* AP endonuclease-independent DNA base excision repair in human cells. *Mol. Cell* **15**, 209–20 (2004).
177. Loizou, J. I. *et al.* The Protein Kinase CK2 Facilitates Repair of Chromosomal DNA Single-Strand Breaks Venetian Institute for Molecular Medicine. **117**, 17–28 (2004).
178. Audebert, M., Salles, B., Weinfeld, M. & Calsou, P. Involvement of polynucleotide kinase in a poly(ADP-ribose) polymerase-1-dependent DNA double-strand breaks rejoining pathway. *J. Mol. Biol.* **356**, 257–65 (2006).
179. Jilani, A. *et al.* Molecular Cloning of the Human Gene, PNKP, Encoding a Polynucleotide Kinase 3'-Phosphatase and Evidence for Its Role in Repair of DNA Strand Breaks Caused by Oxidative Damage. *J. Biol. Chem.* **274**, 24176–24186 (1999).
180. Karimi-Busheri, F. *et al.* Molecular Characterization of a Human DNA Kinase. *J. Biol. Chem.* **274**, 24187–24194 (1999).
181. Whitehouse, C. J. *et al.* XRCC1 Stimulates Human Polynucleotide Kinase Activity at Damaged DNA Termini and Accelerates DNA Single-Strand Break Repair. *Cell* **104**, 107–117 (2001).
182. Della-Maria, J. *et al.* The interaction between polynucleotide kinase phosphatase and the DNA repair protein XRCC1 is critical for repair of DNA alkylation damage and stable association at DNA damage sites. *J. Biol. Chem.* **287**, 39233–44 (2012).
183. Zhang, Y. *et al.* Association of XRCC1 gene polymorphisms with the survival and clinicopathological characteristics of gastric cancer. *DNA Cell Biol.* **32**, 111–8 (2013).
184. Zhang, Y., Wang, Y., Wu, J. & Li, L.-J. XRCC1 Arg194Trp polymorphism is associated with oral cancer risk: evidence from a meta-analysis. *Tumour Biol.* **34**, 2321–7 (2013).
185. Fang, Z. *et al.* XRCC1 Arg194Trp and Arg280His polymorphisms increase bladder cancer risk in Asian population: evidence from a meta-analysis. *PLoS One* **8**, e64001 (2013).
186. Prendergast, F. G., Meyer, M., Carlson, G. L., Iida, S. & Potter, J. D. Synthesis, spectral properties, and use of 6-acryloyl-2-dimethylaminonaphthalene

- (Acrylodan). A thiol-selective, polarity-sensitive fluorescent probe. *J. Biol. Chem.* **258**, 7541–4 (1983).
187. Mani, R. S. & Kay, C. M. Calcium-dependent regulation of the caldesmon-heavy meromyosin interaction by caltropin. *Biochemistry* **32**, 11217–11223 (1993).
 188. Masson, M. *et al.* XRCC1 is specifically associated with poly(ADP-ribose) polymerase and negatively regulates its activity following DNA damage. *Mol. Cell. Biol.* **18**, 3563–71 (1998).
 189. Marintchev, A. *et al.* Solution structure of the single-strand break repair protein XRCC1 N-terminal domain. *Nat. Struct. Biol.* **6**, 884–93 (1999).
 190. Hanahan, D. & Weinberg, R. a. Hallmarks of cancer: The next generation. *Cell* **144**, 646–674 (2011).
 191. Jones, R. E. *et al.* Escape from telomere-driven crisis is DNA ligase III dependent. *Cell Rep.* **8**, 1063–76 (2014).
 192. Cosme-Blanco, W. & Chang, S. Dual roles of telomere dysfunction in initiation and suppression of tumorigenesis. *Exp. Cell Res.* **314**, 1973–9 (2008).
 193. Perera, S. A. *et al.* Telomere dysfunction promotes genome instability and metastatic potential in a K-ras p53 mouse model of lung cancer. *Carcinogenesis* **29**, 747–53 (2008).
 194. Olivier, M., Hollstein, M. & Hainaut, P. TP53 mutations in human cancers: origins, consequences, and clinical use. *Cold Spring Harb. Perspect. Biol.* **2**, a001008 (2010).
 195. Sallmyr, A., Tomkinson, A. E. & Rassool, F. V. Up-regulation of WRN and DNA ligase IIIalpha in chronic myeloid leukemia: consequences for the repair of DNA double-strand breaks. *Blood* **112**, 1413–23 (2008).
 196. Tobin, L. a *et al.* Targeting abnormal DNA double-strand break repair in tyrosine kinase inhibitor-resistant chronic myeloid leukemias. *Oncogene* **32**, 1784–1793 (2012).
 197. Tobin, L. A. *et al.* Abstract 5495: ALT NHEJ is a therapeutic target in hormone therapy resistant ER/PR/HER+ and ER/PR/HER- breast cancers. *Cancer Res.* **71**, 5495–5495 (2011).
 198. Tomkinson, A. E., Howes, T. R. L. & Wiest, N. E. DNA ligases as therapeutic targets. *Transl. Cancer Res.* **2**, (2013).

199. Chen, X. *et al.* Rational design of human DNA ligase inhibitors that target cellular DNA replication and repair. *Cancer Res.* **68**, 3169–77 (2008).
200. Tomkinson, A. E., Vijayakumar, S., Pascal, J. M. & Ellenberger, T. DNA ligases: structure, reaction mechanism, and function. *Chem. Rev.* **106**, 687–99 (2006).
201. Kulczyk, A. W., Yang, J.-C. & Neuhaus, D. Solution structure and DNA binding of the zinc-finger domain from DNA ligase III α . *J. Mol. Biol.* **341**, 723–38 (2004).
202. Ahel, I. *et al.* The neurodegenerative disease protein aprataxin resolves abortive DNA ligation intermediates. *Nature* **443**, 713–6 (2006).
203. Dobson, C. J. & Allinson, S. L. The phosphatase activity of mammalian polynucleotide kinase takes precedence over its kinase activity in repair of single strand breaks. *Nucleic Acids Res.* **34**, 2230–7 (2006).
204. Pommier, Y. Repair of and checkpoint response to topoisomerase I-mediated DNA damage. *Mutat. Res. Mol. Mech. Mutagen.* **532**, 173–203 (2003).
205. Gueven, N. *et al.* Aprataxin, a novel protein that protects against genotoxic stress. *Hum. Mol. Genet.* **13**, 1081–93 (2004).
206. Chiang, S.-C., Carroll, J. & El-Khamisy, S. F. TDP1 serine 81 promotes interaction with DNA ligase III α and facilitates cell survival following DNA damage. *Cell Cycle* **9**, 588–595 (2010).
207. Freschauf, G. K. *et al.* Identification of a small molecule inhibitor of the human DNA repair enzyme polynucleotide kinase/phosphatase. *Cancer Res.* **69**, 7739–46 (2009).
208. Mani, R. S. *et al.* XRCC1 stimulates polynucleotide kinase by enhancing its damage discrimination and displacement from DNA repair intermediates. *J. Biol. Chem.* **282**, 28004–13 (2007).
209. Kubota, Y., Takanami, T., Higashitani, A. & Horiuchi, S. Localization of X-ray cross complementing gene 1 protein in the nuclear matrix is controlled by casein kinase II-dependent phosphorylation in response to oxidative damage. *DNA Repair (Amst)*. **8**, 953–60 (2009).
210. Ström, C. E. *et al.* CK2 phosphorylation of XRCC1 facilitates dissociation from DNA and single-strand break formation during base excision repair. *DNA Repair (Amst)*. **10**, 961–9 (2011).
211. Parsons, J. L. *et al.* XRCC1 phosphorylation by CK2 is required for its stability and efficient DNA repair. *DNA Repair (Amst)*. **9**, 835–41 (2010).

212. Mani, R. S. *et al.* Dual modes of interaction between XRCC4 and polynucleotide kinase/phosphatase: implications for nonhomologous end joining. *J. Biol. Chem.* **285**, 37619–29 (2010).
213. Dong, Z. & Tomkinson, A. E. ATM mediates oxidative stress-induced dephosphorylation of DNA ligase IIIalpha. *Nucleic Acids Res.* **34**, 5721–279 (2006).